PREPARATION OF MULTILAYER CAPSULES CONTAINING DODECAHYDRO-*CLOSO*-DODECABORATE LOADED POLYMER MICELLES

A THESIS SUBMITTED TO
THE GRADUATE SCHOOL OF NATURAL AND APPLIED SCIENCES
OF
MIDDLE EAST TECHNICAL UNIVERSITY

BY

UMUT AYDEMİR

IN PARTIAL FULFILLMENT OF THE REQUIREMENTS
FOR
THE DEGREE OF MASTER OF SCIENCE
IN
BIOCHEMISTRY

SEPTEMBER 2021

Approval of the thesis:

PREPARATION OF MULTILAYER CAPSULES CONTAINING DODECAHYDRO-*CLOSO*-DODECABORATE LOADED POLYMER MICELLES

submitted by **UMUT AYDEMİR** in partial fulfillment of the requirements for the degree of **Master of Science in Biochemistry, Middle East Technical University** by,

Prof. Dr. Halil Kalıpçılar
Dean, Graduate School of **Natural and Applied Sciences** _____

Assoc. Prof. Dr. Yeşim Soyer
Head of the Department, **Biochemistry** _____

Assoc. Prof. Dr. İrem Erel Göktepe
Supervisor, **Biochemistry, METU** _____

Prof. Dr. Akın Akdağ
Co-Supervisor, **Chemistry, METU** _____

Examining Committee Members:

Prof. Dr. Sreeparna Banerjee
Biological Sciences, METU _____

Assoc. Prof. Dr. İrem Erel Göktepe
Chemistry, METU _____

Prof. Dr. Akın Akdağ
Chemistry, METU _____

Prof. Dr. Gülay Ertaş
Chemistry, METU _____

Prof. Dr. Atilla Cihaner
Chemical Engineering, Atılım University _____

Date: 09.09.2021

I hereby declare that all information in this document has been obtained and presented in accordance with academic rules and ethical conduct. I also declare that, as required by these rules and conduct, I have fully cited and referenced all material and results that are not original to this work.

Name Last name : Umut Aydemir

Signature :

ABSTRACT

PREPARATION OF MULTILAYER CAPSULES CONTAINING DODECAHYDRO-*CLOSO*-DODECABORATE LOADED POLYMER MICELLES

Aydemir, Umut
Master of Science, Biochemistry
Supervisor: Assoc. Prof. Dr. İrem Erel Göktepe
Co-Supervisor: Prof. Dr. Akın Akdağ

September 2021, 124 pages

Boron Neutron Capture Therapy (BNCT) is a non-invasive radiotherapy technique which is based on delivery of non-radioactive ^{10}B compounds to cancer cells and irradiation of the tumour tissues with low energy thermal neutrons. It is a promising radiotherapy technique due to reduce the side effects of the treatment.

The main goal of this thesis is to prepare a non-toxic polymer vehicle to provide efficient delivery of ^{10}B to cancer cells. Dodecahydro-*closo*-dodecaborate $(B_{12}H_{12})^{2-}$ (B12) anion was utilized as a model ^{10}B containing agent because of its high boron concentration. Quaternized poly(2-vinyl pyridine)-*b*-poly(ethylene oxide) (QP2VP-*b*-PEO) was chosen as a model neutral-cationic block copolymer to construct the carrier. The electrostatic association between QP2VP and B12 induced self-assembly of QP2VP-*b*-PEO, resulting in micelles with (B12+QP2VP)-core and PEO-corona. (B12+QP2VP)-*b*-PEO micelles were found to be not stable against dilution in biological medium.

Layer-by-Layer (LbL) deposition technique was used to self-assemble these micelles onto colloidal $CaCO_3$ microparticles to enhance their stability. Tannic acid (TA) was used to drive the LbL assembly through hydrogen bonding interactions between hydrogen accepting PEO-corona and hydrogen donating TA. Stability of LbL capsules in biological medium was assured by construction of barrier layers composed of poly(N-vinyl-caprolactam) (PVCL) and TA on top of (B12+QP2VP)-*b*-PEO micelles and TA multilayers.

Cytotoxicity and cellular association of LbL capsules was assessed in non-hollow and hollow form using Hep G2 cell line. Capsules were found to show no systematic cytotoxicity on Hep G2 cell line.
Cellular association studies and boron concentrations determined through inductively coupled plasma optical emission spectroscopy (ICP-OES) showed that both non-hollow and hollow capsules associated with Hep G2 cells and delivered boron to the cells.

Overall, this study generated fundamental knowledge on B12 induced micellization and stabilization of micelles in biological medium. These findings may form a basis to develop polymer carriers for boron delivery for BNCT.

Keywords: Self-assembly, Layer-by-Layer Self-assembly Technique, Boron Neutron Capture Therapy, Microcapsules

ÖZ

DODEKAHİDRO-*KLOSO*-DODEKABORAT YÜKLÜ POLİMER MİSELLER İÇEREN ÇOK KATMANLI KAPSÜLLERİN HAZIRLANMASI

Aydemir, Umut
Yüksek Lisans, Biyokimya
Tez Yöneticisi: Doç. Dr. İrem Erel Göktepe
Ortak Tez Yöneticisi: Prof. Dr. Akın Akdağ

Eylül 2021, 124 sayfa

Bor Nötron Yakalama Terapisi (BNCT), radyoaktif olmayan ^{10}B bileşiklerinin kanser hücrelerine taşınması sonrasında tümör dokularının düşük enerjili termal nötronlarla ışınlanmasına dayanan ve invazif olmayan bir radyoterapi tekniğidir. Tedavinin yan etkisinin az olması nedeniyle bu teknik umut vadeden bir radyoterapi biçimidir.

Bu tezin temel amacı, ^{10}B'nin kanser hücrelerine verimli bir şekilde taşınmasını sağlamak için toksik olmayan bir polimer taşıyıcı geliştirmektir. Dodekahidro-*kloso*-dodekaborat $(B_{12}H_{12})^{2-}$ (B12) anyonu yüksek bor içeriğinden dolayı ^{10}B içeren model ajan olarak kullanılmıştır. Kuaternize poli(2-vinil piridin)-*b*-poli(etilen oksit) (QP2VP-*b*-PEO) ise, taşıyıcıyı oluşturmak için model bir nötr-katyonik blok kopolimer olarak seçilmiştir. QP2VP ve B12 arasındaki elektrostatik etkileşim, QP2VP-*b*-PEO'nun kendi kendine yapılanmasını sağlamış, (B12+QP2VP)-çekirdek ve PEO-korona yapısına sahip misellerin oluşmasını tetiklemiştir. Fakat (B12+QP2VP)-*b*-PEO misellerinin biyolojik ortamda seyrelmeye karşı kararlı olmadığı tespit edilmiştir.

(B12+QP2VP)-*b*-PEO misellerinin kararlılıklarını artırmak için katman-katman biriktirme (LbL) yöntemi ile kolloidal $CaCO_3$ mikroparçacıklar üzerine (B12+QP2VP)-*b*-PEO miselleri kendiliğinden yapılandırılmıştır. Katman-katman yapılanma, TA kullanılarak hidrojen kabul edici PEO-kabuk ve hidrojen verici TA arasında kurulan hidrojen bağları etkileşimi sayesinde gerçekleştirilmiştir. LbL kapsüllerin biyolojik ortamdaki kararlılığı, (B12+QP2VP)-*b*-PEO miseller ve TA çok-katmanlı kapsüllerinin üzerinde biriktirilen poli(N-vinil-kaprolaktam) (PVCL) ve TA'dan oluşan bariyer tabaka ile sağlanmıştır.

LbL kapsüllerin sitotoksisitesi ve hücre ile etkileşimleri, Hep G2 hücre hattı kullanılarak içi boş olmayan ve içi boş kapsüller ile takip edilmiştir. Kapsüllerin, Hep G2 hücre hattı üzerinde majör sistematik sitotoksisite göstermediği tespit edilmiştir.

Hücre ile etkileşim çalışmaları ve indüktif eşleşmiş plazma optik emisyon spektroskopisi (ICP-OES) yöntemiyle belirlenen bor derişimi analizleri, içi boş olmayan ve içi boş kapsüllerin hücrelerle etkileştiğini ve hücrelere bor taşınabildiğini göstermiştir.

Genel olarak, bu çalışma B12 ile tetiklenmiş miselizasyon ve misellerin biyolojik ortamlardaki kararlılığı hakkında temel bilgi üretilmesini sağlamıştır. Bulgular, BNCT'e yönelik bor taşınımı yapacak polimer taşıyıcılar geliştirmek için bir temel oluşturabilecek niteliktedir.

Anahtar Kelimeler: Kendiliğinden Yapılanma Katman-Katman Kendiliğinden Yapılanma Tekniği, , Bor Nötron Yakalama Terapisi, Mikrokapsüller

To the dearest existence of my grandmother, Ayşe Cemmedo

ACKNOWLEDGMENTS

First and the biggest appreciation needs to be done to my supervisor Assoc. Prof. Dr. İrem Erel Göktepe. She was always very kind, helpful, and patient to me even during the times I got demotivated, she encourages me to do my best. İrem Hoca has believed and supported me in every mean. She thought me how to be a scientist, how to be a future's proper academician candidate and how important the work we are doing in the lab is. Her discipline of studying, scientific work ethic and ambition to do more in the field inspires me every day.

I appreciate the guidance of my co-supervisor Prof. Dr. Akın Akdağ to find which chemistry related discipline best suits for me. Akın Hoca is one of the few people strongly believes the capacity I have and had before. He motivates me for gaining an interdisciplinary perspective whenever we had a discussion. His immense knowledge in organic chemistry, boron chemistry and biochemistry has enriched my thesis study.

I would like to thank to Prof. Dr. Sreeparna Banerjee for the opportunity she gave me to study and experience by hand the biological aspects of my project. Her navigation and advices have brought my studies a very sophisticated viewpoint.

I would like to thank for the other defence committee members; Prof. Dr. Atilla Cihaner and Prof. Dr. Gülay Ertaş for their presence, time and valuable comments.

My family, especially my mother Şansel Aydemir, my father Salih Aydemir and my brother Selçuk Uluç Aydemir have shown me the biggest support during my lifetime. I would like to thank them for being there whenever I need and for their unconditionally love.

I would like to thank my colleagues in the lab; Dilara Gündoğdu, Gökçe Tidim, Esma Uğur and Çağrı Turan who were always supportive and have constructed a

welcoming, warm, home-like atmosphere in the workplace. We are friends beyond colleagues, and we stand with each other against every obstacle.

I would like to thank all Banerjee Cancer Systems Research Group members; especially Çağdaş Ermiş, Aydan Torun, and Esin Gülce Seza. Çağdaş has patiently trained me in biology laboratory techniques and I owe what I know to him. Aydan and Esin were always supportive, and they discussed my results with me in every detail.

I would also like to thank the members of Akın Akdağ Research Group especially Perihan Öztürk Düzenli, Gizem Ünay, Sevban Doğan and Fatmanur Aydemir for their contribution in my work. I especially thank to Fatma Nur Aydemir for her effort in the synthesis of B12.

I would like to thank to my close friends especially Nihad Aliyev, Tuğçe Demirsöz, Mehmet Fırat Aydın, Sena Tarım, Berçin Verda Asya, Gökçe Tidim, Ege Hoşgör, Doruk Baykal, Bengi Şentürk, Ece Ayça Erdoğan Dilan Ece Dikbıyık and İrem Kolay for their presence and support.

We acknowledge National Boron Research Institute for supporting the project financially.

The times I spent during my MSc studies were extraordinary. We tried to do our bests in one of the darkest times of humanity. COVID-19 pandemic had changed everything from top to bottom. Now, I better know the importance of each breath, I appreciate being healthy and enjoy the assurance of knowing my beloved ones are safe and sound. That is why I would like to thank with a reverence to Dr. Özlem Türeci and Dr. Uğur Şahin for saving millions of lives.

My cat, Kiwi was also one of my biggest supporters, thank you Kiwi!

TABLE OF CONTENTS

LIST OF TABLES

LIST OF FIGURES

LIST OF SCHEMES

LIST OF ABBREVIATIONS

ATRP	Atom transfer radical polymerization
ATR-FTIR	Attenuated total reflectance- fourier transform infrared
B12	Dodecahydro-*closo*-dodecaborate
BCP	Block copolymers
BNCT	Boron neutron capture therapy
BPA	L-4-dihydroxy-borylphenylalanine
BSH	Sodium mercaptoundecahydro-*closo*-dodecaborate
CMC	Critical micellization concentration
CMT	Critical micellization temperature
CUR	Curcumin
DI	Deionized
DMF	N,N- Dimetylformamide
DNA	Deoxyribose nucleic acid
DOTAP	1,2-dioleoyl-3-trimethylammonium-propane
DS	Dextran sulphate
EGFR	Epidermal growth factor
EDTA	Ethylenediaminetetraacetic acid
ICP-OES	Inductively coupled plasma- optical emission spectroscopy
HS	Heparin sulphate

HVJE Hemagglutinating virus of Japan envelope

LBL Layer by layer

LCST Lower critical solution temperature

MeI Iodomethane

MSNP Mesoporous silica nanoparticle

NGF Nerve growth factor

NMR Nuclear magnetic resonance

P2VP-*b*-PEO Poly(2-vinylpyridine-*b*-ethylene oxide)

***β*PDMA-b-PDPA** Poly[3-dimethyl (methacryloyloxyethyl) ammonium propane sulfonate]-*b*-poly[2-(diisopropylamino)ethyl methacrylate]

PAA Poly(acryclic acid)

PAH Poly(allylamine hydrochloride)

PArg Poly-arginine

PAAM Poly(acrylamide)

PAMAM Polyamidoamino

PCL Poly(ε-caprolactone)

PDDA Poly(diallyldimethylammonium chloride)

PDEA Poly[(2-dimethylamino)ethyl methacrylate]

PDEAM Poly(N,N-diethylacrylamide)

PGEA Poly(guanidium ethyl acrylate)

P(Glu) Poly(glutamic acid)

PMAA Poly(methacrylic acid)

PMMA	Poly(methyl methacrylate)
PNAGA	Poly(N-acryloylglycinamide)
PNIPAAm	Poly(N-isopropylacrylamide)
PNNPAM	Poly(N-n-propylacrylamide)
PPO	Poly(ethylene oxide)
PSS	Poly(sodium 4-styrenesulfonate)
PS-*b*-PAA	Poly(styrene-*b*-acrylic acid)
PVCL	Poly(N-vinylcaprolactam)
PVP	Poly(N-vinylpyrrolidone)
PVS	Poly(vinyl sulphate)
RAFT	Reversible addition-fragmentation chain transfer radical polymerization
RES	Reticulo endothelial system
SEM	Scanning electron microscopy
SDS	Sodium dodecyl sulphate
SRPs	Stimuli responsive polymers
SPP	3-[N-(3-methacrylamidopropyl)-N,N-dimethyl] ammoniopropane sulfonate (SPP)
SWCNT	Single walled carbon nanotubes
TA	Tannic acid
TEM	Transmission electron microscopy
UCST	Upper critical solution temperature

CHAPTER 1

INTRODUCTION

1.1 Self-Assembly of Block Copolymers

Block copolymers (BCP) have two or more different blocks of homopolymers with different chemical structures which are linked to one another [1]. Block copolymers are synthesized using two or more monomers through various polymerization routes such as cationic and anionic polymerization, atom transfer radical polymerization (ATRP) and reversible addition-fragmentation chain transfer radical polymerization (RAFT) [2]. Both functional groups of monomers and integration procedures influence their topology [3].

“Amphiphilic” is a characteristic property which means "loving both" or "having an affinity for both". This feature is commonly shown toward water and oil. However, amphiphilicity can also be displayed towards any two solvents that are incompatible with each other [4]. Amphiphilic block copolymers have two separate parts, including hydrophilic (water-loving) and hydrophobic (water-hating) parts. Amphiphilic block copolymers have been of interest to polymer scientists for more than three decades [5] and represent a new family of functional polymers that serve as one-of-a-kind building blocks for a variety of applications, most notably energy and structural control of materials interfaces [6]. Anionic, cationic, group transfer, and radical polymerization techniques can all be used to perform sequential controlled or live polymerizations for the synthesis of amphiphilic block copolymers [7]. When amphiphilic block copolymers are dissolved in a solvent, each block may interact differently with the solvent molecules which affects the conformation of each block in that particular solvent [8]. Because of the amphiphilic character, the two components of the block copolymer may interact significantly different with

either a polar/nonpolar solvent or surface [4]. In order to avoid energetically unfavourable hydrophobe–water interactions, amphiphilic block copolymers may undergo self-assembly in aqueous solution [9].

The concept "self-assembly" refers to a dynamic process in which system components assemble themselves into ordered structures without any external direction [10]. However, the definition of "self-assembly" is not definite. It may vary depending on the processes happened within a particular system [11]. When self-assembly of amphiphilic molecules is in question, the two parts of the same amphiphilic molecule behave quite differently when interacting with a polar/ nonpolar solvent or polar/ nonpolar surface. There are two main approaches to make favourable intermolecular interactions while reducing unfavourable ones: i) self-assembly in solution and ii) adsorption to a surface/interface [4]. Self-assembly of amphiphilic block copolymers is a reversible process mediated by the solution thermodynamics. The entropy of the solution decreases as the concentration of polymer is increased due to the unfavourable arrangement or ordering of solvent molecules. As the concentration approaches a critical value, so called “critical micellization concentration (CMC)”, the association among the hydrophobic blocks of the polymer chains is enhanced. This non-covalent association among the hydrophobic blocks results in formation of micellar aggregates and an increase in entropy of solution [7, 12]

The morphology of self-assembled BCP is determined by the inherent molecular curvature and its effect on the packing of copolymer chains. The following formula defines dimensionless packing parameter (p) and provides information about the shape of the molecule. In this formula, v is the hydrophobic chain volume, a_o is the optimal head group area and I_c is the hydrophobic tail length [13].

$$p = \frac{v}{a_0 \, I_C}$$

For a theoretical point of view, micelles exhibiting spherical shape are favoured when packing parameter, $p \leq \frac{1}{3}$, micelles with cylindrical shapes are favoured when $\frac{1}{3} \leq p \leq \frac{1}{2}$ and vesicles are favoured when $\frac{1}{2} \leq p \leq 1$ [14].

As mentioned above, micelles are formed above a certain concentration (CMC). When a solution of micelles is diluted to concentrations lower than 10^{-3} mM, number of molecules inside the medium become sufficiently low to drive a self-assembly. Instead, they favour to distribute themselves inside the medium [15]. Thus, CMC is an important parameter in the formation, characterization and stability of micelles in a medium [16]. Micelles have diameters ranging from 10 to 100 nm. Amphiphilic block copolymer micelles are characterized by a core-shell architecture in which the core contains the hydrophobic blocks and corona contains the hydrophilic blocks of the amphiphilic block copolymer. The core region of block copolymer micelles provide a cargo space for the solubilization of lipophilic drug molecules [17]. The hydrophilic blocks in the corona region become water bound and splayed [18]. Corona expected to sterically restrict opsonization by the blood components and prevent macrophage phagocytosis. In this way, reticulo-endothelial system (RES) clearance is reduced providing longer circulation times in the blood [19].

Micelles are not the only outcome of self - assembled BCP. Amphiphilic BCP can also form nanoparticles. However, the equilibrium dynamics of nanoparticle formation is different than that of micelles. The formation of nanoparticles can be controlled kinetically via temperature [20], pH [21], solvent content and presence of electrolytes [20]. Nanoparticles are formed by the nucleation and growth of the dispersed block copolymer chains. Growth occurs by the insertion of unimers into self-assembly and this occurs until unimers are energetically unfavourable to insert into the formed particle where particles become kinetically frozen [22]. A polymeric nanoparticle is a solid colloidal particle with a matrix in which pharmaceuticals can be encapsulated, adsorbed, or chemically bonded, to the polymer matrix [23]. The size of the nanoparticles usually varies from 100 to 200 nm [24]. Nanoparticle core

serves as a container for the dissolution or encapsulation of hydrophobic pharmaceuticals [25]. On the other hand, the shell serves as a barrier to aggregation/coagulation and phagocytosis. Even though the size of the nanospheres delays elimination, clearance is still unavoidable due to capture by the RES, which sequesters particles within organs like the liver and spleen [26]. The shells of the nanoparticles have been demonstrated to be very vulnerable to opsonization and clearing by the RES [27].

In addition to micelles and nanoparticles, amphiphilic BCPs can also self-assemble into polymersomes. Polymersomes are hollow structures surrounded by a polymer bilayer membrane. The structure of liposomes - spherical, nano- or micron-sized vehicles made of phospholipids that self-assemble in order to form lipid bilayers- has been used as a model to study polymersomes [28]. Polymersomes have been generated from amphiphilic macromolecules with a variety of topologies (diblock, triblock, graft, hyperbranched, and so on) and molecular weights which varying from hundreds up to thousands of Da [29]. Polymersomes are made up of amphiphilic block copolymers with two or more chemically different monomer sequences linked via a covalent connection that self-assemble. These blocks are typically immiscible within each other; however, the covalent connection prevents them from separating in macrophase. To limit the contact between the blocks, the copolymers microphase segregate. These microphase separated copolymers form sheets, or lamellas, as the most efficient shape for minimizing their contact area, when the block sizes are properly proportioned. These sheets final morphology is a spherical polymersome [30]. Polymersomes are promising prospects for drug delivery applications because of their outstanding robustness and stability, chemical diversity for variable membrane characteristics, and surface functionalization [31]. Basic illustration of micelle, nanoparticle and polymersome architectures is represented in Figure 1.

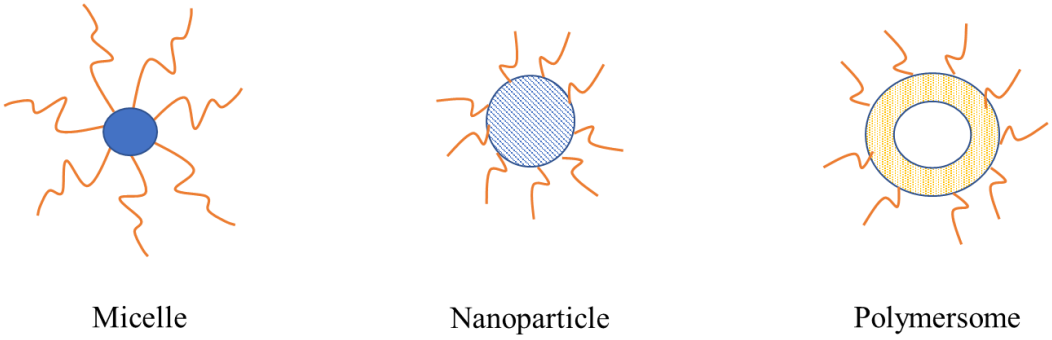

Figure 1. Illustration of nanostructures obtained from the self-assembly of BCPs.

1.2 Stimuli Responsive Polymers

As the synthetic techniques and engineering aspects have been developed by the sake of technology, polymers which alter their chemical and/or physical properties in response to change in stimuli such as temperature [32], pH [33], light [34], and ionic strength, so called "stimuli responsive polymers" (SRPs) have been synthesized [35]. Upon exposure to these stimuli, these polymers can be altered in a variety of ways at the macromolecular level, including changes in hydrophilic-to-hydrophobic balance, conformation, and solubility [36,37].

1.2.1 Temperature Responsive Polymers

Temperature-responsive polymers have gained a lot of attention in bioengineering and biotechnology applications since certain diseases cause temperature changes [38]. In general, temperature-responsive polymers show a critical solution temperature at which the hydrophobic and hydrophilic interactions between the polymer chains and the aqueous media alter rapidly along a limited temperature range [39].

The solubility of temperature responsive polymers changes rapidly as the critical temperature is reached and such polymers display reversible, temperature-dependent sol-gel transitions [40]. The ratio of hydrophilic and hydrophobic portions on the polymer chain is critical on the temperature at which the phase transition occurs. Basically, temperature-responsive polymers are classified into two categories: i) polymers exhibiting upper critical solution temperature (UCST) behaviour and ii) polymers exhibiting lower critical solution temperature (LCST) behaviour.

Polymer solutions with UCST behaviour phase separate below a certain temperature but exist as a single phase beyond the same temperature [41]. Polymer solutions that appear monophasic below a certain temperature but biphasic beyond that temperature are said to have LCST behaviour [7]. UCST and LCST are schematically described on Figure 2.

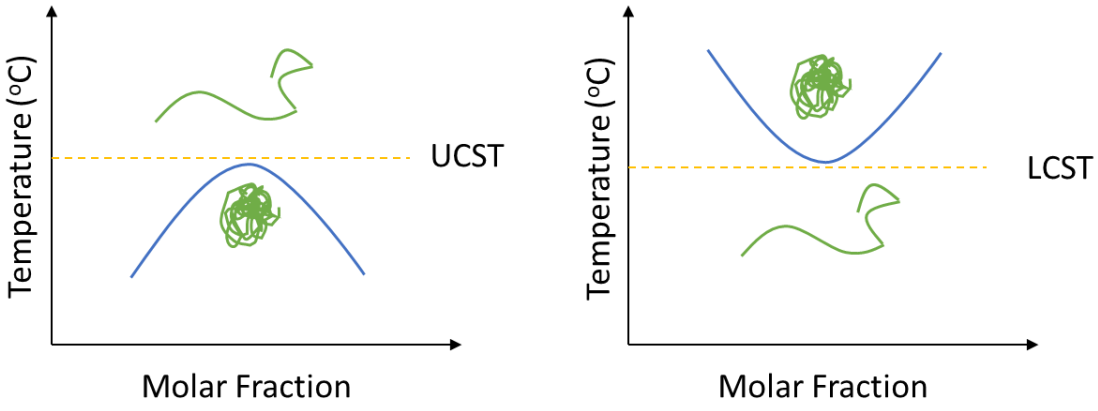

Figure 2. UCST and LCST polymer phase diagrams, the phase separation border is indicated by the yellow dashed line. The schematic is modified from Gibson and O'Reilly, Chem Soc Rev. (2013) [42].

1.2.2 pH Responsive Polymers

pH-responsive polymers are a class of stimuli-responsive polymers that can modify their structure and properties such as chain conformation, surface activity,

configuration, and solubility in response to variations in the solution pH [43]. The term "pH-responsive polymers" refers to polymers with ionisable basic or acidic functional groups. Therefore, ionization of the polymer is affected by the pH of the solution. Under particular pH conditions, the functional groups present on the side chains of polymer or in the backbone will ionize and led to a conformational shift in the polymer that results in dissolution or swelling [43]. pH responsive polymers find use in various applications, including drug delivery, sensors, preparation of smart surfaces, gene delivery, and chromatography [44]. Polymers containing acidic functional groups, polyacids, accept protons especially at pH values lower than pK_a of the polyacid. For example, poly(acrylic acid) (PAA) with a pK_a of 4.25 deprotonate especially at pH values higher than 4.25 (Scheme 1) and the swelling of PAA in water is explained by the electrostatic repulsion among the carboxylate groups [43].

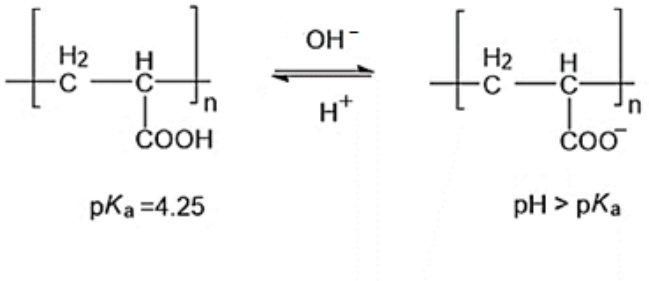

Scheme 1. Schematic illustration of ionization of PAA above its pK_a (Modified from ref [43], Chan et al., Adv. Drug Deliv. Rev. (2012)).

Polybases accept protons below their pK_a values. Solubility of polybases is lost at pH above their pK_a. An example to commonly used polybases is poly[(2-dimethylamino)ethyl methacrylate] (PDEA) with a pK_a of 7.3. Scheme 2 shows protonation/deprotonation of tertiary amine groups of PDEA [43].

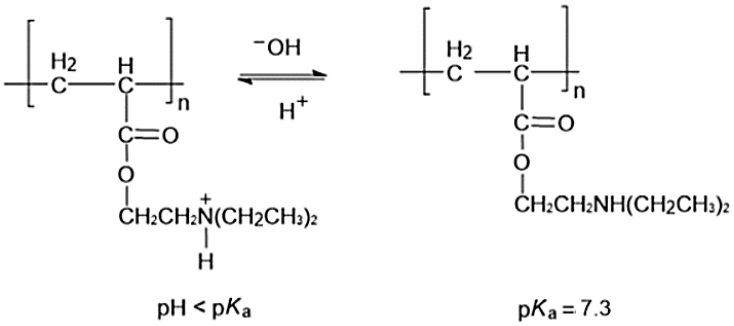

Scheme 2. Schematic illustration of PDEA's ionization below its pK_a (Modified from ref [43], Chan et al., Adv. Drug Deliv. Rev. (2012)).

1.3 Stimuli Responsive Micellization

Poor water solubility of certain therapeutics make effective delivery of therapeutic compounds challenging [45]. For example, the majority of anti-cancer drugs have limited solubility in aqueous environment, and the standard solubilizing chemicals employed to formulate those are frequently hazardous [19]. Colloidal vehicles function as effective solubilizing agents in such circumstances and this has been obviated by recent developments in drug formulations [46]. Block copolymer micelles have the ability to improve the solubility of hydrophobic compounds [47]. Incorporation of drug molecules into micellar cores was discovered as an efficient strategy to increase the aqueous solubility of anti- cancer drugs [48]. Additionally, encapsulating drug molecules into micellar cores was found to result in a significant reduction in systemic toxicity of Doxorubicin [48,49], Paclitaxel [50,51] and many other anti-cancer clinical formulations [52]. Regarding the effectiveness of polymeric micelles as drug carriers, clinical trials have revealed a variety of problems such as early drug release from micelles in the circulation or insufficient drug release after micelle accumulation in the tumour interstitium [53]. As a solution

to these challenges, micelles which can release their cargo in a controlled manner by applying an internal or external stimuli have attracted attention. By applying a kind of stimuli (e.g. temperature and/or pH change), micelle destabilization can be promoted in a regulated way and in this manner, drug delivery specificity can be improved [54]. Block copolymer micelles which show response to changes in environmental conditions are obtained through stimuli-triggered self-assembly of block copolymers.

1.3.1 pH Induced Micellization

pH is a vital physiological measure in cellular and tissue homeostasis. The presence of a dysregulated pH level has been identified as a characteristic of cancer and it is known that the pH of tumour interstitial fluid is lower than that of normal tissues [55]. Endocytosis is used to internalize the micelles, which then end up in the acidic environment of endosomes and lysosomes [56]. pH-sensitive micelles may be capable of overcoming intracellular barriers in the drug's (or gene's) pathway to its target, such as endosomal or lysosomal membranes [57]. Many pH-sensitive polymeric micellar systems have been developed using this phenomenon for the delivery of anti-cancer drugs to tumours. The release of the drug can be promoted if the micelles could be disintegrated upon arriving at the target in response to pH change at tumour tissue [58].

pH-responsive micelles can be obtained using a double hydrophilic block copolymer with at least one polyacid/polybase block. When the pH-sensitive block is rendered water-insoluble above/below the pK_a of the polybase/polyacid, enhanced association among the insoluble blocks yield in formation of block copolymer micelles. For example, Martin et al. studied pH-triggered micellization of poly(2-vinyl pyridine)-*b*-polyethylene oxide (P2VP-*b*-PEO) with polybasic P2VP block and neutral PEO block [59]. PEO was soluble regardless of pH. However, P2VP block was soluble only when pyridine units of P2VP were protonated. When the pH was risen to neutral

or basic conditions, P2VP block deprotonated and the self-assembly was induced due to enhanced association among P2VP blocks. The resulting micelles had PEO-corona and P2VP-core structure [59]. In another study by Giacomelli et al., pH-induced micellization of a triblock-copolymer, poly(ethylene oxide)-*b*-poly(glycerol monomethacrylate)-*b*-poly[2-(diisopropylamino)ethyl methacrylate] (PEO-*b*-PG2MA-*b*-PDPA) was examined. When the pH of the aqueous solution of PEO-*b*-PG2MA-*b*-PDPA was increased above pH 6.8 (pK_a of PDPA ~ 6.8), PDPA deprotonated and induced micellization as well as encapsulation of poorly water-soluble drug, paclitaxel. These micelles provided a pH response within 6.30 < pH < 6.95, suitable for the drug release in the tumour microenvironment [60].

1.3.2 Temperature Induced Micellization

Temperature is one of the most studied stimuli for drug delivery since it can operate as both an internal and exterior stimulation. Temperature changes in specific tissues can happen as a consequence of certain disorders (e.g., tumor, inflammation, or infection) or as a result of the use of an external heating source/device [61]. The elevated temperature, commonly known as "hyperthermia," might cause extra damage to tumour cells by inhibiting deoxyribose nucleic acid (DNA) synthesis and repair, disrupting microtubules, and changing receptor expression [62]. As a result, temperature responsive drug delivery systems are among the most studied stimuli-responsive treatment routes [63] .

The development of thermo-responsive polymeric micelles as intelligent drug delivery systems that respond to slight changes in the temperature has received a lot of interest recently. Temperature-induced micellization was generally obtained using block copolymers with at least one hydrophilic and one temperature-responsive block. For example, block copolymers containing poly(N-alkylacrylamide)s with LCST-type phase behaviour, such as Poly(N-n-propylacrylamide) (PNNPAM), Poly(N,N-diethylacrylamide) (PDEAM), Poly(N-vinylpyrrolidone) (PVP) Poly(N-

vinylcaprolactam) (PVCL), poly(N-isopropylacrylamide) (PNIPAAm) [64]. PNIPAAm have been extensively studied to obtain temperature-responsive block copolymer micelles [64]. In case of micellization in the presence of a block with LCST-type phase behaviour, micelles are formed above the critical temperature and hydrophobic drugs are encapsulated during micellization. For example, Hennink and co-workers demonstrated micellization of PEG-*b*-PNIPAAm. PNIPAAm transformed from extended to globular form above its LCST, desolubilized and formed the micellar cores [65]. There are also studies concerning micellization of block copolymers composed of a block with LCST and a hydrophobic block. For example, Wei et al. reported micellization of PNIPAAm–poly(methyl methacrylate) (PNIPAAm–PMMA) below LCST of PNIPAAm while encapsulating an anti-inflammatory drug, prednisone acetate. The resulting micelles had PNIPAAm-corona and PMMA-core. The study investigated the release rate difference with respect to the temperature changes [66].

Although polymers that exhibit LCST behavior have received greater attention, thermoresponsive polymers that exhibit decreasing solubility upon cooling are another significant group of polymers so, UCST behaviour is becoming increasingly popular. RAFT polymerization was used to make poly(N-acryloylglycinamide) (PNAGA), a polyacrylamide with a terminal amide functional group. The resultant polymer underwent a protein-like gel–sol transition in aqueous phase, transitioning from a hydrogel at ambient temperature to a flowing liquid at higher temperatures [67]. The first instance of UCST responsiveness in PNAGA was reported by Agarwal and colleagues. While the thermogelation of PNAGA at low temperatures had previously been described, a definite UCST had not been published until this communication [68] . Laschewsky and co-workers explained the two different phase transition temperatures for PNIPAM and 3-[N-(3-methacrylamidopropyl)-N,N-dimethyl] ammoniopropane sulfonate (SPP) driven by UCST of the SPP block and the LCST of the NIPAM-block [69] .Yusan et al. had prepared pH-induced micelles from zwitterionic poly[3-dimethyl (methacryloyloxyethyl) ammonium propane

sulfonate]-block-poly[2-(diisopropylamino)ethyl methacrylate] copolymer (*β*PDMA-*b*-PDPA) and observed that below 15 ^{o}C aggregation of micelles occurred because βPDMA coronal blocks lose their solubility below their UCST [70].

1.3.3 Salt Induced Micellization

Salt-induced micellization has drawn less attention to prepare micelles because the salt ions in buffers used *in vitro* experiments and in physiological conditions induce competitive interactions with the block copolymer and result in disintegration of micelles [71]. There are many studies reporting on the salt-induced micellization of poly(ethylene oxide)-poly(propylene oxide)-poly(ethylene oxide) (PEO-PPO-PEO) (Pluronic® or poloxamer) triblock copolymer and physicochemical properties such as critical micellization temperature (CMT), viscosity and rheology [72,73]. For example, Patel et al. examined micellization of PEO-PPO-PEO triblock copolymer (Pluronics® F88) in the presence of KCl, entraped orange OT dye into micellar core [74]. Through hydrogen bonding, the salts enhance the self-hydration of water, lowering the hydration of the Pluronics. This strongly lowers the CMC and CMT for Pluronics and increase in the standard entropy / enthalpy of micellization. With this regard, Pluronics morphologically prefer to be in a spherical shape with PEO corona and PPO core [75].

In another study, Bahadur and co-workers reported that self-assembly of ethylenediamine tetrakis-block-propoxylate-*block*-ethoxylate tetrol (Tetronic 1307) could be induced simply by NaCl addition [76]. The salt induced Tetronic 1307 micelles had more hydrophobic cores than temperature induced Tetronic 1307 micelles since salts had been reported to decrease the hydrophilicity of the central ethylenediamine group of copolymer by interfering the electric double layer of central group [76,77]. Üstoğlu et al. demonstrated salt-induced micellization of quaternized P2VP-*b*-PEO (QP2VP-*b*-PEO) in the presence of potassium ferricyanide ($K_3[Fe(CN)_6]$) [78]. The electrostatic association among quaternized

P2VP block and $Fe(CN)_6^{3-}$ multivalent ion induced formation of block copolymer micelles with PEO-corona and ($QP2VP^+[Fe(CN)6]^{3-}$) cores [79]. Jia et al. also used multivalent counterions to induce micellization of PEO-*b*-P2VP through electrostatic interaction between P2VP block (at strongly acidic pH where the P2VP block was protonated) and persulphate ions of potassium persulphate ($K_2S_2O_8$) as illustrated in the Scheme 3 [80].

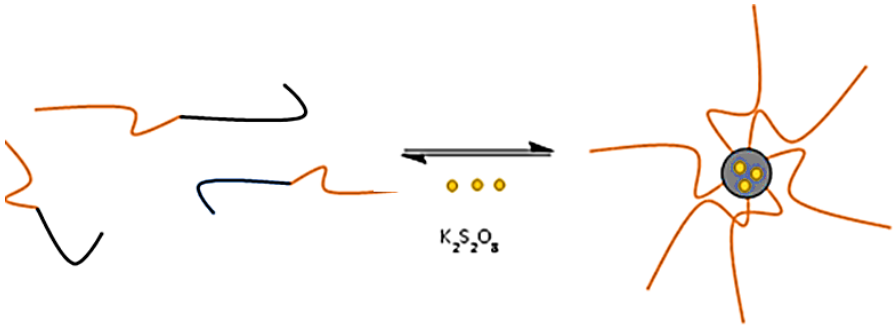

Scheme 3. Schematic illustration of salt induced micellization of P2VP-*b*-PEO. Modified from ref. [80], Jia et al, Chemcomm (2006).

1.4 Layer by Layer Self Assembly

Layer by Layer (LbL) self-assembly is a simple and straightforward thin film production process. LbL self-assembly is based on alternating adsorption of oppositely charged (or interacting) species (e.g. polymers, inorganic salts, nucleic acids, graphene oxide, nanoparticles, lipids, or any biological entities including cells) on a definite substrate [81]. It can produce nanostructured materials in a variety of compositions, and morphologies. This technique is of interest for a wide range of biological applications since LbL assembly allows effective coating of large surfaces with nanoscale precision [82]. On the other hand, the moderate, aqueous assembly conditions permit incorporation of tiny molecules and biological agents while avoiding destabilizing effects of solvents [83]. The applications of LbL films vary in a wide range including encapsulation and controlled release of drugs [84],

preparation of antifouling and antimicrobial materials, tissue engineering and regenerative medicine applications [85] and the production of biosensors, e.g. detection of glucose [86] and cholesterol [87].

Iller and co-workers was the first to discover the LbL approach in 1966. The work demonstrated alternating deposition of positively and negatively charged colloidal particles onto a substrate [88]. In 1997, for the first time, Decher et al. applied this process to construct polyelectrolyte multilayer films using oppositely charged polyelectrolytes, i.e. poly(allylamine hydrochloride) (PAH) and poly(sodium 4-styrenesulfonate) (PSS). The driving force for multilayer growth was electrostatic interactions among the oppositely charged polyelectrolytes. Scheme 4A shows the chemical structures of PAH and PSS, and schematic representation of LbL self-assembly process (Scheme 4B). The negatively charged substrate is first dipped into a polycation solution, followed by generally two rinsing steps to remove the loosely bound polycations from the surface. Then the substrate is dipped into a polyanion solution. This step is also followed by two rinsing steps to remove the loosely bound polyanions. This cycle is continued until desired number of layers are deposited at the surface. It is worth to note that rinsing steps are crucial in a LbL process to avoid contamination as well as to prevent polyelectrolyte complexation in solution and deposition of polyelectrolytes at the surface in the form of polyelectrolyte complexes [89].

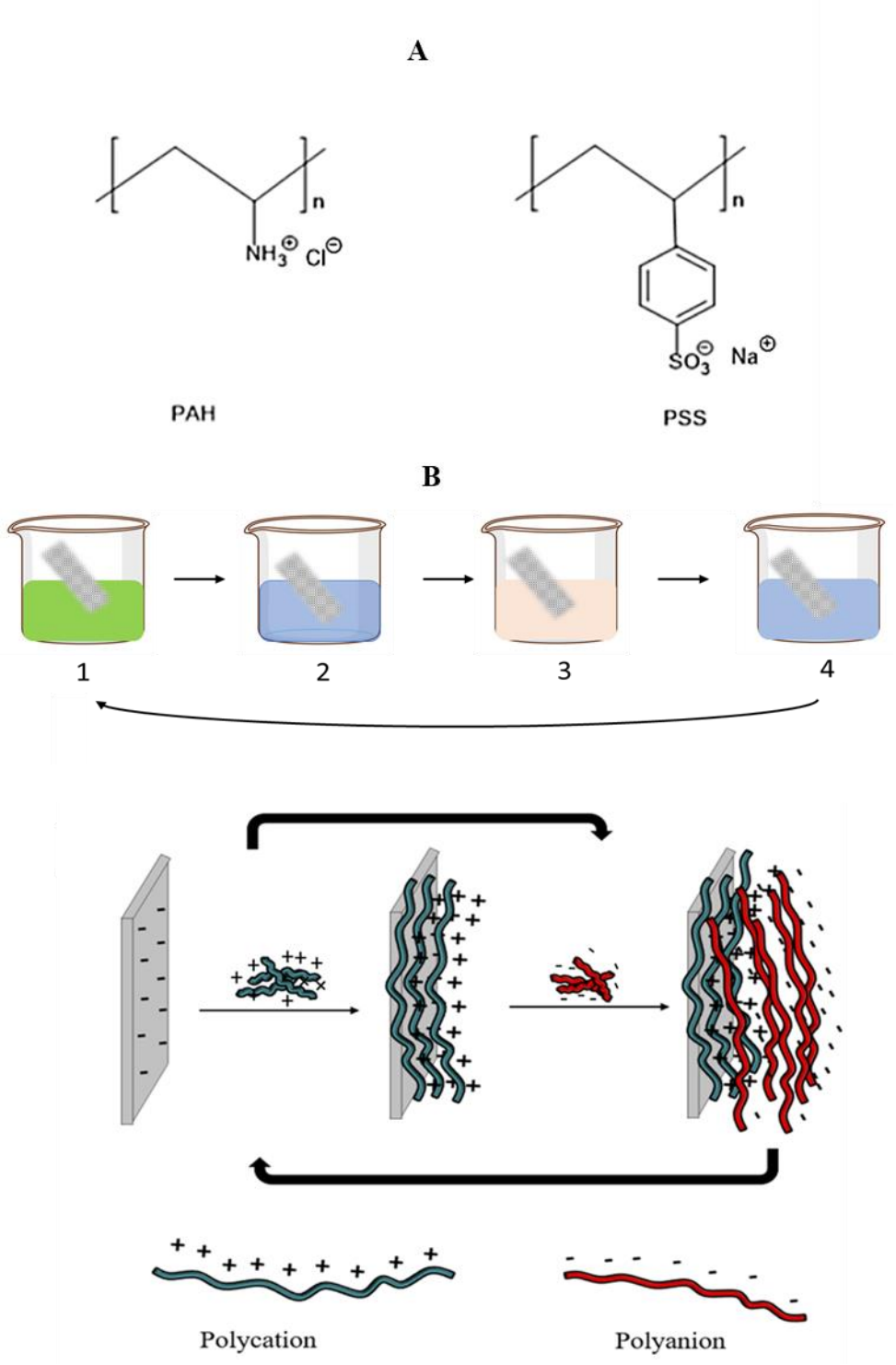

Scheme 4. (A) Chemical structures PSS and PAH (Reproduced from Decher, Science (1997) [89], **(B)** Schematic representation of LbL self-assembly process.

Besides electrostatically driven LbL self-assembly, polymer layers can also be deposited at the surface through hydrogen bonding interactions. Hydrogen bonded multilayers are specifically important for biomedical applications since the process allows the employment of neutral polymers and reduce the toxicity caused by the polycation components [90]. By utilizing polyaniline and neutral polymers such as PVP and poly(acrylamide) (PAAM), Stockon and Rubner succeeded growth of multilayers. The driving force for LbL growth was hydrogen bonding interactions between the amine- imine groups' N bearing on polyaniline and the carbonyl oxygens of PVP and PAAM [91]. For a hydrogen bonding driven multilayer assembly, the pH of the polymer solutions is very important. DeLongchamp et al. showed that multilayers of poly(methacrylic acid) (PMAA) and PEO could be grown through hydrogen bonding interactions between carboxylic acid group of PMAA and the ether oxygens of PEO (Figure 3) when the pH was below 3.5 [92]. Film deposition was totally prohibited above pH 3.5 due to ionization of carboxylic acid groups and disruption of hydrogen bonding interactions [93].

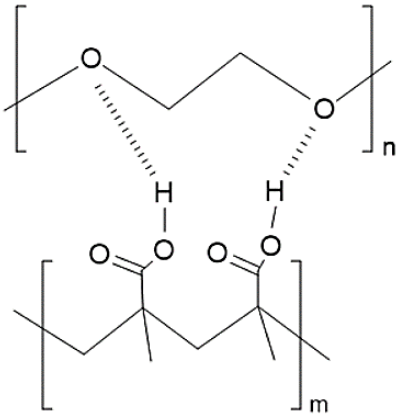

Figure 3. Hydrogen bonding interactions between PEO and PMAA.

1.5 Layer by Layer Assemblies onto Colloidal Substrates

Drug-delivery field needs designing systems that can distribute precise amounts of a therapeutic payload at a particular target location or tissue with a designed release profile upon a specific trigger [94]. Micro-engineered capsules with tailored properties are emerging because of their potential applications and promising solutions for drug delivery and diagnostics [95]. LbL technique is a promising method to fabricate nano-sized coatings on colloidal substrates. The colloidal substrates are classified as hard (SiO_2, $CaCO_3$, etc.) and flexible (liposomes, red blood cells, microgels, etc.) [96]. The deposition onto colloidal substrates requires a suspension of particles in solvent, generally water [97]. The assembly process is more complicated due to the necessity to follow a separation process after deposition steps through centrifugation and redispersing in rinsing buffers to remove unbounded components. As the components adsorb onto the colloidal substrates, centrifugation of the assembly media will yield a sedimentation at the bottom of the centrifugation tube. The coated particles are then used as substrates for the new layer deposition. LbL growth onto colloidal particles is generally followed by the change in zeta-potential of the particles [97-99]. The LbL process on 3D substrates are illustrated on Scheme 5A.

For drug delivery purposes, SiO_2 particles are drawing attention since it is possible to fabricate extremely monodisperse capsules. Colloidal silica substrates have been explored as drug carrier materials because of their meso-porous structure which have fixed pore sizes over a length range of nanometres to tens of nanometres, provide consistent nano spaces for drug accommodation [100]. Furthermore, due to their enormous pore volumes per unit mass of material, one may entrap significant amounts of therapeutics [101]. Use of SiO_2 template becomes problematic when one prepares hollow capsules. LbL hollow capsules are a unique type of core-shell particles in which the core of the particles consist of air or solvent, and draw a tremendous interest due to their possible applications [102]. The shell of LbL hollow

capsules is formed by the sequential adsorption of oppositely charged species around a charged spherical template. The compartment is formed after the sacrificial template is removed and has large storage volume in which chemical reactions can be carried out [103] and a variety of materials ranging from small molecules to macromolecules can be encapsulated [104]. Besides, the core protects unstable cargo from the hostile environment while at the same time increases biodistribution and solubility of hydrophobic drugs [105]. The hollow capsule preparation schematic is given on scheme 5B. In case of SiO_2 particles as templates, the requirement of hydrofluoric acid to dissolve SiO_2 core and obtain hallow capsules limits its application [97].

Calcium carbonate crystals are popular templates for LbL and exists as calcite, vaterite and aragonite polymorphs in the nature [106]. The most stable polymorph of $CaCO_3$ is calcite but draws a lower attention in biomedical applications since it has low drug loading capacity due to its non-porous structure. Vaterite polymorph has a suitable internal structure for hosting different drugs or molecules of interest [107]. Additionally, decomposition of the templates can be performed using unharmful chemicals under mild conditions [108]. While $CaCO_3$ decomposes slowly at physiological conditions, they show faster decomposition in the tumour environment (around pH 6.5), providing controlled release of anticancer agents [109,110].

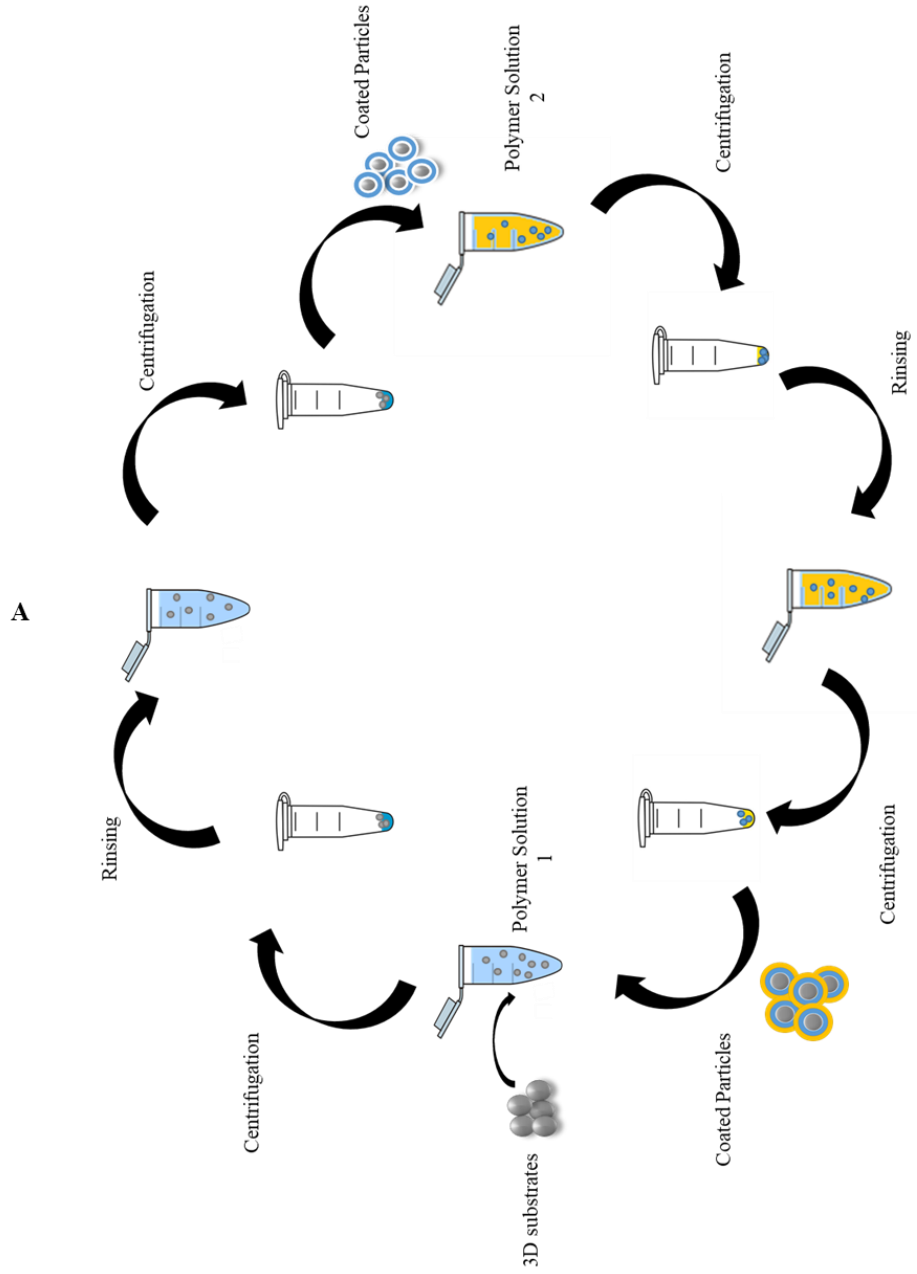
A
3D substrates
Polymer Solution 1
Centrifugation
Rinsing
Centrifugation
Coated Particles
Polymer Solution 2
Centrifugation
Rinsing
Centrifugation
Coated Particles

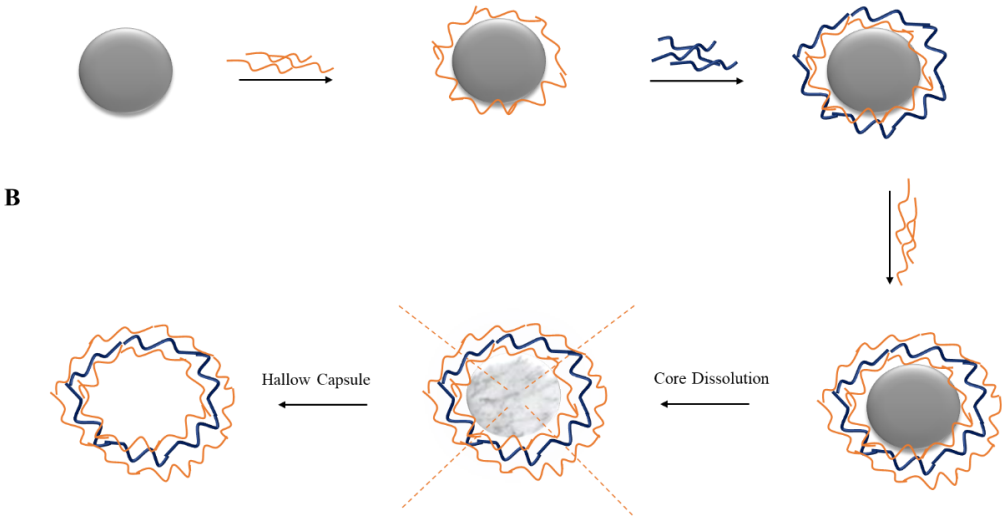

Scheme 5. (A) LbL deposition process on 3D particulate, **(B)** Hollow capsule preparation by dissolving sacrificial core.

Several studies on preparation of LbL capsules have been reported which used vaterite $CaCO_3$ substrates for the controlled release of bioactives and drugs. For example, microcapsules constructed by i) heparin sulphate (HS) and poly-arginine (pARG) [111], ii) dextran sulphate (DS) and pARG [112], iii) Protamine (PR) and DS [113], and iv) hyaluronic acid (HA) and poly-L-lysine (PLL) [114] have been reported. In another study, Yoshida et al. prepared LbL capsules of insulin including $CaCO_3$ microparticles by depositing PAH/PSS, PAH/poly(vinyl sulphate) (PVS) and PAH/ dextran sulphate (DS) pairs and evaluated the pH dependent insulin release through fluorescence spectroscopy after core dissolution [115]. A work of Kopach et al. demonstrated the specific channel blocker delivery to peripheral nerves. Nerve growth factor loaded (NGF) $CaCO_3$ templates were LbL-coated with poly-$_L$-arginine (PArg) and DS, followed by core dissolution to obtain hollow capsule. The results showed site specific actions of neurotrophins for stimulating synaptic circuit formation [116].

1.6 Layer by Layer Deposition of Micelles

In LbL based drug delivery, many studies used to be based on direct integration of pharmaceuticals into multilayers [117], encapsulation of drug molecules within a polyelectrolyte matrix [118], and use of polymer-bound prodrugs [119]. However, it has been difficult to directly insert tiny, uncharged, and hydrophobic therapeutics into multilayer thin films due to the absence of functional groups. Considering that around 40% of FDA (U.S. Food and Drug Administration) -approved drugs are hydrophobic therapeutics, development of new strategies for incorporation of hydrophobic drugs into multilayers has become important. Integration of hydrophobic pharmaceuticals into core region of amphiphilic block copolymer micelles and including these block copolymer micelles as building blocks into LbL films turned to be an efficient strategy [120]. On the other hand, integration of block copolymer micelles within multilayers had been showed to increase the drug loading efficacy rather than simply loading a drug directly within the polymer multilayers [121]. Moreover, the swelling capacity of multilayers and stabilities had reported to be enhanced [122]. There are several studies which the micelles have been incorporated 2D [123,124] and 3-D self-assembled multilayer films [125,126]. The deposited micelles may show different responsiveness upon a specific stimulus such as temperature [122,127,128] and pH [129-131]. Ma et al. constructed a 2D LbL multilayer films using poly(diallyldimethylammonium chloride) (PDDA) and micelles obtained from the self-assembly of poly(styrene-*b*-acrylic acid) (PS-*b*-PAA) in aqueous media. Pyrene was post-incorporated into PS-core before LbL deposition. Following the sequential adsorption of PS-*b*-PAA micelles and PDDA, the release of pyrene from multilayers was investigated in solutions of varying ionic strength [132]. Hammond and co-workers constructed the very first H-bonded micelle including multilayer films. PEO-*b*-poly(ε-caprolactone) (PEO-*b*-PCL) was self-assembed in aqueous media resulting in micelles with PEO-corona and PCL-core. PEO-*b*-PCL micelles were then self-assembled at the surface using PAA

through H-bonding interactions between PEO corona's ether oxygen and PAA's carboxylic acid groups. Post-loading an antibacterial agent, triclosan, into PCL micellar cores and release of triclosan from multilayers was investigated in the same study [120]. In another study, Biggs et al. prepared multilayers on SiO_2 particles composed of solely micelles. As the positively charged building block, PDMA-*b*-PDEA was self-assembled at pH 7, forming micellar aggregates with PDMA-core and cationic PDEA-corona. As the negatively charged building block, PDEA-*b*-PMAA was self-assembled at alkaline conditions, forming micellar aggregates with PDEA-core and cationic PMAA-corona. micelles The hydrophobic dye, Orange OT, which was pre-loaded into the micelles prior to multilayer capsule preparation, was followed after SiO_2 core was dissolved and hollow capsules were obtained [133]. In another study by Addison et al., same building blocks were loaded with a hydrophobic dye, Chrysoidine, and then coated onto $CaCO_3$ microparticles. Once $CaCO_3$ template was dissolved and hollow capsules were obtained, through TGA analysis the group had investigated if there is any residual $CaCO_3$ core and successful removal of core was reported [134].

1.7 Boron Neutron Capture Therapy (BNCT)

Radiotherapy is one of the most common cancer treatments [135]. Within the scope of cancer treatment, 50 % or more patients are needed to be involved in radiotherapy because it is very effective in localized tumours and legions [136]. With these in mind, the patients are generally suffering from acute and cytotoxic outcomes of radiotherapy as side effects because of DNA cleavage and subsequent cell death [137]. When the glioblastoma multiforme is the case, which is the most aggressive and fatal type of all cancer types, despite the intense treatment with all types of current therapies, patients have a lifespan of 5 years at most [138]. When the glioblastoma is high grade, chemotherapy is not sufficient to cure the patients since they are not successful to penetrate tumour cells [139].

Boron Neutron Capture Therapy (BNCT), gives opportunity to kill malignant cells by differentiating them from the normal cells [140]. BNCT is based on nuclear fission reaction. It relies on the irradiation of nonradioactive, naturally occurring ^{10}B with a low energy thermal neutron which yields a linear high energy transfer to α particle (^{4}He) and recoiling to ^{7}Li nuclei [141]. The radiochemical reaction of ^{10}B upon low energy thermal neutron capturing is given below and illustrated in Scheme 6.

$$^{10}B + n_{th}\ (0.025\ eV) \rightarrow [^{11}B] \rightarrow {}^{4}He + {}^{7}Li + 2.79\ MeV\ (6\%)$$

$$\rightarrow {}^{4}He + {}^{7}Li + 2.31\ MeV\ (94\%)$$

$$\downarrow$$

$$^{7}Li + \gamma + 0.48\ MeV$$

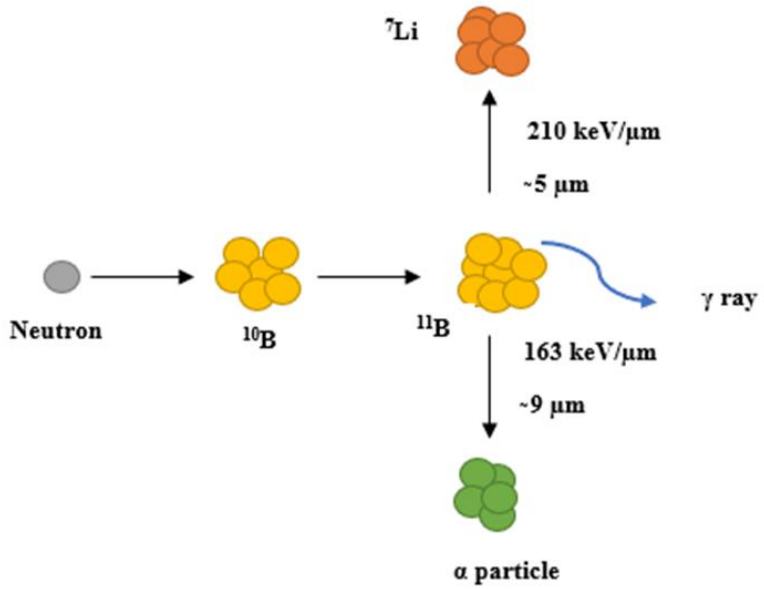

Scheme 6. Schematic Representation of Boron's Neutron Capturing. (Revised from ref. [142], Pitto-Barry et al., Polymer Chem.(2021)).

The Boron Neutron Capture Therapy was first mentioned theoretically by Locher in 1936. The first clinical trials were held by Farr and Sweet in 1951 at Brookhaven Graphite Research Reactor with the patients who were suffering from gliomas [143]. The high energy particles have a scope of 5 to 9 µm travel and the cytotoxic effect of the procedure is limited within the boron including cells or tissues [144]. BNCT is highly desired for acute glioma and cerebral tumour [140]. Recently, it has found interest in liver cancer and early stages of skin cancer (milenoma) [145].

1.8 Boron Including Compounds Suitable for BNCT and Boron Delivery Agents

The BNCT lies beyond a radiochemical reaction. The most important part of the treatment is to obtain a successful delivery of boron including compounds specifically to the cancer cells together with an effective concentration of boron in the delivered cells [146].

Boron delivery agents are expected to possess the following properties for BNCT:

- Boron delivery agents need to show low cytotoxicity upon the normal cell uptake,
- The boron concentration of approximately 20 μgB/g tumour should be achieved,
- Should sustain a fast clearance in the blood stream,
- Should accumulate cancer cells/ tumours effectively [147].

The very first trials were conducted with boric acid and boric acid derivatives (Scheme 7A). However, these simple chemicals were not selective towards cancer cells and their accumulation to tumour sites were low. Therefore, a successful treatment was not achieved [142]. As the technology and synthetic approaches have been improved, many boron bearing low molecular weight molecules have been synthesized. Scheme 7B and 7C show (L)-4-dihydroxy-borylphenylalanine (BPA) and a polyhedral boron anion, sodium mercaptoundecahydro-*closo*-dodecaborate (BSH) synthesized by Snyder et al. [148] and Soloway et al. [149], respectively.

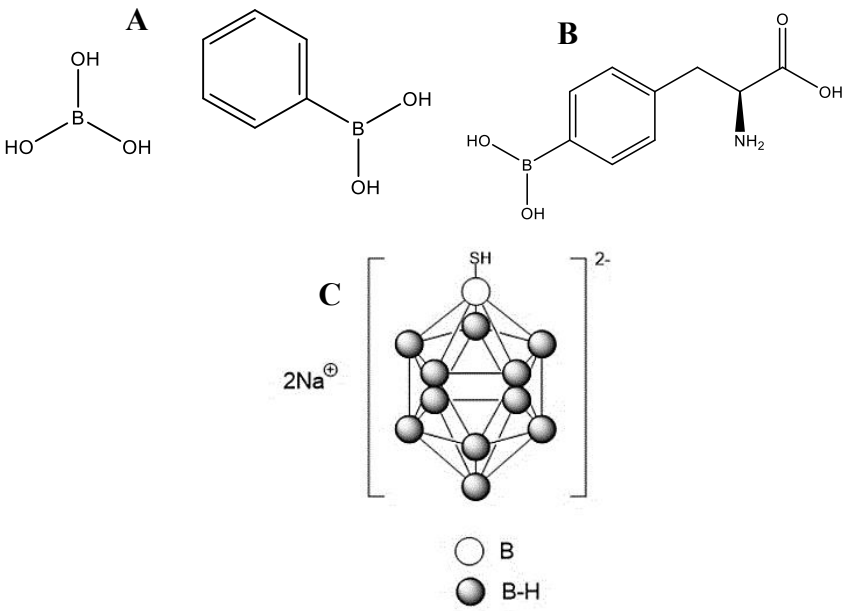

Scheme 7. Chemical Structures of **(A)** boric acid, phenylboronic acid, **(B)** BPA, and **(C)** BSH

Other approaches generally include a stable boron group, or a boron cluster linked to a tumour specified moiety for instance monoclonal antibodies. The epidermal growth factor receptors (EGFR) and their mutant isoform (EGFRvIII) are over expressed on high grade gliomas [150]. Functionalizing boron agents with these receptors provide higher accumulation of boron at the tumour site [151]. Boronated amino acids are also attached to the boron clusters and widely used in the clinical trials. Especially cysteine, tyrosine, glycine and aspartic acid were conjugated with boron clusters to improve tumour accumumulation [152]. Another approach is conjugating boron with porphyrin derivatives. Porphyrin modified molecules strongly complex with DNA and yield in a high ^{10}B accumulation at the tumour tissues [153].

1.8.2 Dendrimers

Dendrimers are subject of interest due to their low cytotoxicity, ease of synthetic functionalizing and their ability of encapsulating the boron species in their cores. Poly(amidoamine) dendrimers are extensively studied for BNCT applications. Wu et al. utilized the thiol–maleimide “click” reaction to boronate EGFR through different ways. An isocyanato polyhedral borane was used to functionalize starburst dendrimers constituted of repeating polyamidoamino (PAMAM) moieties on terminal amine groups present. EGF has maleimide groups and for conjugation with EGF, primarily functionalized dendrimer moieties were further functionalized with thiol groups [155]. In human glioblastomas, EGFR gene is frequently amplified and tumour cells express approximately 100 times more receptors than normal cells [142]. The approach reached an effective boron accumulation towards $F98_{EGFR}$ cells.

Barth and co-workers. attached the antibody IB16-6 to PAMAM dendrimers that were again functionalized with isocyanato decaborane cluster which isocyanato groups reacts with free amino groups on the dendrimer structure. This derivatized moieties enable attachment with IB16-6 antibody through maleimide groups present in their structure. Antibody was aimed to prevent random attachments and retaining the antibody's localizing characteristics in *in vivo* tests [156]. *In vivo* investigations on rats with B16 melanomas, however, revealed a tendency for the tumour to concentrate in the liver and spleen, as well as a lack of specificity for the tumour.

1.8.1 Nanomaterial Based Delivery of Boron

Nanomaterials gained enormous importance in drug delivery field due to their favourable nanometric sizes, optical and physicochemical properties and the possibility of conjugating and functionalizing them with tumour targeting moieties to achieve higher accumulation to cancer tissue. Moreover, they are important in delivering higher concentrations of boron to the tumour since nanoparticles are

capable of carrying higher concentrations of boron rather than a single molecule [154].

1.8.3 Liposomes

Liposomes have been widely used in diagnostic and therapeutic applications due to their unique characteristics, such as the ability to entrap hydrophilic actives and avoid premature release into bloodstream [142]. Liposomes have been modified to carry boron agents for potential applications in the field of BNCT. Hawthorne et al. demonstrated that the liposomes could carry sufficient amount of boron in order to show therapeutic efficacy with a high retention time [157]. Yanagie et al. published the first example of a ^{10}BSH-encapsulated liposome conjugated with a monoclonal antibody. The immunoliposomes were demonstrated to selectively reach tumor cells and supress the growth of tumour *in vivo* after thermal neutron irradiation [158]. Martini et al. conjugated the zwitterionic 1,2-dioleoyl-sn-glycero- 3-phosphoethanolamine to 1,2-dioleoyl-3-trimethylammonium-propane (DOTAP) and electrostatically entrapped BPA [159]. Hawthorne et al. created a bilayer membrane with $Na_3[1\text{-}(20\text{-}B_{10}H_9)\text{-}2\text{-}NH_3B_{10}H_8]$ and reported a boron concentration of 67.8 μg/g tumour tissue. BNCT mediated by these liposomes provided sustained, effective tumour suppression in the hamster cheek pouch oral cancer model over a 16-week follow-up period. [160].

1.8.4 Mesoporous Silica Nanoparticles

Mesoporous silica nanoparticles (MSNP) are also potential drug delivery agents with functionalizable surface, high biocompatibility, and controllable size. Lai et al. functionalized the surface of MSNP with galactosyl ligands while encapsulating *o*-carborane inside the MSNP [161]. Glyco-functionalized nanoparticles have been shown to be effective carbohydrate carriers with excellent affinity to tumour cells

due to binding specificities between targeted receptors and carbohydrate ligands on the surface of tumour tissues [162]. In another study, Feng et al. functionalized boron nitride nanoparticles with mesoporous silica and then conjugated this system with folate in order to increase cellular uptake of MSNP to HeLa cells [163].

1.8.5 Carbon Nanotubes

Carbon nanotubes were discovered in 1991 by Iijima et al [164]. C_2B_{10} cages were inserted to single walled carbon nanoparticles (SWCNT) by Zhu et al. The nanotubes were found to display high accumulation at EMT6 tumor cells of young female BALB/c mice [165].

1.8.6 Polymer Conjugates and Polymeric Nanoparticles

Polymer conjugates and polymeric NP are studied widely as drug delivery agents. Their sizes can be controlled and successful accumulation to tumour cells can be achieved [166]. Most of the studies in the literature are based on linking boron clusters or boron including compounds to the polymer chains. Srebnic and co-workers synthesized a triblock copolymer including an acrylamide attached block, N-acryloyl-2-(dihydroxyborolanyl) aniline attached block and cationic N-acryloyl-diaminoethane block into target colon polyps in rats. Findings claimed success in brain targeting led to the selection of aminophenylboronic acid [167] [168]. Besides this, a block copolymer, PEO-*b*-poly(glutamic acid) [PEO-*b*-P(Glu)] conjugated with BSH through disulphide bond [PEG-*b*-P(Glu-SS-BSH)] increased the cellular uptake of boron [143].

Huang and colleagues synthesized amphiphilic carborane-conjugated polycarbonates by ring-opening polymerization of a carborane cyclic carbonate monomer using a poly(ethylene oxide) macroinitiator. The carborane conjugated amphiphilic block copolymer underwent self-assembly in aqueous media and

micelles were formed with PEO corona and carborane containing core. Outcomes of the study showed that micelles encapsulated and delivered sufficient boron concentration to initiate BNCT and tumour bearing mouse models proved the efficacy of the system [169].

Tsukahara and colleagues coated the surface of inactivated Hemagglutinating Virus of Japan Envelope (HVJE)due to strong fusion ability as well as the capacity to activate anti-tumour immune response which makes HVJE a promising option for use in cancer therapy [170]. HVJ-E surface was functionalized with galactose and then HVJ-E was coated with a block copolymer containing zwitterionic 2-methacryloyloxyethyl phosphorylcholine and methacrylamide benzoxaborole blocks. High boron accumulation and the suppression of haemolysis was recorded on Hep G2 cells [171] .

In a recent study, Matejicek and colleagues obtained self-assembled PEO-*b*-poly(2-(N,N,N',N'-tetramethyl guanidium) ethyl acrylate) (PEO-*b*-PGEA) nanoparticles using *closo*-dodecaborate, $[B_{12}H_{12}]^{2-}$ through electrostatic association between guadinium units and *closo*-dodecaborate, $[B_{12}H_{12}]^{2-}$. They examined the effect of aggregate shape and morphology on the internalization of $[B_{12}H_{12}]^{2-}$ containing PEO-*b*-PGEA nanoparticles by U87 cells [172].

1.9 Aim of Thesis

Boron Neutron Capture Therapy (BNCT) is a non-invasive radiotherapy technique that enables scientists to kill malignant cells with a cell-specific effect while lowering side effects. BNCT relies on the nuclear fission reaction of non-radioactive ^{10}B isotope upon neutron capturing. This process produces highly energetic α particles (^{4}He) and a recoiling to ^{7}Li nuclei [138].

In recent years, the design of drug delivery systems that will enable the controlled and targeted release of therapeutic molecules for more effective treatment of diseases has been a rapidly developing research area. Some of the advantages of drug delivery systems are increasing the biocompatibility of drugs, making them act specific to the desired type of cells, improving their pharmacokinetic/pharmacodynamic properties, preventing their degradation by proteolytic enzymes, and making their concentrations in the body controllable for a long time. Polymers have become a preferred material class in the design of drug delivery systems because they can show very different properties depending on their chemical structures, can be produced at an industrial scale, and can be chemically modified after synthesis. Polymeric drug delivery vehicles are being studied extensively for BNCT purposes due to the ease of architecture tailoring and prospering accumulation to tumour cells [142].

This thesis study aimed at developing a polymer carrier encapsulating stable boron compounds for potential applications in the field of BNCT. B12 was chosen as a model ^{10}B including agent due to its high boron concentration. P2VP-*b*-PEO was chosen as a model neutral-cationic block copolymer for the preparation of delivery vehicles. It was hypothesized that:

i) self-assembly of P2VP-*b*-PEO could be induced in the presence of B12 molecules in aqueous solution through electrostatic association among B12 and P2VP blocks. In this way, a simple strategy would be developed to encapsulate B12 in polymer micelles.

ii) stability of the resulting micellar aggregates could be affected by the varying pH, salt concentration and the presence of biological molecules in the environment. In such a case, LbL self-assembly of these micellar aggregates at a surface would be an appropriate strategy to further enhance the stability of the carriers.

The study was planned to be completed in four different parts:

i) preparation of B12 containing block copolymer micellar aggregates,

ii) evaluation of the stability of the aggregates in PBS and biological medium,

iii) adsorption of the micellar aggregates onto colloidal particles in case of instability of the micellar aggregates in biological medium,

iv) examination of cytotoxicity and cellular association of the polymer particles.

As also mentioned in Section 1.8.6, there are limited number of studies reporting polymer based B12 encapsulating carriers. Recently, in 2020, triggering self-assembly of a diblock copolymer using B12 has been recently reported [172]. The group examined the morphologies of self-assembled aggregates and the effect of morphology on the internalization by U87 cells. However, no detailed analysis of micellar stability against varying environmental conditions tabulated. Also, the concentration of B12 loaded inside the micellar aggregates and the amount of boron delivered to cells were not reported. Different from this study, this thesis study aimed at examining the stability of B12 containing micelles at varying pH and ionic strength conditions as well as against dilution with biological medium. Moreover, the loading capacities of B12 inside the micellar aggregates and the concentration of boron delivered to cells had been reported. In the light of the findings, developing new strategies to enhance the stability of micellar aggregates was aimed.

CHAPTER 2

EXPERIMENTAL

2.1 Materials

Poly(2-vinylpyridine-*b*-ethylene oxide) (P2VP-*b*-PEO) (M_n(P2VP) = 13,500 g/mol; M_n(PEO) = 21,000 g/mol) and poly(N-vinyl caprolactam) (PVCL) (M_w =1,800 g/mol; M_n =1,300 g/mol) were purchased from Polymer Source Inc. Phosphate buffer saline (PBS) (tablet), calcium chloride ($CaCl_2$, anhydrous, granular), sodium carbonate (Na_2CO_3) (powder, ≥ 99.5%, ACS reagent), Curcumin (CUR) and poly(sodium 4-styrenesulfonate) (PSS) (70,000 g/mol) were purchased from Sigma-Aldrich Chemical Co. Sodium dihydrogen phosphate dihydrate ($NaH_2PO_4.2H_2O$), Tannic Acid (TA, M_w 1701), N,N- Dimetylformamide (DMF) (> 99%), iodomethane (MEI, > 99%), sulfuric acid (H_2SO_4, 98%), polyvinylpyrrolidone (PVP) (Mw:10,000 g/mol) sodium hydroxide (NaOH) (pellet), SpectroPor7 regenerated cellulose dialysis membrane (molecular weight cut off: 3.5 kDa) and Spectra/Por Float-A-Lyzer G2 Dialysis device were purchased from Merck Chemicals. Deionized (DI) H_2O was purified by passage through a Milli-Q system (Millipore) at 18.2 MΩ. Sodium dodecyl sulphate (SDS, used in the synthesis of CUR loaded $CaCO_3$) was purchased from BioShop® Canada Inc.. Ethanol (≥ 99.9%) was purchased from Isolab® Chemicals. Eagle's minimum essential medium (EMEM) was purchased from Thermo Fisher Scientific, Boston, MA, USA. Hep G2 cells were purchased from ATCC® HB-8065™. SDS BioChemica and Triton®X-100 was purchased from AppliChem (used in the viability and cellular association assays). Plasmocin was purchased from Invivogen, San Diego, CA, USA. Fetal Bovine Serum (FBS), Na-Pyruvate, L-glutamine, and non-essential amino acids were purchased from Biological Industries, Beit Haemek, Israel. 3-(4,5-

dimethylthiazol-2-yl)-2,5-diphenyltetrazolium bromide Vybrant MTT assay kit was purchased from Invitrogen, Carslbad, CA, USA. Phalloidin-iFluor 405 Reagent used for the staining actin filaments in the formaldehyde fixed cells were purchased from abcam®. Dulbecco's Phosphate Buffered Saline (D-PBS) was purchased from Biowest (Nuaillé, France). T25, T75 and other cell culture plates were purchased from Greiner Bio-One (Kremsmünster, Austria).

Table 1. Chemical structures of Polymers and molecules used in the experiments.

Molecule	**Chemical Structure**
P2VP-*b*-PEO	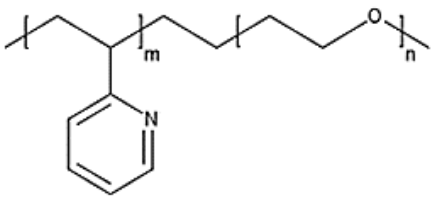
QP2VP-*b*-PEO	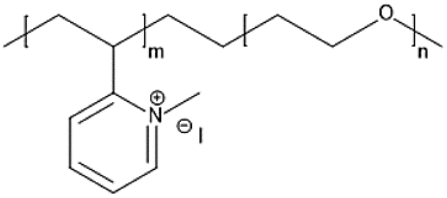

PVCL	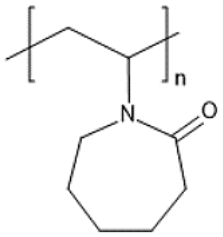
PSS	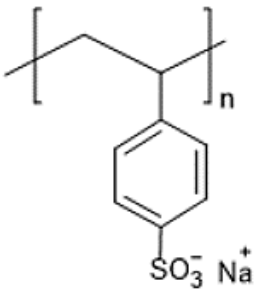
PVP	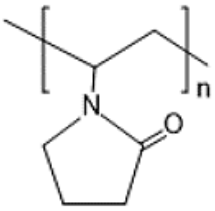
CUR	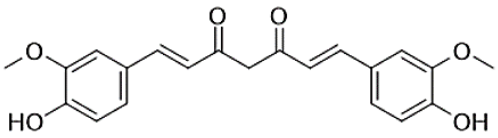

TA	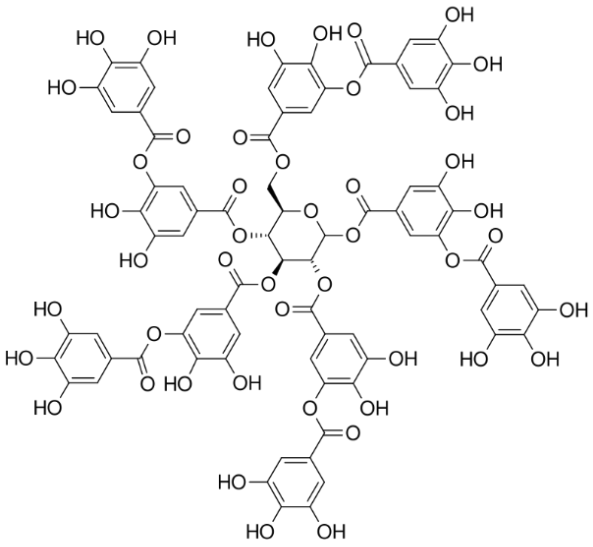
SDS	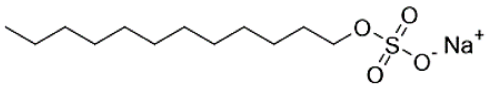
3-(4,5-dimethylthiazol-2-yl)-2,5 diphenyltetrazolium bromide	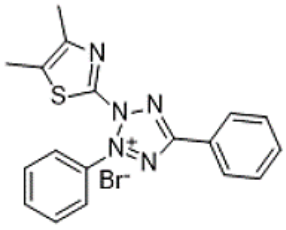

2.2 Methods

2.2.1 Quaternization of P2VP-*b*-PEO

P2VP-*b*-PEO (34 mg) was dissolved in DMF (9.6 mL) for 4 hours. Iodomethane (MeI) (12 μL) was added to P2VP-*b*-PEO solution, and the mixture was agitated at 400 rpm at room temperature for 3 days in the dark. A rotary evaporator was used to extract DMF and unreacted MeI. In DI water, quaternized P2VP-*b*-PEO (QP2VP-*b*-PEO) was dissolved, dialysed against DI water for 3 days and lyophilized. ^{1}H NMR P2VP-*b*-PEO and QP2VP-*b*-PEO were characterized by ^{1}H NMR and ATR-FTIR.

2.2.2 Synthesis of $[(CH_3CH_2)_3NH]_2[B_{12}H_{12}]$

$[(CH_3CH_2)_3NH]_2[B_{12}H_{12}]$ was synthesized by a modified procedure published earlier [173]. I_2 (0.25 mol, 62.66 g) was completely dissolved in diglyme (70.0 mL). Then, added dropwise via a dropping funnel for six hours onto a suspension of $NaBH_4$ (0.79 mol, 30.00 g) in diglyme (200 mL) at 105 ^{o}C under a well-sealed argon atmosphere. By the addition of I_2, the reaction medium colour had changed into a yellowish colour and the amount of $NaBH_4$ retained insoluble was decreased. The temperature kept at 105 ^{o}C and reaction medium was refluxed for 24 hours to form a white precipitate. Afterwards, the reaction medium temperature was increased to 185 ^{o}C and it was stirred for an additional 24 hours. Following, the reaction medium was cooled to room temperature, diglyme was removed by distillation and a white solid was observed. The remaining white solid was dissolved by the addition of distilled water (180 mL) and prior to complete dissolution, 84.0 mL of 37% HCl solution was added dropwise to the medium with the extreme care of **hydrogen gas evolution**. To precipitate boric acid crystals in the medium, it was kept at +4 ^{o}C overnight. The precipitated crystals were vacuum filtered, and the filtrate was added 150 mL of $(CH_3CH_2)_3N$ under moderate agitation overnight for finalizing the

precipitation of a mixture of boric acid and $[(CH_3CH_2)_3NH]_2[B_{12}H_{12}]$. Purification of $[(CH_3CH_2)_3NH]_2[B_{12}H_{12}]$ from boric acid was performed by resuspending the white crystals in hot distilled water and the reaction medium was mixed for another 6 hours. After that, precipitated white solid was characterized as $[(CH_3CH_2)_3NH]_2[B_{12}H_{12}]$. ^{11}B NMR and ATR-FTIR spectra of B12 that is used in this study were previously reported [174].

2.2.3 Synthesis of vaterite $CaCO_3$ microparticles

Bare $CaCO_3$ microparticles and CUR loaded $CaCO_3$ microparticles were synthesized by Esma Uğur in our research laboratory. CUR loaded $CaCO_3$ microparticles were synthesized by using the procedure described by Mc Donald et al. [80]. 50 mg SDS, 25 mg CUR, and 50 mg PVP were dissolved in 5.0 mL ethanol and magnetically stirred at 1000 rpm for 1 hour. 10 mg of PSS was added into 5.0 mL of 0.5 M Na_2CO_3 solution and mixed for 20 minutes at 1000 rpm in a round bottom flask. Then, 5.0 mL of 0.5 M $CaCl_2$ solution and previously prepared SDS/CUR/PVP solution was simultaneously added to the PSS-Na_2CO_3 mixture and continued stirring at 1000 rpm for 2 minutes in dark at room temperature. CUR loaded $CaCO_3$ microparticles were separated through suction filtration and dried in the oven at 65^{o}C for 2 hours. CUR-loaded $CaCO_3$ microparticles were characterized using FTIR-ATR and XRD. In ATR-FTIR spectrum, the peaks of $CaCO_3$ vaterite microparticles around 744, 875 and 1084 cm^{-1} were attributed to the four vibrational modes of CO_3^{2-} [175]. The bands cantered 1185, 1128, 1040 and 830 cm^{-1} belongs to PSS's specific absorption of $R\text{-}SO_3^-$ group [176]. The XRD pattern with the peaks at 2 Θ = 21.004 ^{o}, 24.900 ^{o}, 27.047, 32.778 ^{o}, 42.759 ^{o}, 43.848^o, 50.077 ^{o}, 55.805 ^{o}, 62.868 ^{o}, 71.967 ^{o} and 73.593 ^{o} are characteristic peaks for vaterite polymorph tabulated in PDF#33-0268. In XRD analysis, the appearance of CUR's characteristic peaks had disappeared (The 2Θ values have been reported before to be in the range of 5^o -30^o). This supports the fact that the crystalline curcumin has become into an amorphous structure during

dispersion in ethanol with PVP. Where this phenomenon was reported before in the concept of integrating hydrophobic drugs into the carrier materials [177-179]. Calcite peaks were also observed however, a pure single crystal grow is not expected as have been reported in the literature [180]. For SEM imaging, samples were prepared by diluting 40 μL of microparticle solution with 1000 μL of DI water at pH 6.5 and dropping 50 μL of prepared solution onto 1x1 cm Si wafer (Si wafers were acid and base treated, which the procedure will be described in section 2.2.5). Following, the Si wafers were dried in the vacuumed desiccator.

2.2.4 Preparation of (B12+ QP2VP)-*b*-PEO micelles

6.6 x 10^{-2} M B12 was prepared in DI water at pH 7.5. 0.5 mg/mL QP2VP-*b*-PEO solution was prepared at pH 7.5 and 25^{o}C overnight using 10.0 mM phosphate buffer. Dropwise addition of B12 solution to QP2VP-*b*-PEO solution was used to promote micellization. After addition of 300 μL B12, (B12 concentration in the mixture = 4.6 x 10^{-3} M) the mixture was stirred at 100 rpm for 45 minutes. For the micellization of 0.1 mg/mL and 1.0 mg/mL QP2VP-*b*-PEO, final B12 concentrations in the micellar solution were 6.5 x 10^{-4} M and 1.1 x 10^{-2} M, respectively. The resulting micelles are denoted as "(B12+QP2VP)-*b*-PEO micelles". Micelles were characterized by hydrodynamic size measurements using dynamic light scattering technique (DLS), zeta potential measurements and TEM.

Dialysis of micelles was carried out against 10.0 mM phosphate buffer at pH 7.5 and 25 ^{o}C for 1 day using a Spectra/Por Float-A-Lyzer G2 Dialysis device to remove excess B12. 50 μL of dialysed (B12+QP2VP)-*b*-PEO micellar aggregates at pH 7.5 was placed on the surface of a copper grid coated with a carbon substrate. Samples were air-dried upon deposition of (B12+QP2VP)-*b*-PEO micelles at the surface.

2.2.5 Preparation of LbL films on silicon wafers

(B12+QP2VP)-*b*-PEO micellar solution was prepared by adding 800 μL of 6.6 x 10^{2-} M B12 solution into 400 mL of 1 mg/mL QP2VP-*b*-PEO solution according to the procedure described in Section 2.6. 1.0 mg/mL TA and PVCL solutions were prepared by dissolving the polymers in 10.0 mM phosphate buffer at pH 6.5. To follow LbL growth, multilayers were first deposited onto silicon wafers.

Before LbL construction, the wafers were immersed into 12 M H_2SO_4 for 85 minutes, rinsed with DI water for 2 minutes and dried under N_2 gas. Silicon wafers were then treated with 0.25 M NaOH for 10 minutes, rinsed with DI water and dried under N_2 gas. Afterwards, silicon wafers were dipped into 1.0 mg/mL TA solution at pH 6.5 and 25°C solution for 15 minutes. Then the wafers were rinsed twice with pH 6.5, 10.0 mM phosphate buffer each for 2 minutes. Following, substrates were immersed into (B12+ QP2VP)-*b*-PEO micellar solution at pH 7.5 and 25°C for 15 minutes and were rinsed twice with pH 7.5, 10.0 mM phosphate buffer each for 2 minutes. This process was repeated until deposition of either 2- or 4-layers of TA and (B12+ QP2VP)-*b*-PEO micelles. For construction of barrier layers, 1 bilayer PVCL (1.0 mg/mL, prepared using 10.0 mM phosphate at pH 6.5) and TA was deposited at pH 6.5. Each layer deposition was followed by 2 rinsing steps using 10.0 mM phosphate buffer at pH 6.5. Thickness measurements during LbL growth were conducted using a Optosense spectrometric ellipsometer (OPT-S6000, USA).

2.2.6 Preparation of LbL capsules

$CaCO_3$ microparticles were dispersed in 10.0 mM pH 6.5 phosphate buffer with a final concentration of 10 mg/mL and vortex mixed for roughly 2 hours at 25 ^oC and 2500 rpm prior to capsule fabrication. The LbL deposition was performed in a 2 mL Eppendorf tube. $CaCO_3$ microparticles were dispersed into 1.0 mL TA solution (1.0 mg/mL) and shaked for 120 minutes at 2500 rpm using a VWR Vortex 100. Particles

were settled down at 2500 rpm for 1 minute using a Hettich Universal 320 centrifuge and the supernatant was discarded. Particles were then rinsed 3 times with 10.0 mM pH 6.5 phosphate buffer at 25 ^{o}C by shaking the particles at 2500 rpm for 2 minutes using a vortex. The particles were settled down again at 2500 rpm through centrifugation for 1 minute. The deposition of micelles (prepared from 1.0 mg/mL QP2VP-*b*-PEO) was carried out using the same procedure except the pH of both micellar and rinsing solutions was 7.5. This cycle was repeated until 2- or 4- layers of TA/(B12+ QP2VP)-*b*-PEO micelles were deposited onto $CaCO_3$ microparticles. For construction of barrier layers, same procedure was applied using 1.0 mg/mL PVCL and 1.0 mg/mL TA. LbL growth was followed through zeta potential measurements after every layer deposition. For zeta-potential measurements, 40 µL of particle solution was diluted with 1.0 mL of 10.0 mM phosphate buffer at pH 6.5 or pH 7.5 (for the micellar layers).

For preparation of hollow capsules, LbL-coated $CaCO_3$ microparticles were dispersed into 0.25 M ethylenediaminetetraacetic acid (EDTA) solution at pH 5 and shaked at 2500 rpm for 10 minutes using a vortex. Particles were suspended by centrifugation at 2500 rpm for 1 minute. EDTA cycle were repeated for 3 times. The particles were then rinsed with DI water at pH 6.5 through vortex mixing at 2500 rpm for 2 minutes and centrifugation at 2500 rpm for 1 minute. This rinsing cycle was repeated for 3 times.

For SEM imaging, the sample preparation procedure described in section 2.2.3 was used again. Samples were prepared by diluting 40 µL of capsule solution with 1000 µL of DI water at pH 6.5 and dropping 50 µL of this solution onto acid and base treated (described in 2.2.5) 1x1 cm Si wafer. Following, the Si wafers were dried in the vacuumed desiccator.

2.2.7 Determination of Boron Concentration of (B12+QP2VP)-*b*-PEO Micelles by Inductively Coupled Plasma Optical Emission Spectroscopy (ICP-OES)

Perkin Elmer Optima 4300 DV ICP-OES device was used to determine the boron concentration in (B12+ QP2VP)-*b*-PEO micelles. (B12+QP2VP)-*b*-PEO micelles were prepared from 0.1 mg/mL, 0.5 mg/mL and 1.0 mg/mL QP2VP-*b*-PEO at 6.5 x 10^{-4} M, 4.6 x 10^{-3} M, and 1.1 x 10^{-2} M B12, respectively. Samples were dialysed prior to analysis. 1.0 mL of the samples for boron concentration determination were digested by 1.0 mL of 1% HNO_3 (v/v) at 65 ^{o}C for 1 hour.

2.2.8 Cell Culture

Hep G2 cells (ATCC® HB-8065™) were grown in EMEM with 1% penicillin-streptomycin, 10% FBS, 1.0 mM Na-pyruvate, 2.0 mM L-glutamine, and non-essential amino acids at 37°C in a humidified incubator with 95% air and 5% CO_2. In a T25 flask, the cells were grown to proper confluency following the treatments. To prevent mycoplasma contamination, cells were treated with plasmocin (2.5 μg/mL).

2.2.9 Cell Viability Assays

The Viability of Hep G2 cells was determined by using MTT assay after a concentration dependent (0, 50, 75, 100 ppm) 24 h time point treatment of B12, QP2VP-*b*-PEO, [(TA/(B12+QP2VP)-*b*-PEO)]+(TA/PVCL) capsules, hollow [(TA/(B12+QP2VP)-*b*-PEO)] + (TA/PVCL)] capsules, [(TA/(B12+QP2VP)-*b*-PEO)]$_2$+(TA/PVCL) capsules and hollow [(TA/(B12+QP2VP)-*b*-PEO)]$_2$+(TA/PVCL) capsules. Prior to the 80% confluency, the Hep G2 cells were counted by Thoma cell counting chamber and collected via centrifugation. Hep G2 cells were seeded by 8.000 cells/well in each well of 96-well plate as 25x25 wells.

After 24 hours treatment, the medium was removed, 100 μL of 1.2 mM MTT reagent was added in PBS and incubated for 4 hours. Upon formation of formazan crystals, 1% SDS (dissolved in 0.01 M HCl) was added to dissolve crystals. Absorbance values were measured by plate reader at 570 nm.

2.2.10 Cellular Association of LbL Capsules

Hep G2 cells were grown up to a confluency of 80% in a T75 flask with the same cell culture supplements and conditions described in the cell culture section and counted by Thoma cell counting chamber. After that, the cells were collected via centrifugation and seeded by 500.000 cells/well 5 well of 6-well plate. After 24 h treatment, cells were stained with Phalloidin-iFluor 405 reagent. The medium on the cells was removed and cells were washed with PBS. Following, PBS was removed, and the cells were fixed with 4 % paraformaldehyde for 15 mins at 25 ^{o}C. Then, the cells were washed with PBS and treated with 0.5 μL/well of TritonX buffer to enhance the membrane permeability for 5 mins in dark. After that, the cells were treated with 0.5 μL/well of ICC blocking solution to supress the auto-fluorescence caused by cellular entities. Afterwards, phalloidin-iFluor 405 reagent was added with 1x concentration to stain actin filaments of cytoskeleton and the cells were incubated for 1 hour at 37 ^{o}C. The associations of capsules were evaluated upon merging the green (482 nm) and red-light (586 nm) wavelengths on by Floid® Cell Imaging Station. Capsules were provided green fluorescence because of encapsulated CUR within the capsule core while Phalloidin-iFlour 405 stained cells were red-coloured.

2.2.11 Determination of Boron Concentration of Capsules and Capsule-Associated Cells by ICP-OES.

Perkin Elmer Optima 4300 DV ICP-OES device was used to determine the boron concentration of capsules and capsule-associated cells. All capsules were prepared by the procedure described in section 2.2.6, 1.0 mL of capsule solution is digested with 1.0 mL of 1% (v/v) HNO_3 at 65 ^oC for 1 hour. For the determination of boron concentration associated with Hep G2 cells, the cells were washed several times with PBS. It was assumed that the cytotoxicity of capsules was ~ 0 % and all capsules associated with cells in 1.0 mL volume. Therefore, it was assumed that the number of cells before and after cellular association experiments (described in 2.2.10) were similar and were about 500.000 cells/well. The cells were scrapped with a scrapper until there were no cells attached to well-plate. 1.0 mL of scrapped cells were collected and digested in 1.0 mL of 1% (v/v) HNO_3 at 65 ^oC for 1 hour.

2.3 Instrumentation

2.3.1 ^{1}H Nuclear Magnetic Resonance Spectroscopy

^{1}H NMR spectra of P2VP-*b*-PEO and QP2VP-*b*-PEO were taken using a Brucker Spectrospin Avance DPX-400 Ultra shield instrument, operating at 400 MHz (Solvent: $CDCl_3$).

2.3.2 Fourier Transform Infrared Spectroscopy

ATR-FTIR spectra of P2VP-*b*-PEO, QP2VP-*b*-PEO, B12 and Cur loaded $CaCO_3$ were recorded using a Nicolet iS10 ATR-FTIR.

2.3.3 pH Meter

Ohaus Starter 3000 pH meter was used for pH adjustments prior to the experiments.

2.3.4 X-ray Diffractometry

Rigaku X-ray Diffractometer with a miniflex goniometer operated at 30 kV and 15 mA Cu-Kα line (α =1.54 Å) as the X-ray source was used for XRD measurements.

2.3.5 Scanning Electron Microscopy (SEM)

JSM-6400 Scanning Electron Microscope (SEM) (JEOL, equipped with NORAN system 6 X-ray Micro-analysis system and semaphore digitizer, Westhorst, NL) was used for tracking SEM micrographs.

2.3.6 Dynamic Light Scattering and Zeta Potential Measurements

Zetasizer Nano-ZS equipment (Malvern Instruments Ltd., U.K.) was used for hydrodynamic size and zeta potential measurements which the results were obtained by cumulants analysis of the autocorrelation data. Zeta potential values were obtained from electrophoretic mobility values using the Smoluchowski approximation.

2.3.7 Transmission Electron Microscopy (TEM)

TEM micrographs of micellar aggregates was obtained by using a FEI Tecnai G2 Spirit Bio-Twin CTEM operating at an acceleration voltage of 20–120 kV.

2.3.8 Spectroscopic Ellipsometer

Thickness measurements during LbL growth were conducted using a Optosense spectrometric ellipsometer (OPT-S6000, USA).

2.3.9 Inductively Coupled Plasma-Optical Emission Spectroscopy (ICP-OES)

Perkin Elmer Optima 4300 DV ICP-OES device was used to determine the boron concentration in (B12+ QP2VP)-*b*-PEO micelles, LbL capsules and cells.

2.3.9 Plate Reading Spectrophotometer

Absorbance values for MTT assays were measured by Thermo Fisher Scientific, Waltham, MA, USA Plate Reader which operates at 570 nm.

2.3.10 Cell Imaging

Cell imaging was done by Floid® Cell Imaging Station which operates at 482 nm for green light and 586 nm for red light.

2.4 Statistical Analysis

DLS measurements were performed as ten different measurements in succession. Zeta potential measurements were done as three different measurements in succession. The thickness of 2D ultra-thin LbL films were conducted as three different measurements which are detected from different points on Si substrates. For ICP-OES measurements 3 different samples were prepared and measurements were done as three different measurements in succession. For biological applications, minimum three technical replicates were used in each independent

biological replicate. Graphing and statistical analysis were conducted out using OriginLab® software, MA, USA. The t-test or ANOVA were used to detect the statistical difference between the samples. Following ANOVA, Holm-Sidak's test was used as a multiple comparisons test. A p value of less than 0.05 was judged significant be of importance.

CHAPTER 3

RESULTS AND DISCUSSION

3.1 B12 induced micellization of P2VP-*b*-PEO

3.1.1 Micellization at acidic conditions

Micellization was first performed at pH 3. P2VP-*b*-PEO was dissolved in 10.0 mM phosphate buffer at a concentration of 0.5 mg/mL. The temperature was kept constant at 25 °C. P2VP has a pK_a ~4.6 [181], thus pyridine units of P2VP blocks of P2VP-*b*-PEO are protonated at pH 3. Solubility of B12 decreases as the pH is decreased. To obtain greater solubility, B12 was dissolved in DI water at pH 7.5 and the pH was adjusted to pH 3 prior to micellization. The highest concentration of B12 solution at pH 7.5 was prepared as 6.6 x 10^{-2} M. 6.6 x 10^{-2} M B12 solution was gradually added to 0.5 mg/mL P2VP-*b*-PEO solution at pH 3. The self-assembly was induced through electrostatic association among positively charged P2VP and negatively charged B12. The formation of micellar aggregates was followed using dynamic light scattering technique. The hydrodynamic size of P2VP-*b*-PEO increased as the micellar aggregates formed. Figure 4 shows the evolution of hydrodynamic size as a function of final B12 concentration in the mixture. The size did not increase significantly above 6.0 x 10^{-3} M B12. Formation of micellar aggregates [(B12+P2VP)-*b*-PEO micelles] was optimized at 4.6 x 10^{-3} M B12 where the standard deviation in size measurements was minimum (as shown by the arrow in the Figure 4). Scheme 8 shows schematic representation of micellization at pH 3.

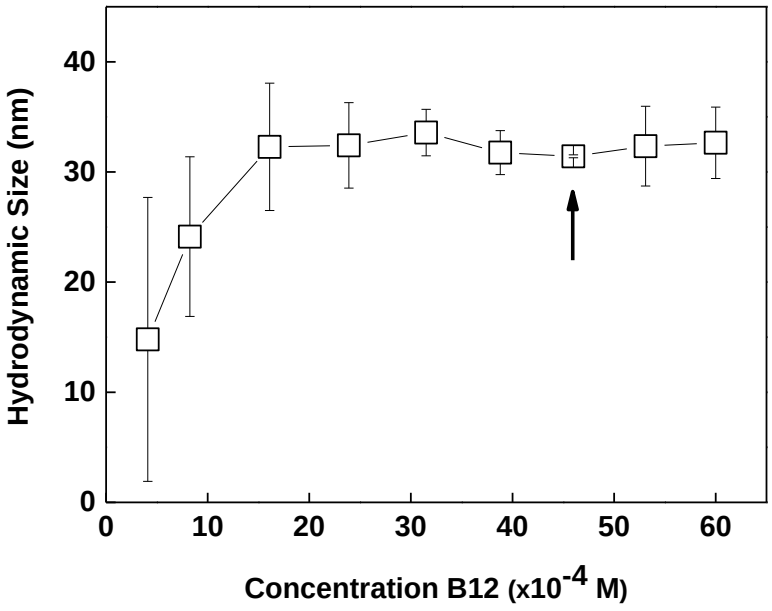

Figure 4. Evolution of hydrodynamic size of P2VP-*b*-PEO with respect to B12 concentration.

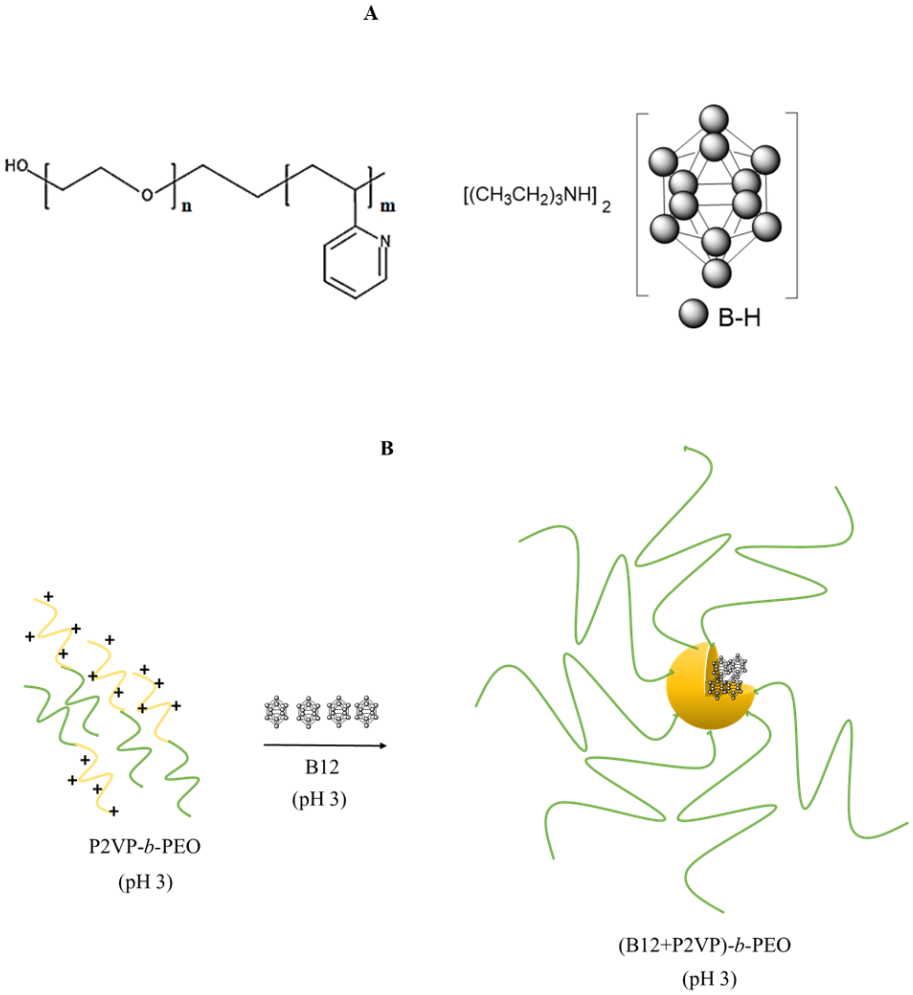

Scheme 8. (A) Chemical structure of P2VP-*b*-PEO and B 12. **(B)** Schematic illustration of B12 induced micellization of P2VP-*b*-PEO at pH 3.

For the potential applications in the field of BNCT, preparation of boron carriers which are stable at physiologically related pH conditions is desired. Therefore, stability of (B12+P2VP)-*b*-PEO micelles against increasing pH was assessed by comparing the hydrodynamic size of (B12+P2VP)-*b*-PEO micelles at pH 3 and pH 7.5. Micelles disintegrated when pH was elevated to neutral conditions. As seen in Figure 5, size distribution curve of P2VP-*b*-PEO shifted to lower values, indicating dissolution of (B12+P2VP)-micellar cores. Disintegration of micelles can be explained by deprotonation of pyridine units of P2VP and disruption of electrostatic

association between P2VP and B12. To enhance stability of (B12+P2VP)-*b*-PEO micelles at neutral pH conditions, it was aimed to prepare micelles whose stability was not affected by varying pH conditions.

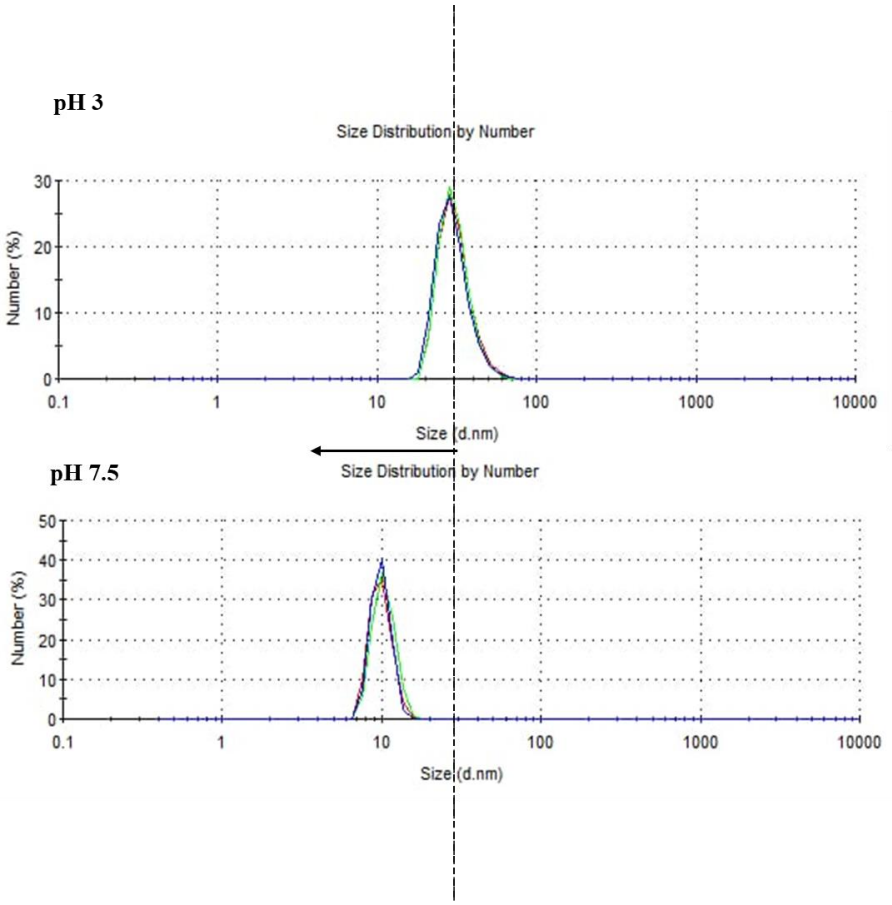

Figure 5. Size distribution curves of (B12+P2VP)-*b*-PEO micelles at pH 3 and pH 7.5. Dotted line is drawn to compare the peak positions of the two size distribution curves.

3.1 2 Micellization studies at neutral pH conditions

It was hypothesized that by introducing permanent charge on P2VP blocks of P2VP-*b*-PEO, electrostatic association between B12 and P2VP would not be affected by the varying pH conditions. In this way, stable micelles would be obtained at neutral pH. In this context, first, permanent charge on P2VP block was obtained.

3.1.2.1 Quaternization of P2VP-*b*-PEO

P2VP blocks of P2VP-*b*-PEO were quaternized using CH_3I. The quaternized polymer will be denoted as QP2VP-*b*-PEO in the rest part of the thesis. Figure 6 shows the ^1H NMR spectra of P2VP-*b*-PEO before and after quaternization. Quaternization of P2VP-*b*-PEO was confirmed through the methyl protons on pyridinium units around 4.2 ppm. Ethylene protons of PEO blocks were detected around 3.6 ppm with a strong singlet peak. The low intensity broad peak at 8.3 ppm represented the aromatic protons of pyridinium units which were adjacent to the nitrogen atoms. Other aromatic protons were detected between 6.3-7.3 ppm. Aliphatic protons of P2VP (CH_2 and CH) block overlapped in the range of 1.8-2.2 ppm.

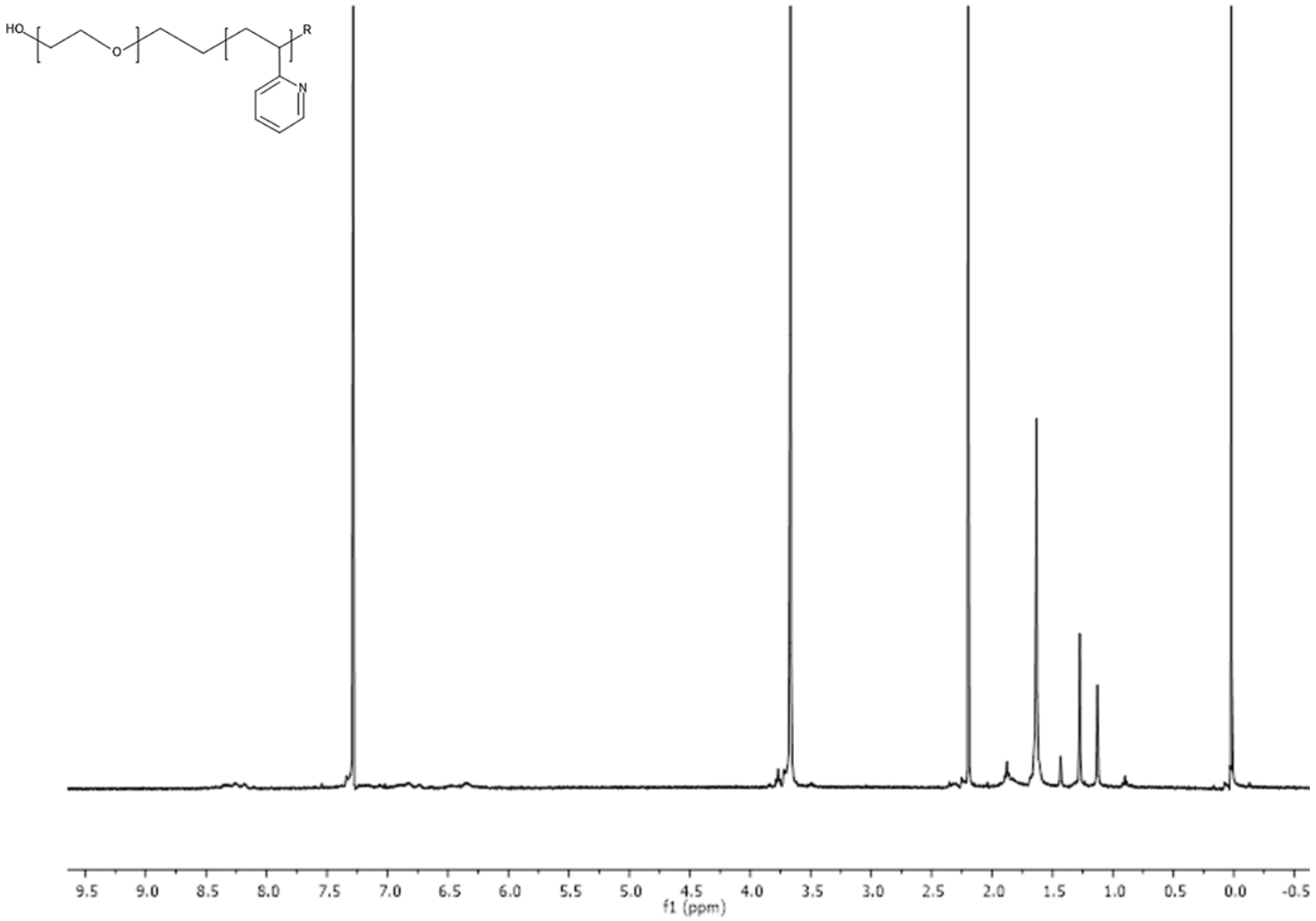
HO
O
R
N
9.5
9.0
8.5
8.0
7.5
7.0
6.5
6.0
5.5
5.0
4.5
4.0
3.5
3.0
2.5
2.0
1.5
1.0
0.5
0.0
-0.5
f1 (ppm)

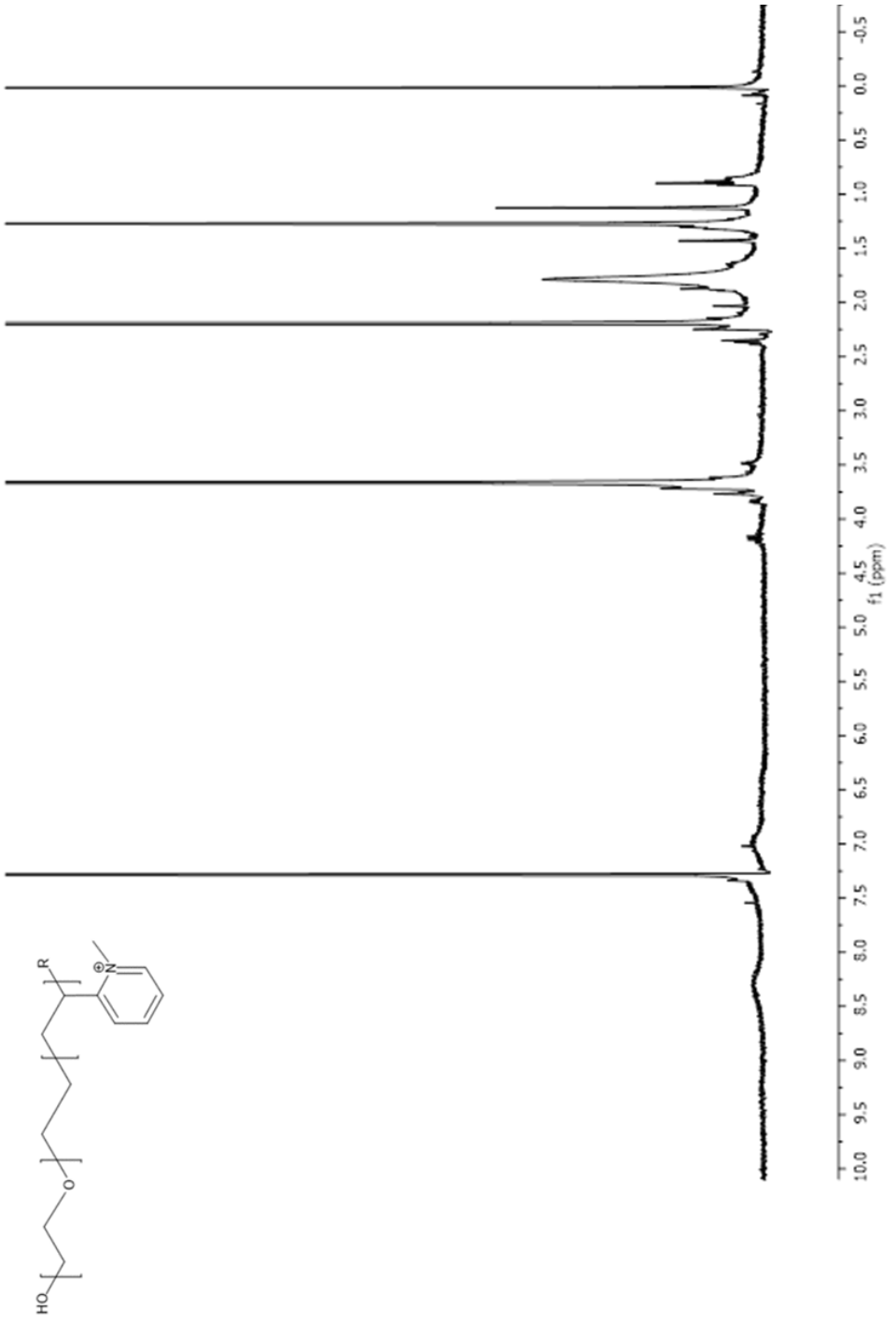

Figure 6. ^{1}H NMR spectra of P2VP-*b*-PEO before and after quaternization (Solvent: $CDCl_3$).

ATR-FTIR spectra of P2VP-*b*-PEO before and after quaternization are shown in Figure 7. The peak centred at 1590 cm^{-1} (X) corresponded to C=C stretching of pyridine ring on the P2VP block. The intensity of the peak at 1590 cm^{-1} (Y) decreased as the quaternization degree increased. The peak at 1630 cm^{-1} (Z) was related with the methyl group, covalently bound to N atoms of the pyridine units. Therefore, the presence of the peak at 1630 cm^{-1} assured the quaternization of P2VP-*b*-PEO. The percent quaternization was approximated as ~ 85 % using the following formula [46] [182]. The peak at 852 cm^{-1} was chosen as a reference peak for the calculation of quaternization degree.

$$\%\ quaternization = \frac{\left(\left(\frac{X}{A} - \frac{Y}{A}\right) + \frac{Z}{A}\right)}{\frac{X}{A}} * 100$$

X: area under the peak centered at 1590 cm^{-1} of P2VP-*b*-PEO

Y: area under the peak centered at 1590 cm^{-1} of QP2VP-*b*-PEO

Z: area under the peak centered at 1630 cm^{-1} of QP2VP-*b*-PEO

A: area under the peak centered at 852 cm^{-1} of both P2VP-*b*-PEO and QP2VP-*b*-PEO

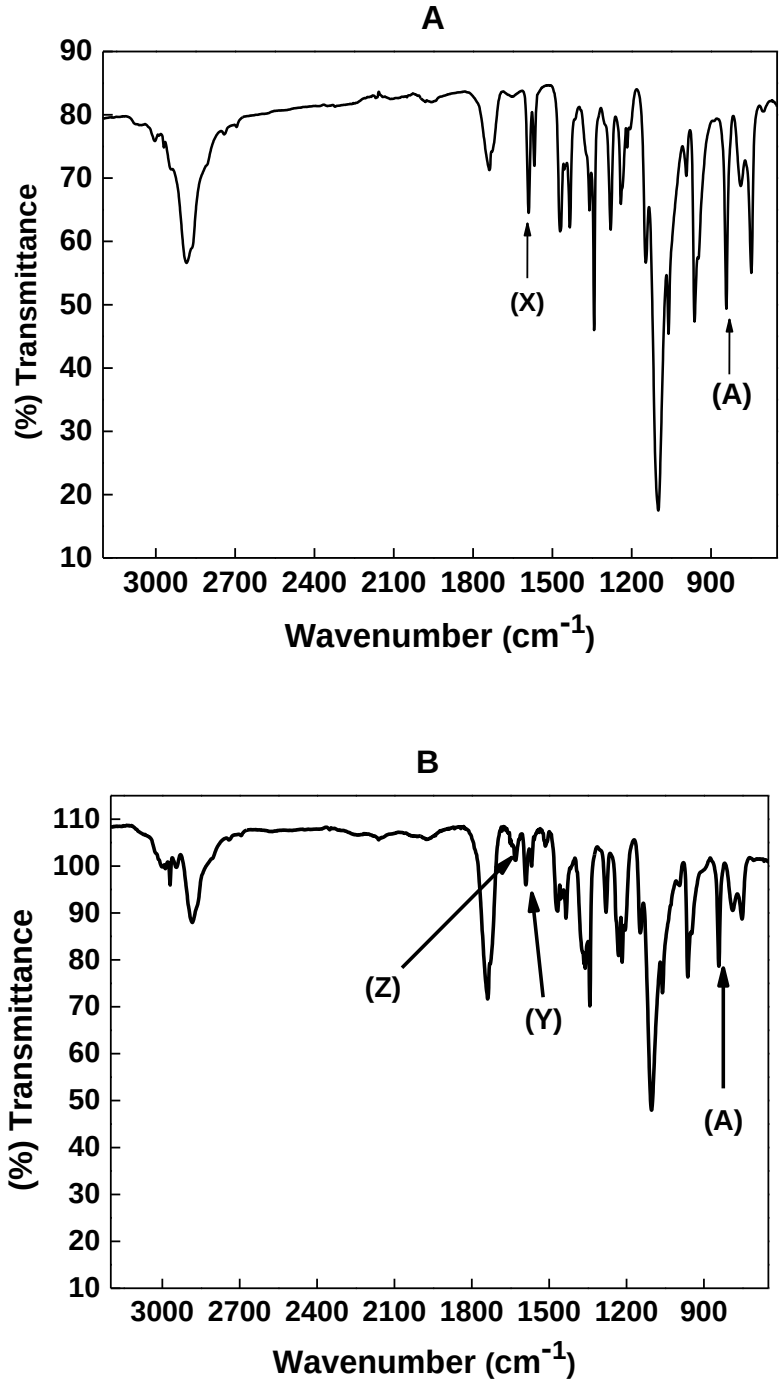

Figure 7. ATR-FTIR spectra of P2VP-*b*-PEO before **(A)** and after **(B)** quaternization.

3. 1.4 Micellization of QP2VP-*b*-PEO

Micellization was performed by adding 6.6 x 10^{-2} M B12 solution (pH 7.5) gradually (100 μL at each) into 0.5 mg/mL QP2VP-*b*-PEO solution at pH 7.5. Micellization was followed by measuring the hydrodynamic size of QP2VP-*b*-PEO as a function of B12 concentration using dynamic light scattering technique. The sharp increase the size was attributed to formation of micellar aggregates. Figure 8A shows the evolution of hydrodynamic size of QP2VP-*b*-PEO as a function of final B12 concentration in the solution. The large error bars between ~ 0.4 x10^{-3} M – 3.0 x10^{-3} M B12 concentration indicate the transition between unimers to micelles. This means that both species exist together in the solution. Formation of micelles with uniform size was recognized with the decrease in the standard deviation of size measurements. Micellization was optimized at 4.6 x 10^{-3} M B12 in the mixture. The size (B12+QP2VP)-*b*-PEO micelles remained nearly constant at ~33 nm between ~ 4.6 x10^{-3} M - ~ 6.0x10^{-3} M B12 concentration. Figure 8B shows the size distribution of (B12+QP2VP)-*b*-PEO micelles at 4.6 x 10^{-3} M B12. Figure 8C illustrates the formation of (B12+QP2VP)-*b*-PEO micelles.

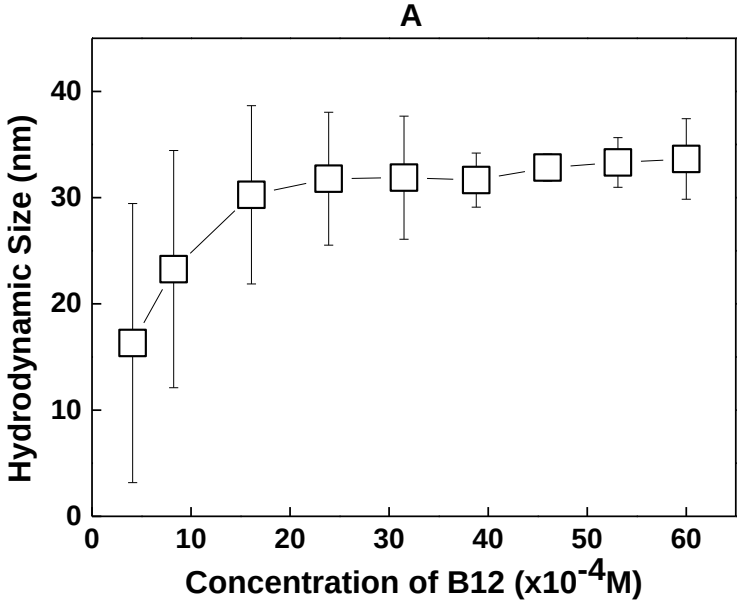

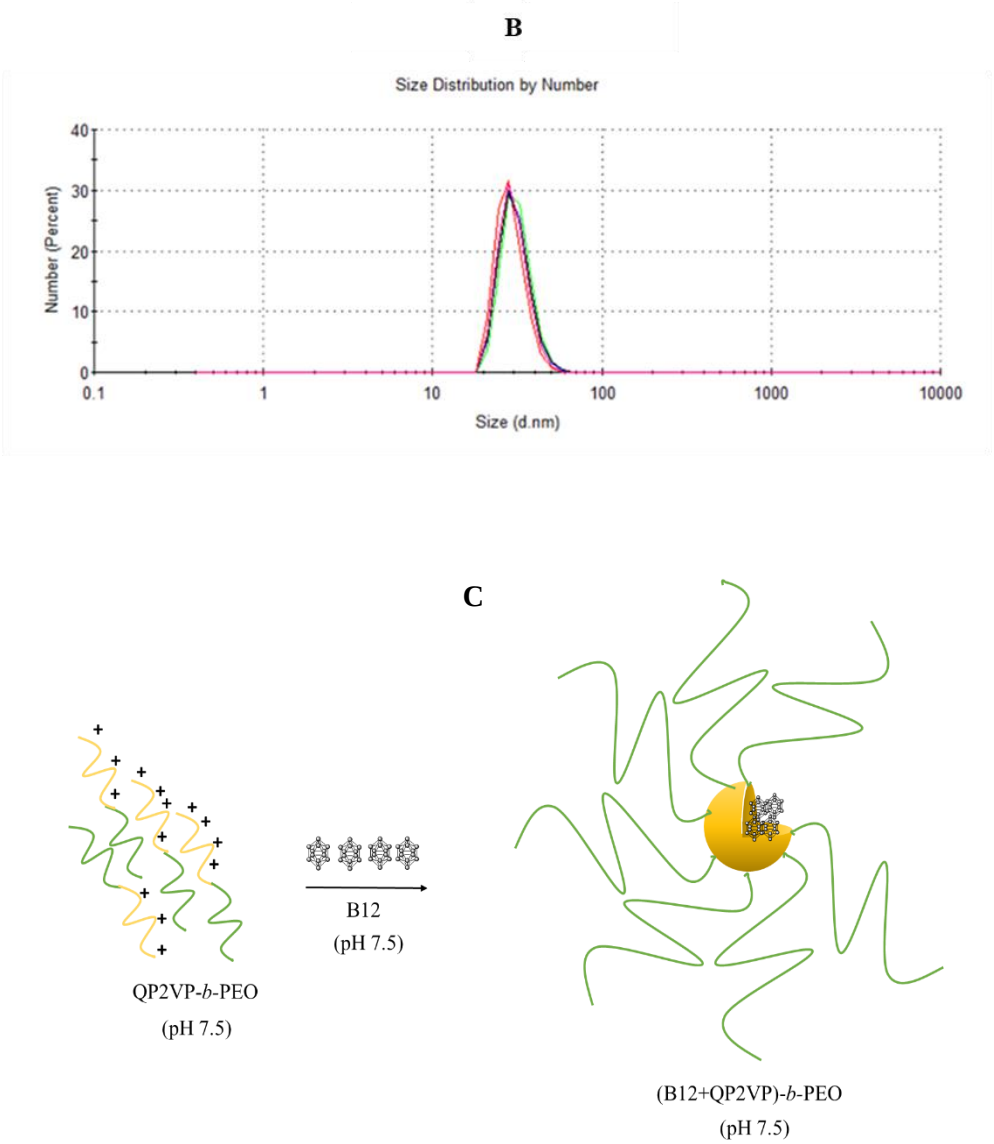

Figure 8. **(A)** Evolution of hydrodynamic size of QP2VP-*b*-PEO at pH 7.5 as a function of final B12 concentration. QP2VP-*b*-PEO solution was prepared at a concentration of 0.5 mg/mL at pH 7.5 and 25 °C. **(B)** Size distribution of (B12+QP2VP)-*b*-PEO micelles at 4.6 x 10^{-3} M B12. **(C)** Basic illustration of the formation of (B12+QP2VP)-*b*-PEO micelles.

For further analysis of (B12+QP2VP)-*b*-PEO micelles, excess B12 which did not participate in the self-assembly and was not encapsulated during micellization was removed by dialysing (B12+QP2VP)-*b*-PEO micelles against 10 mM phosphate buffer at pH 7.5/25 ^{o}C for an overnight period. TEM images shown in Figure 9 confirm the presence of spherical (B12+QP2VP)-*b*-PEO micelles. The particle size histogram of (B12+QP2VP)-*b*-PEO generated from TEM images suggests a size distribution between 25-30 nm (Figure 9).

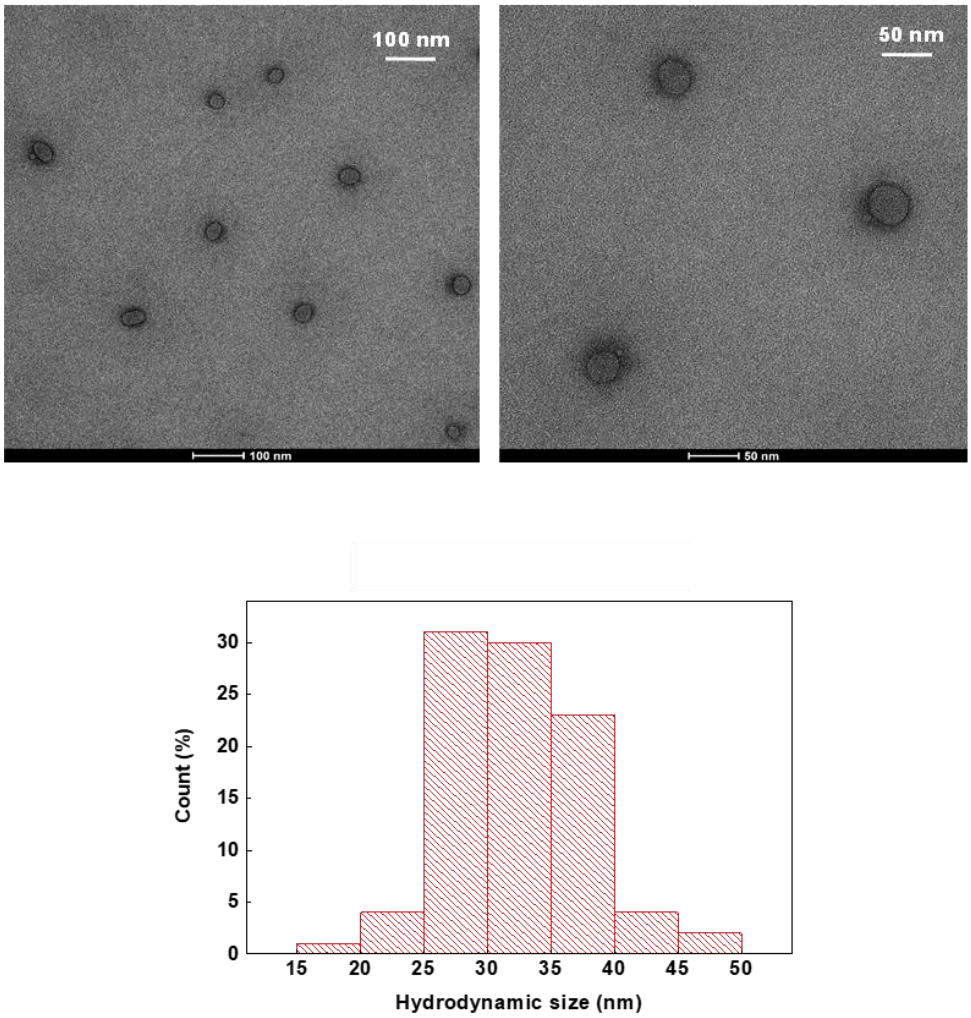

Figure 9. TEM micrographs of (B12+QP2VP)-*b*-PEO micelles and particle size histogram obtained from the TEM micrographs

Figure 10 shows the zeta potential distribution curve of (B12+QP2VP)-*b*-PEO micelles after dialysis process. The average zeta potential of the micelles before and after dialysis was -8.2 ± 0.5 mV and -3.5 ± 0.2 mV, respectively. The shift in zeta potential to less negative values upon dialysis was attributed to removal of the B12 anions which were not encapsulated but loosely adsorbed on the PEO-micellar

corona. The negative zeta potential might be occurred due to anions adsorbing on the PEO coronal chains, resulting in negatively charged QP2VP-*b*-PEO micelles.

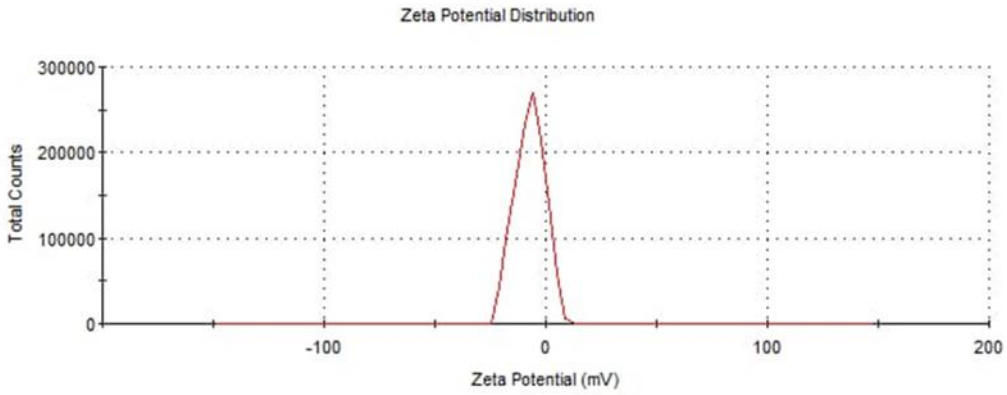

Figure 10. Zeta potential distribution curve of (B12+QP2VP)-*b*-PEO micelles after dialysis.

Finally, the presence of B12 in the micellar aggregates was confirmed through ATR-FTIR Spectroscopy technique. ATR-FTIR spectra of (B12+QP2VP)-*b*-PEO micelles obtained after dialysis, B12 and QP2VP-*b*-PEO are tabulated in Figure 11. In the spectrum of QP2VP-*b*-PEO, the peaks at 1630 cm^{-1} are related with the methylation of pyridinium rings. The peak at 1590 cm^{-1} resembles the specific pyridine rings's C=C stretching [79,182]. In the spectrum of B12, the peak at 2476 cm^{-1} and 3250 cm^{-1} are correlated with B-H stretching and N-H stretching , respectively. The peaks at 3100 cm^{-1} and the bands around 1080 cm^{-1} and 1030 cm^{-1} correspond to the C-H stretching and bending of C-H in plane, respectively [173]. The presence of the peak at 2476 cm^{-1} in the ATR-FTIR spectrum of (B12+QP2VP)-*b*-PEO micelles confirmed the presence of B12 in the aggregates.

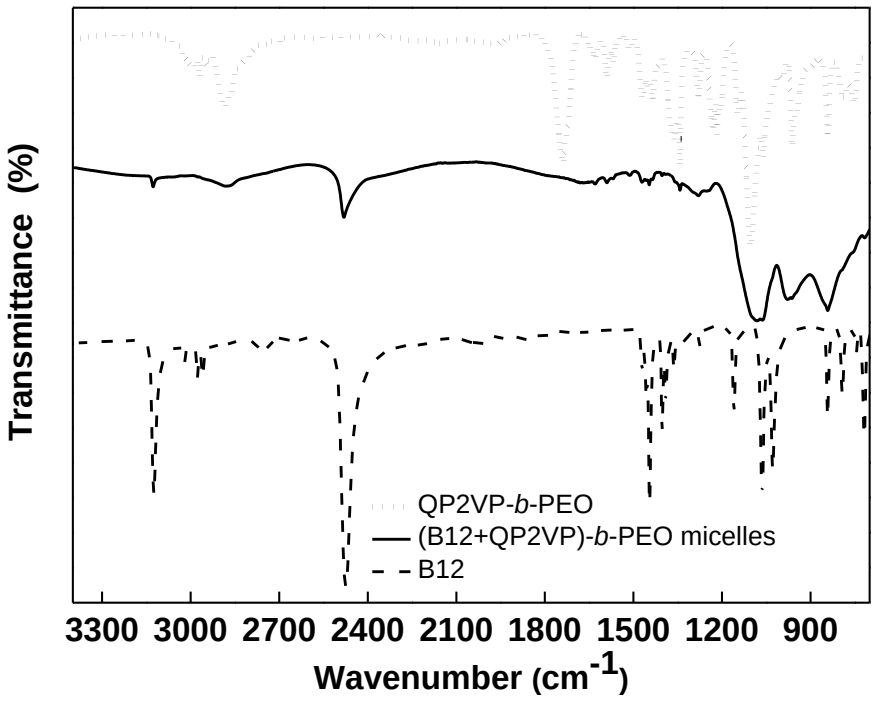

Figure 11. ATR-FTIR spectra of QP2VP-*b*-PEO, B12 and (B12+QP2VP)-*b*-PEO micelles.

3.2 Boron Encapsulation Efficiency of (B12+QP2VP)-*b*-PEO Micelles

The boron concentration encapsulated (B12+QP2VP)-*b*-PEO micelles were quantified by ICP-OES. To examine the effect of polymer concentration on the amount of B12 encapsulation, (B12+QP2VP)-*b*-PEO micelles were prepared at varying concentrations of QP2VP-*b*-PEO, i.e. 0.1 mg/mL and 1.0 mg/mL. Accordingly, the amount of B12 required for micelle formation was optimized prior to analysis. Figure 12 shows the hydrodynamic size of QP2VP-*b*-PEO as a function of B12 concentration in the solution for QP2VP-*b*-PEO concentration at 0.1 mg/mL (Figure 12A) and 1.0 mg/mL (Figure 12B). The optimal B12 concentrations were determined according to the extent of standard deviation in size measurements. The

B12 concentrations were determined as 6.5 x 10^{-4} M and 1.1 x 10^{-2} M for micellization of 0.1 mg/mL and 1 mg/mL QP2VP-*b*-PEO, respectively.

Micellar solutions were dialysed against 10 mM phosphate buffer at pH 7.5 and 25 °C prior to the ICP-OES analysis. This was done to remove excess B12 which was not entrapped /loosely bounded to the micelles. Table 2 expresses the concentrations of B12 and QP2VP-*b*-PEO utilized for the self-assembly process together with boron concentration of (B12+QP2VP)-*b*-PEO micelles analyzed by ICP-OES analysis.

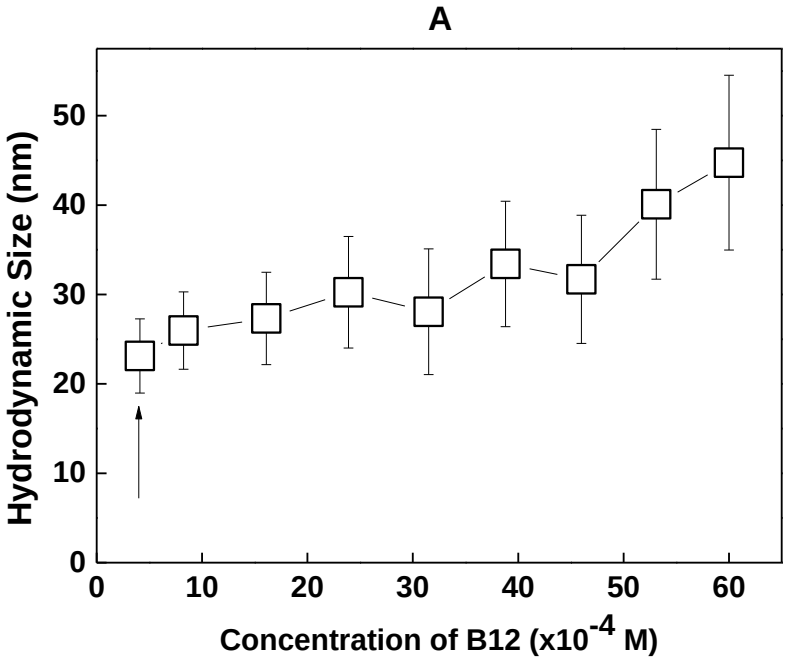

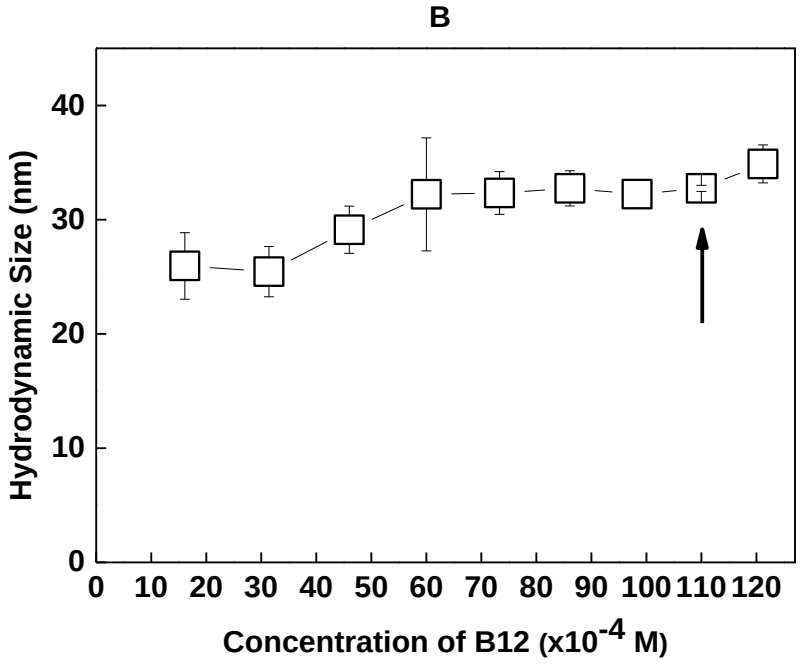

Figure 12. The evolution of hydrodynamic size of QP2VP-*b*-PEO as a function of B12 for QP2VP-*b*-PEO concentration at **(A)** 0.1 mg/mL and **(B)** 1.0 mg/mL.

Table 2. Comparison of the boron concentration and encapsulation % of (B12+QP2VP)-*b*-PEO micelles prepared with different QP2VP-*b*-PEO concentrations.

Concentration of QP2VP-*b*-PEO	**Concentration of B12 to induce micellization**	**Concentration of B after micellization and dialysis**	**% encapsulation**
0.1 mg/mL	6.5×10^{-4} M (0.23 mg/mL)	18 ±1 ppm (0.02 mg/mL)	22 %
0.5 mg/mL	4.6×10^{-3} M (1.60 mg/mL)	82 ±2 ppm (0.08 mg/mL)	14 %
1.0 mg/mL	1.1×10^{-2} M (3.80 mg/mL)	290 ±6 ppm (0.29 mg/mL)	20 %

As seen in Table 2, concentration of B12 required for micellization increases as the polymer concentration increased. However, % encapsulation of boron by the micellar cores remained almost constant. % encapsulation of B12 by micelles was calculated by the ratio of boron concentration detected in the micelles through ICP-OES to boron concentration in B12 added to induce micellization.

3.3 Stability of (B12+QP2VP)-*b*-PEO micelles against dilution with PBS and EMEM cell culture medium

3.3.1 Stability against dilution with PBS

The stability of micelles, prepared using 0.5 mg/mL QP2VP-*b*-PEO solution and 4.6 x 10^{-3} M B12, was examined against dilution with PBS at 37 °C. The total amount of the solution was fixed at 1.0 mL and v/v ratio of micellar solution/PBS was altered from 9:1 to 1:9. In each case, PBS was added to the micellar solution. Dilution with PBS may have the following consequences:

i) (B12+QP2VP)-*b*-PEO micelles were prepared at 10.0 mM phosphate buffer. PBS contains NaCl (137 mmol/L), KCl (2.7 mmol/L), Na_2HPO_4 (10 mmol/L), KH_2PO_4 (1.8 mmol/L). The relatively high salt concentration in PBS may disrupt the association between B12 and QP2VP due to competitive interactions between B12 and the salt ions in PBS.

ii) Micelles are generally formed above a certain concentration which is known as "critical micellization concentration". If the concentration may fall below this critical value, disintegration of micelles may occur.

Figure 13 A shows the hydrodynamic size of (B12+QP2VP)-*b*-PEO micelles as a function of volume of added PBS right after and 24 hours after the dilution, respectively. No significant change in hydrodynamic size was recorded. (B12+QP2VP)-*b*-PEO micelles maintained their integrity in PBS within this dilution range even after 24 hours. To assure the stability of micelles against dilution with PBS, stability of micelles prepared using a solution containing 0.1 mg/mL QP2VP-*b*-PEO and 6.5 x 10^{-4} M B12 was also examined. As seen in the Figure 13 B, micelles disintegrated upon addition of 400 μL PBS indicating the effect of polymer concentration on the stability of micelles.

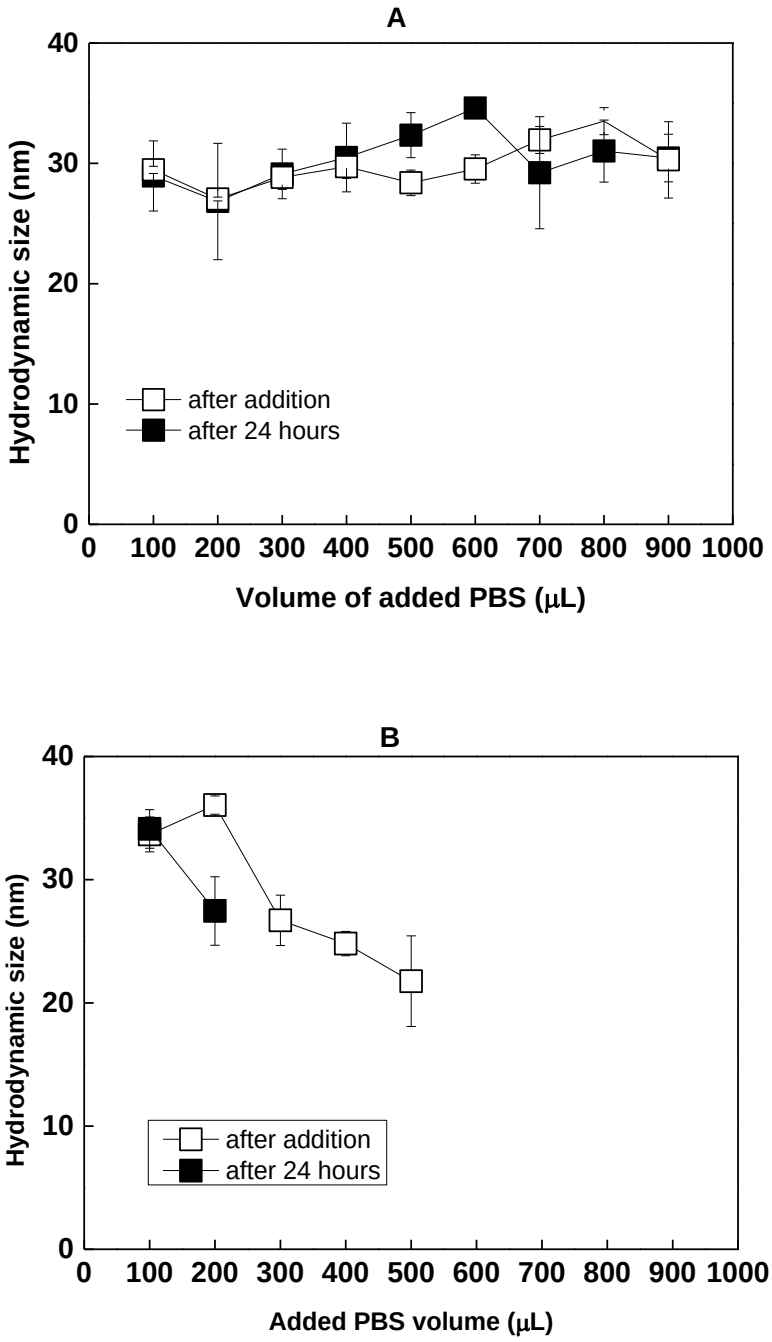

Figure 13. (A) Hydrodynamic size of (B12+QP2VP)-*b*-PEO micelles, prepared using 0.5 mg/mL QP2VP-*b*-PEO solution and 4.6 x 10^{-3} M B12, upon dilution with PBS at pH 7.5 and 37 °C and pH 7.4. **(B)** Hydrodynamic size of (B12+QP2VP)-*b*-

PEO micelles, prepared using 0.1 mg/mL QP2VP-*b*-PEO solution and 6.5 x 10^{-4} M B12, upon dilution with PBS at pH 7.5 and 37 °C and pH 7.4. Empty and filled circles/squares correspond to size data right after dilution and 24 hours after dilution, respectively.

3.3.2 Stability against dilution with Eagle's Minimum Essential Medium EMEM)

Before the biochemical assays to be performed, the stability of (B12+QP2VP)-*b*-PEO micelles (prepared with a solution containing 0.5 mg/mL QP2VP-*b*-PEO and 4.6 x 10^{-3} M B12) was determined against EMEM. In contrast to the stability of the micelles against PBS dilution, shift in the size distribution curve to lower values started even after addition of 100 µL of EMEM into 900 µL of micellar solution. At 200 µL of medium addition into 800 µL of micellar solution, complete disintegration of the micelles occurred. Figure 14 shows the shift in the size distribution curve to lower values upon dilution with EMEM at a v/v ratio of 9:1 and 8:2 ((B12+QP2VP)-*b*-PEO micellar solution: EMEM). The size distribution curve of (B12+QP2VP)-*b*-PEO micelles at pH 7.5 was plotted for comparison.

EMEM contains $CaCl_2$, KCl, $MgSO_4$, NaCl, $NaHCO_3$, NaH_2PO_4. H_2O, D-glucose, phenol red, L-Arginine-HCl, L-cysite, L-Histidine-HCl.H_2O, L-isoleucine, L-Lysine-HCl, L-methionine, L-phenylalanine, L-tryptophan, L-tyrosine, L-valine, D-calcium pantothenate, choline chloride, folic acid, i-inositol, niacinamide, pyridoxal HCl, riboflavin, thiamine HCl, penicillin-streptomycin, fetal bovine serum (FBS), sodium pyruvate, glutamine, and non-essential amino acids. The disintegration of (B12+QP2VP)-*b*-PEO micelles was possibly due to association of P2VP blocks

and/or B12 with the medium ingredients and disruption of QP2VP and B12 interactions.

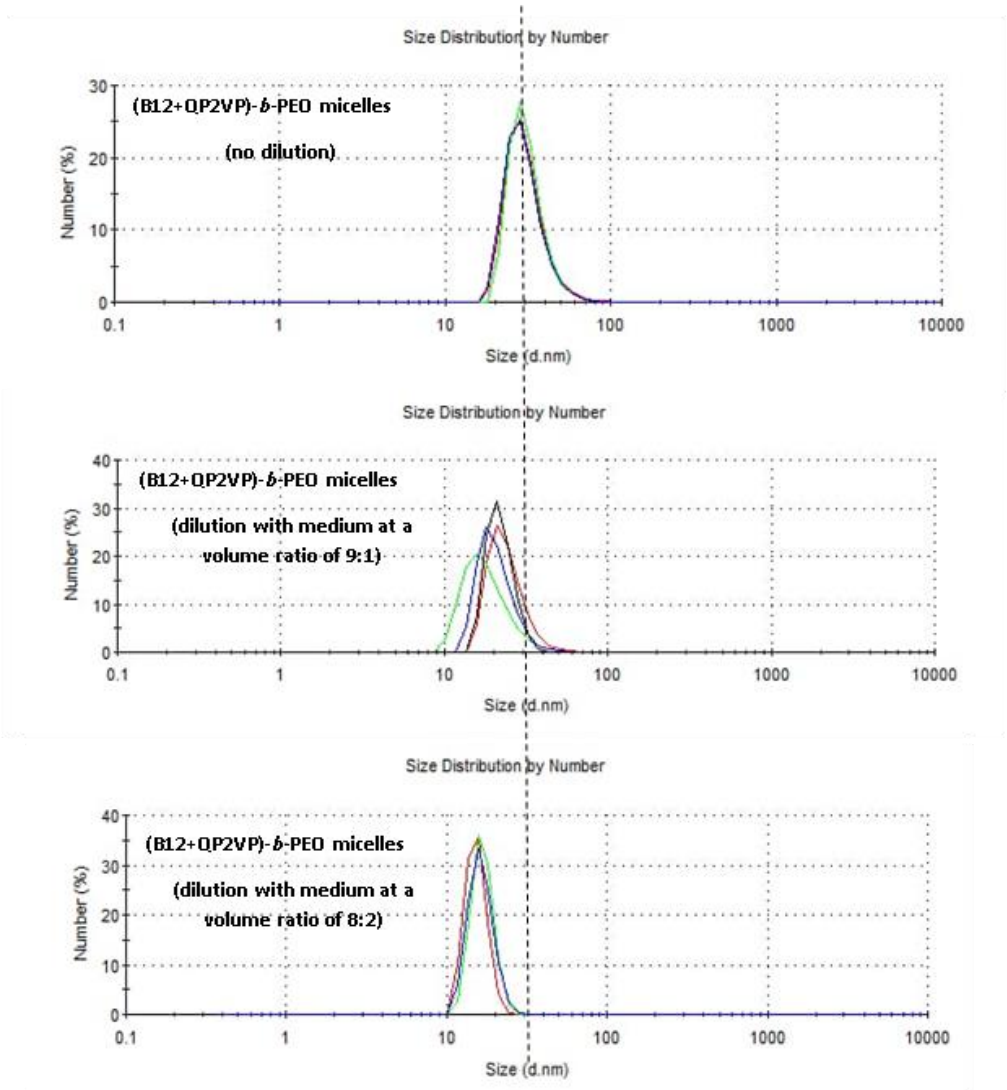

Figure 14. Size distribution of (B12+QP2VP)-*b*-PEO micelles before and after addition of EMEM medium into micellar solution prepared using 0.5 mg/mL QP2VP-*b*-PEO solution and 4.6 x 10^{-3} M B12. Dotted line shows the initial peak position of the size distribution curve for comparison.

3.4 Preparation of B12 containing LbL capsules

As mentioned earlier, the instability of (B12+QP2VP)-*b*-PEO micelles is a concern because BNCT requires release of boron compounds at the target site. Although the micelles rendered stable against pH variations and dilution with PBS, stability against dilution with EMEM could not be succeeded. In order to stabilize the micelles, (B12+QP2VP)-*b*-PEO micelles were self-assembled onto CUR loaded $CaCO_3$ microparticles with TA through hydrogen bonding driven LbL self-assembly. Stabilization of block copolymer micelles upon deposition onto a substrate has been suggested in the literature [183]. The reason for using CUR loaded $CaCO_3$ microparticles was to obtain fluorescence for visualization of microparticles during cellular association experiments.

3.4.1 LbL self-assembly of (B12+QP2VP)-*b*-PEO micelles

(B12+QP2VP)-*b*-PEO micelles and TA were self-assembled on $CaCO_3$ microparticle surface at pH 7.5 and pH 6.5, respectively. The reason for depositing TA at a lower pH was to increase the number of protonated phenolic hydroxyl groups on TA molecules for hydrogen bonding-driven self-assembly. It is also important to mention that $CaCO_3$ microparticles decompose to CO_2 and Ca^{2+} under acidic conditions [184]. Therefore, more acidic deposition pH was avoided to assure the stability of $CaCO_3$ microparticles. LbL growth of (B12+QP2VP)-*b*-PEO micelles and TA was first followed by depositing the multilayers onto a silicon wafer and following the thickness of the films as a function of increasing layer number (Figure 15).

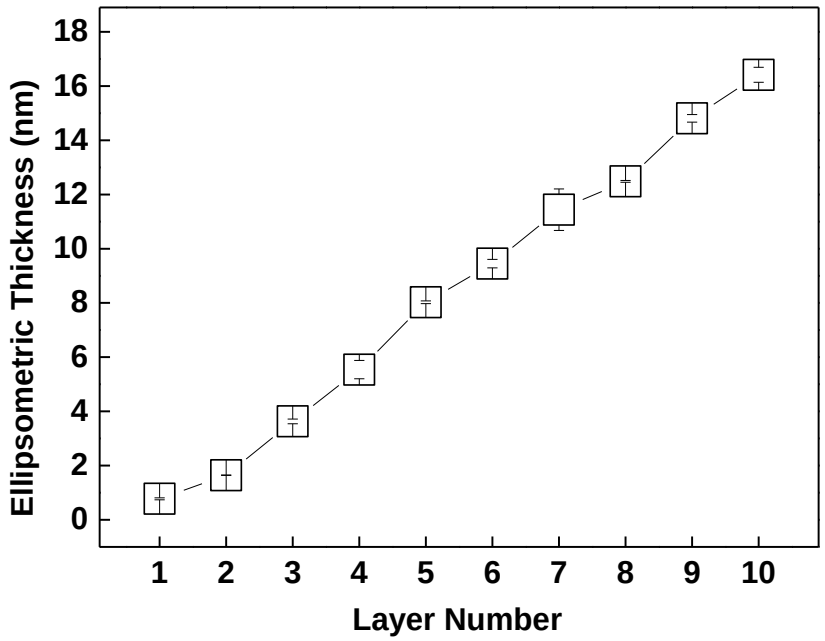

Figure 15. LbL multilayer growth of (B12+QP2VP)-*b*-PEO micelles and TA.

Thickness increased with increasing layer number, indicating successful LbL growth. An average bilayer thickness of ~ 3.6 nm was recorded. The driving force for LbL deposition was hydrogen bonding interactions among ether oxygens of PEO and phenolic hydroxyl groups of TA.

LbL growth of multilayers on $CaCO_3$ microparticles was followed by monitoring the zeta potential of particles with increasing layer number. Figure 16 shows the evolution of zeta potential as a function of layer number. Scheme 10 shows schematic representation of LbL capsules. The mean zeta potential of $CaCO_3$ microparticles changed from -15.7 ± 0.5 mV to -27.4 ± 0.2 mV as the deposition of the first layer (TA). The driving force for the deposition of TA onto microparticles attributed to the hydrogen bonding interactions within SO_3^- units of PSS and the -OH groups of TA. Moreover, π- π stacking interactions between the aromatic rings

of TA and phenyl rings of PSS [188]. The shift of the zeta potential to more negative values was due to phenolate groups of TA (p$K_{a,1}$ ~ 6.5 and p$K_{a,2}$ ~ 8). During the deposition of the remaining layers, the zeta potential oscillated in the negative region. Due to partial screening of the negative surface charge by the neutral PEO coronal chains, less negative zeta potential values were reported after deposition of (B12+QP2VP)-*b*-PEO micellar layers.

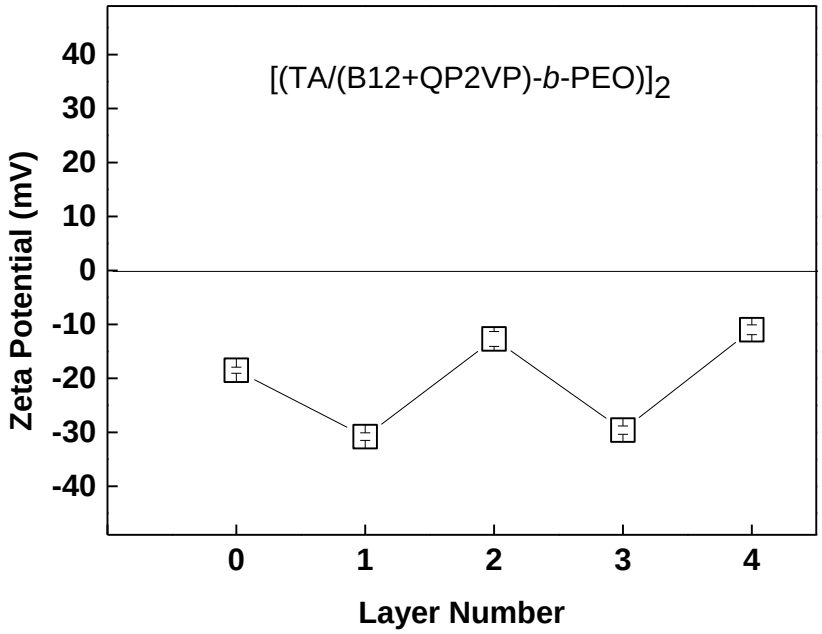

Figure 16. The evolution of zeta potential as a function of layer number prior to the formation of [(TA/(B12+QP2VP)-*b*-PEO)]$_2$. Layer 0 refers to zeta potential of $CaCO_3$ microparticles.

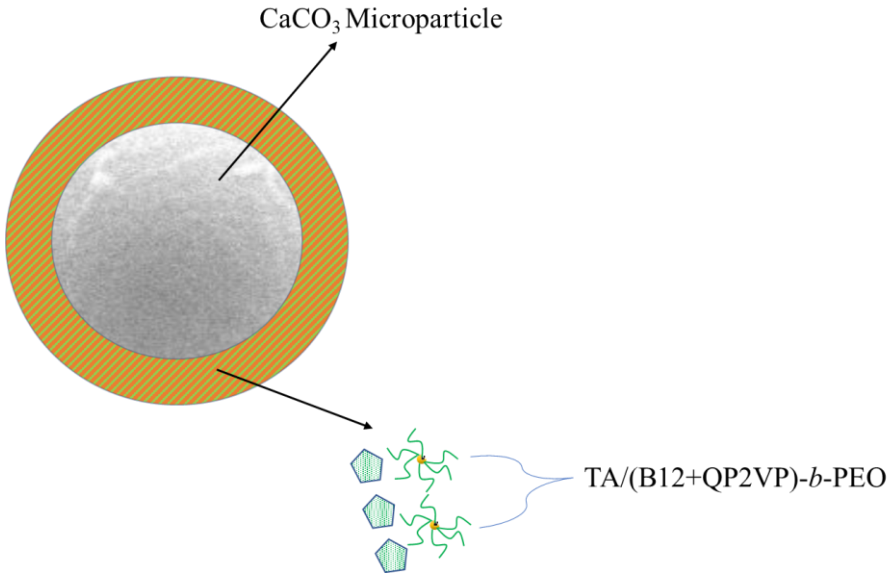

Scheme 9. Schematic representation of LbL capsules of TA and (B12+QP2VP)-*b*-PEO micelles.

Deposition of polymer layers onto $CaCO_3$ microparticles was also confirmed through SEM imaging. As seen in Figure 17, the surface roughness increased as the layers were deposited onto microparticles. Unfortunately, the number of layers that could be deposited onto $CaCO_3$ microparticles was limited to 4 because precipitation of particles turned to be problematic at increasing layer numbers. Increasing the speed of centrifugation triggered the aggregation of particles. Therefore, layer number was limited to 4.

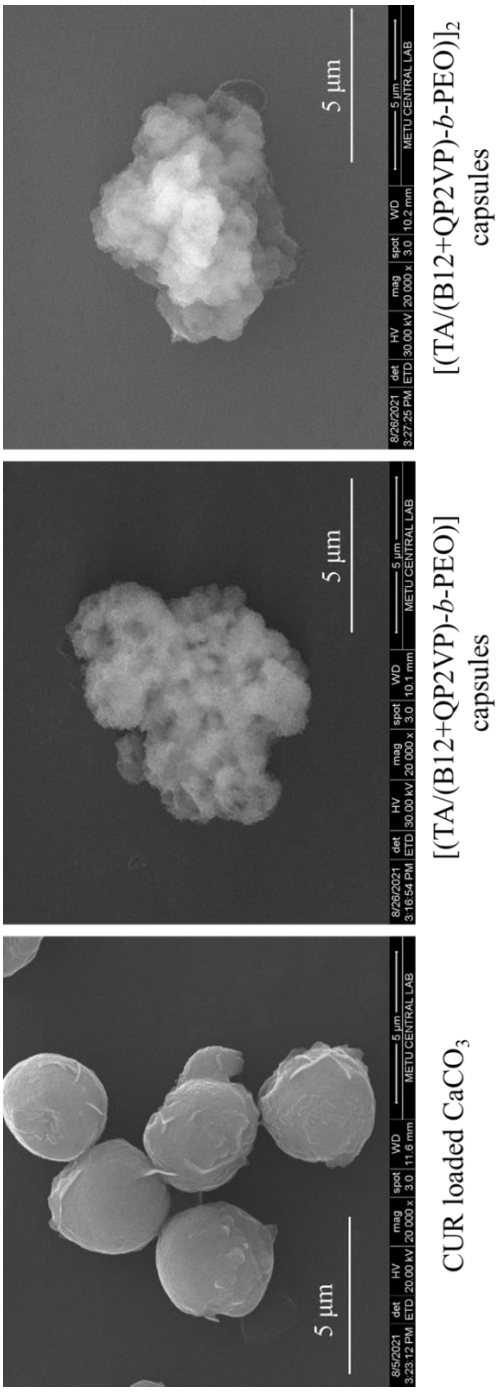

Figure 17. SEM micrographs of bare CUR loaded $CaCO_3$ microparticles, [(TA/(B12+QP2VP)-*b*-PEO)] and [(TA/(B12+QP2VP)-*b*-PEO)]$_2$ capsules.

3.4.2 Stability of LbL capsules

The stability of LbL capsules in EMEM was followed through zeta potential measurements. Although zeta potential measurements do not provide clear information about the stability of micelles, a remarkable change in zeta potential as a function of time was assumed as an indication of instability of LbL capsules. LbL coated microparticles were dispersed in EMEM at 37 °C and Figure 18 shows the evolution of zeta potential of 4-layer capsules - $[(TA/(B12+QP2VP)-b-PEO)]_2$ capsules - as a function of time. The data at time "0" refers to the initial zeta potential of $[(TA/(B12+QP2VP)-b-PEO)]_2$ capsules. The relatively large error bars in zeta potential measurements after the first 1 hour was assumed as layer loss from the surface. The instability of the multilayers was correlated with:

i) penetration of salt ions into multilayers resulting in enhanced ionization of TA and increased osmotic pressure within the multilayers, resulting in loss of hydrogen bonding interactions among the layers. Enhanced ionization of polyacids in the presence of salt ions has been reported [185]. Of note, multilayers were prepared in 10 mM phosphate buffer, whereas the salt concentration in EMEM is higher.

ii) the competitive interactions between the ingredients of EMEM and TA or (B12+QP2VP)-*b*-PEO micelles resulting in partial disintegration of multilayers.

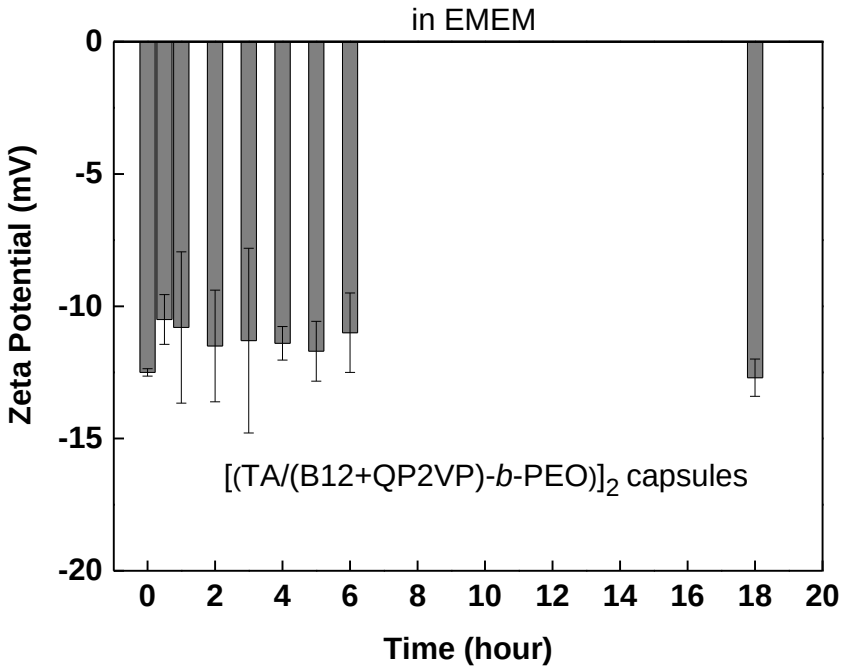

Figure 18. Evolution of zeta potential of $[(TA/(B12+QP2VP)\text{-}b\text{-}PEO)]_2$ capsules upon dispersion into EMEM as a function of time.

3.4.3 Preparation of LbL capsules with barrier stacks

As mentioned in the previous section, the stability of LbL capsules was questionable in EMEM medium. To enhance the stability of capsules, a barrier stack composed of 1 bilayer of PVCL, and TA was deposited on top of $[TA/(B12+QP2VP)\text{-}b\text{-}PEO$ micelles$]_2$. Scheme 10 shows schematic representation of LbL capsules with a barrier stack. The reason for choosing PVCL and TA as a barrier stack was the stronger hydrogen bonding based association between PVCL and TA compared to PEO coronal chains and TA. Prior to preparation of capsules, LbL growth of PVCL and TA onto multilayers of TA/(B12+QP2VP)-*b*-PEO micelles was examined. As seen in Figure 19, TA and PVCL layers could be successfully deposited onto a bottom stack composed of TA and (B12+QP2VP)-*b*-PEO micellar layers.

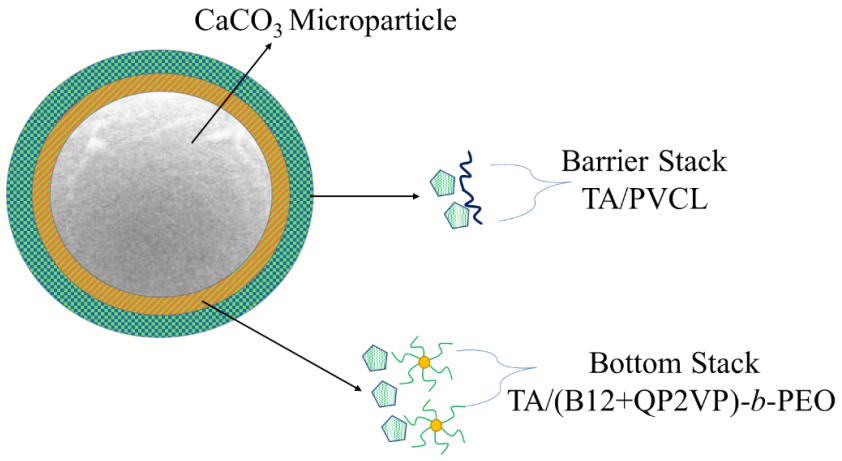

Scheme 10. Schematic representation of $[(TA/(B12+QP2VP)\text{-}b\text{-}PEO)]_2$ + (TA/PVCL) LbL capsule architecture.

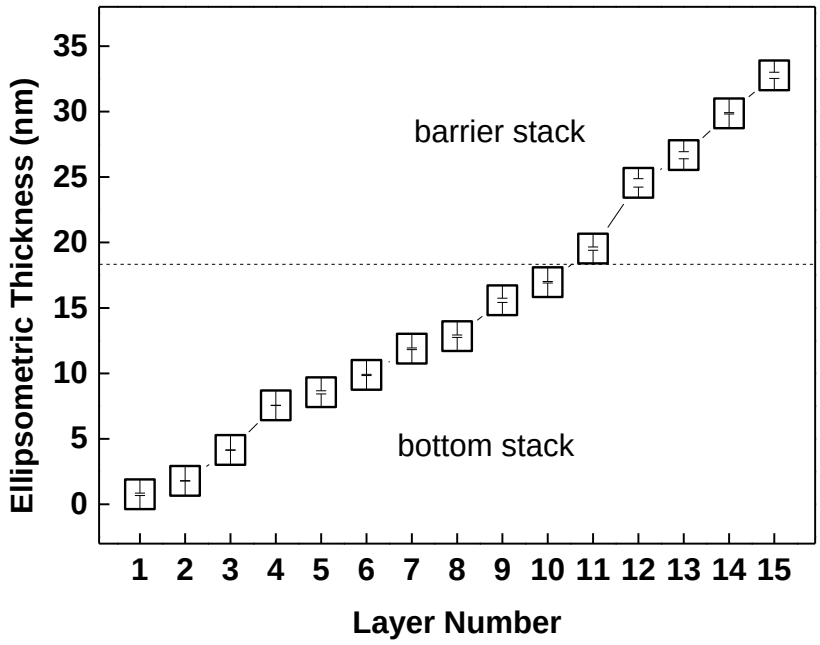

Figure 19. LbL growth of PVCL and TA onto multilayers of TA and (B12+QP2VP)-*b*-PEO micelles, constructed onto silicon wafer.

Deposition of multilayers with a barrier stack onto $CaCO_3$ microparticles was followed through zeta potential measurements. Figure 20 shows the successful deposition of 1 bilayer of TA/PVCL barrier stack onto $[(TA/(B12+QP2VP)\text{-}b\text{-}PEO)]_2$ capsules. The capsules with a barrier will be denoted as "$[(TA/(B12+QP2VP)\text{-}b\text{-}PEO)]_2$ + (TA/PVCL)".

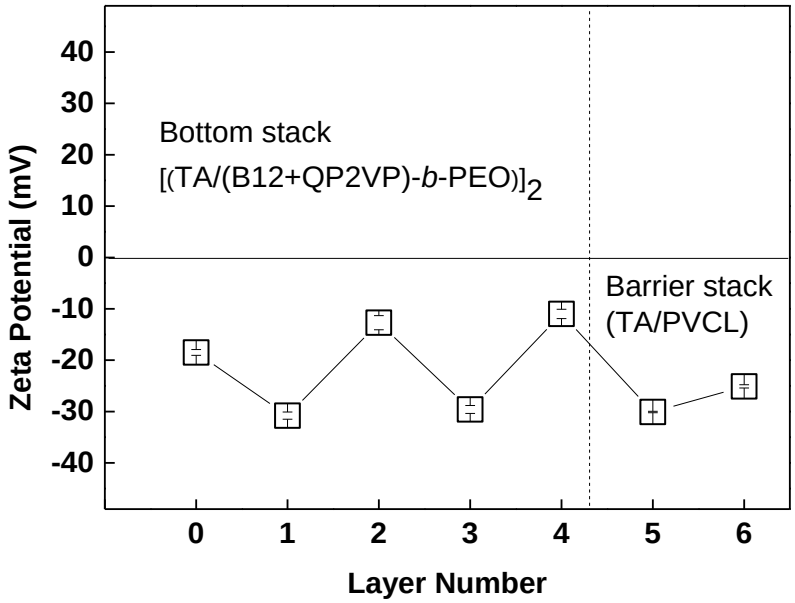

Figure 20. The evolution of zeta potential as a function of layer number prior to the formation of $[(TA/(B12+QP2VP)\text{-}b\text{-}PEO)]_2$ + (TA/PVCL).

LbL capsules with a barrier stack was also assessed through SEM imaging. Figure 21 shows SEM micrographs of 1 micellar layer containing capsule with a barrier stack- [(TA/(B12+QP2VP)-*b*-PEO)] + (TA/PVCL) and 2 micellar layer containing capsule with a barrier stack - $[(TA/(B12+QP2VP)\text{-}b\text{-}PEO)]_2$ + (TA/PVCL). Comparison of the images in Figure 20 shows that aggregation of microparticles enhanced with deposition of additional barrier layers which is more obvious for 2 micellar layer containing capsules.

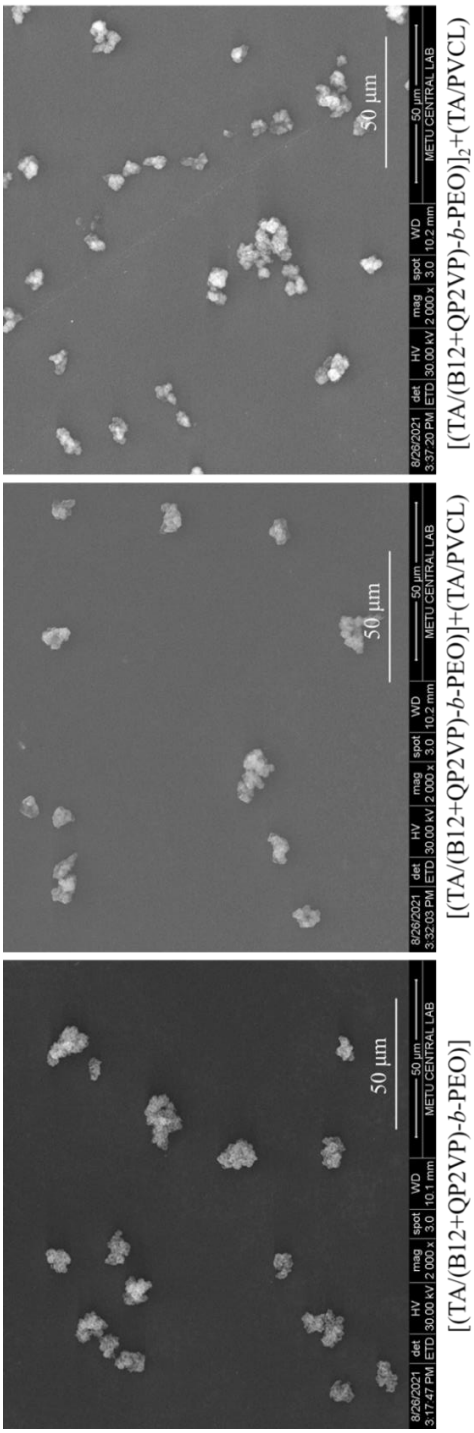

Figure 21. SEM images of [(TA/(B12+QP2VP)-*b*-PEO)] + (TA/PVCL) capsules and $[(TA/(B12+QP2VP)\text{-}b\text{-}PEO)]_2$ + (TA/PVCL) capsules.

The stability of [(TA/(B12+QP2VP)-*b*-PEO)]$_2$ + (TA/PVCL) was again followed through evolution of zeta potential as a function of time. As seen in Figure 22, the zeta potential remained almost constant with relatively small standard deviation compared to capsules without a barrier stack.

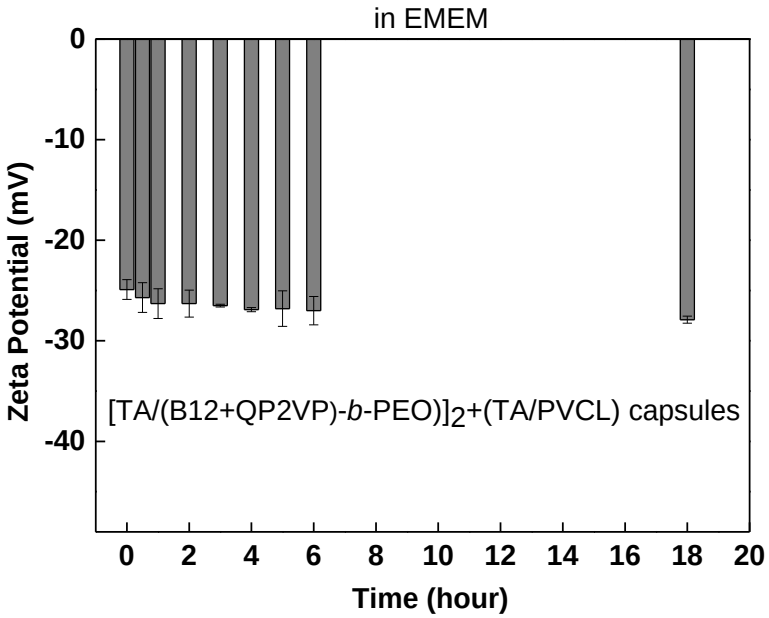

Figure 22. Evolution of zeta potential of [(TA/(B12+QP2VP)-*b*-PEO)]$_2$ + (TA/PVCL) capsules upon dispersion in EMEM as a function of time.

3.5 Preparation of hollow LbL capsules

Hollow LbL capsules were produced by dissolving $CaCO_3$ sacrificial cores in a 0.25 M EDTA solution at pH 5. Importantly, it was found that deposition of barrier layers was necessary not only to increase the stability of capsules in EMEM but also to produce hollow capsules. [TA/(B12+QP2VP)-*b*-PEO micelles]$_2$ capsules without a barrier stack possibly damaged upon treatment with EDTA solution as inferred from zeta potential distribution curves containing multiple peaks. On the other hand, LbL

capsules with a barrier stack produced hollow capsules and the zeta potential distribution curve is shown in Figure 23.

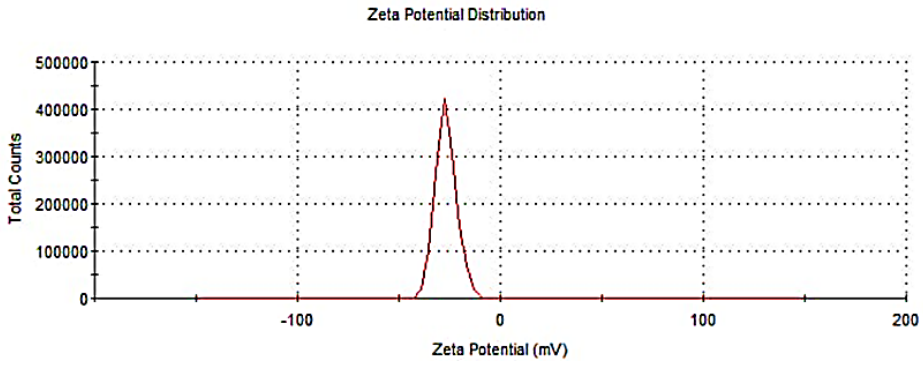

Figure 23. Zeta potential distribution of hollow [(TA/(B12+QP2VP)-*b*-PEO)]$_2$+(PVCL/TA) capsules.

The SEM image and EDX analysis of hollow [(TA/(B12+QP2VP)-*b*-PEO)] + (TA/PVCL) and [(TA/(B12+QP2VP)-*b*-PEO)]$_2$ + (TA/PVCL) capsules are shown in Figure 24. The capsules looked like an empty balloon upon dissolution of the $CaCO_3$ templates.

EDX analysis showed that there were no traces of Ca remained in both capsules after treatment with EDTA, indicating that $CaCO_3$ cores had been successfully removed. For comparison, EDX spectra of non-hollow and hollow [(TA/(B12+QP2VP)-*b*-PEO)] + (TA/PVCL) and [(TA/(B12+QP2VP)-*b*-PEO)]$_2$ + (TA/PVCL) capsules are presented in Figure 24B.

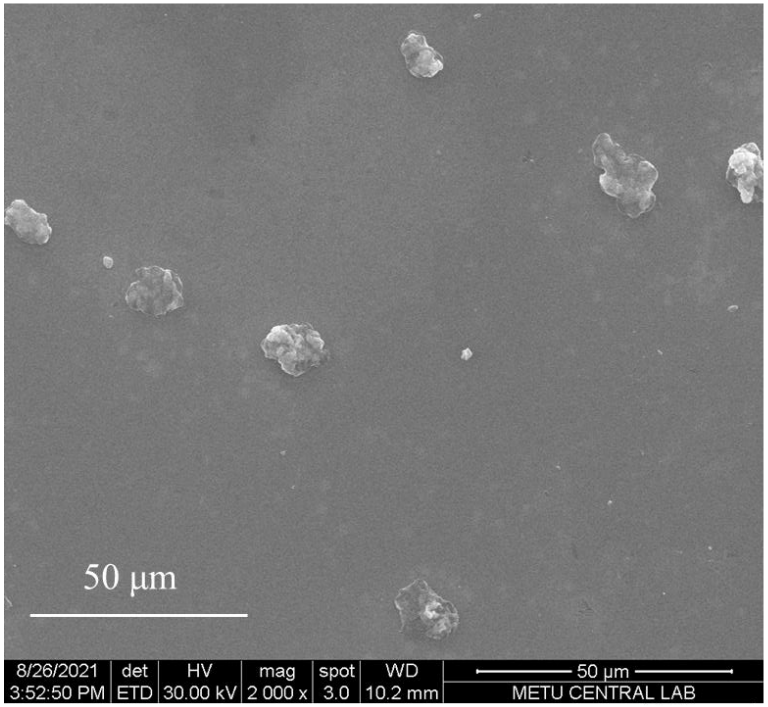

Hollow [(TA/(B12+QP2VP)-*b*-PEO)]+(TA/PVCL) capsules

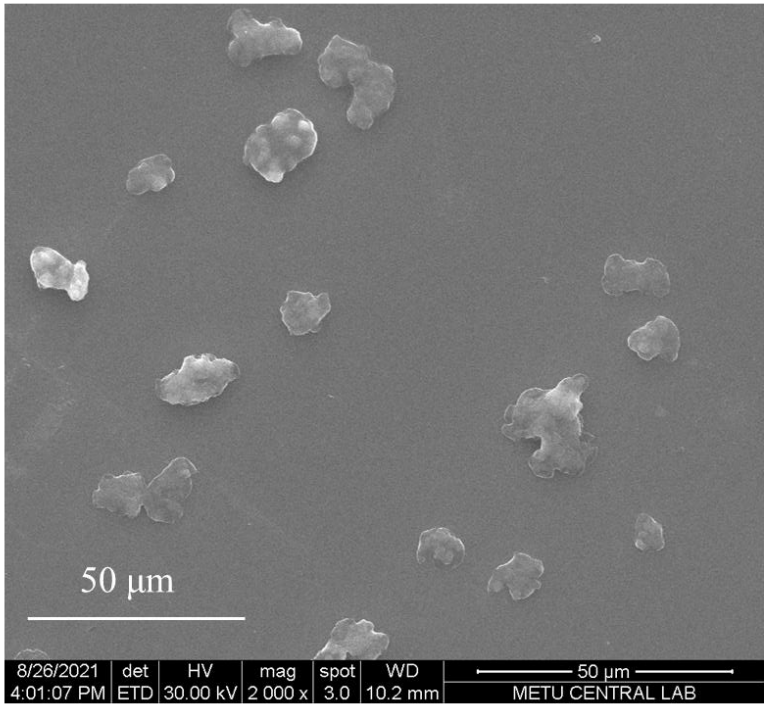

Hollow $[(TA/(B12+QP2VP)\text{-}b\text{-}PEO)]_2$+(TA/PVCL) capsules

B

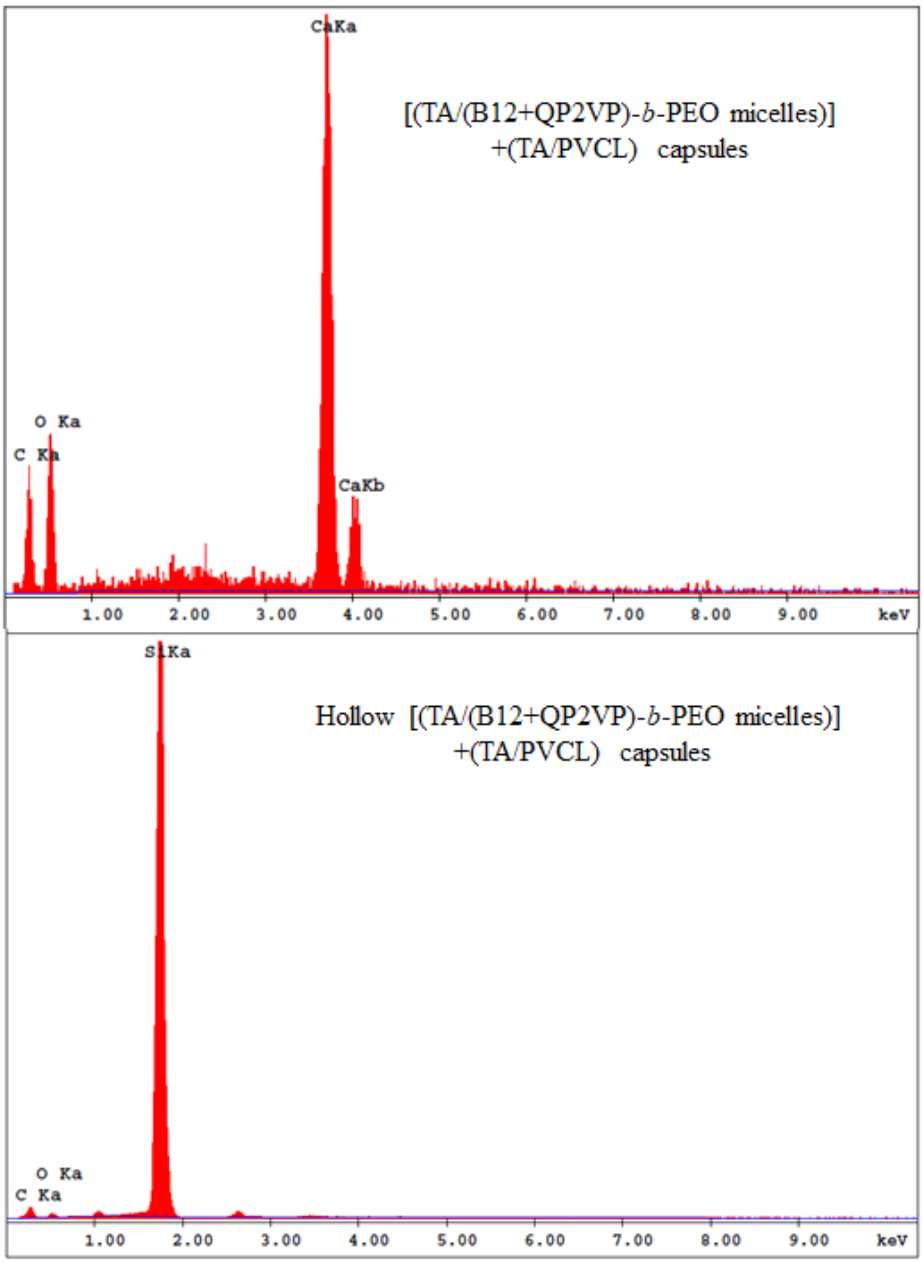
CaKa
[(TA/(B12+QP2VP)-b-PEO micelles)]
+(TA/PVCL) capsules
O Ka
C Ka
CaKb
1.00
2.00
3.00
4.00
5.00
6.00
7.00
8.00
9.00
keV
SiKa
Hollow [(TA/(B12+QP2VP)-b-PEO micelles)]
+(TA/PVCL) capsules
O Ka
C Ka
1.00
2.00
3.00
4.00
5.00
6.00
7.00
8.00
9.00
keV

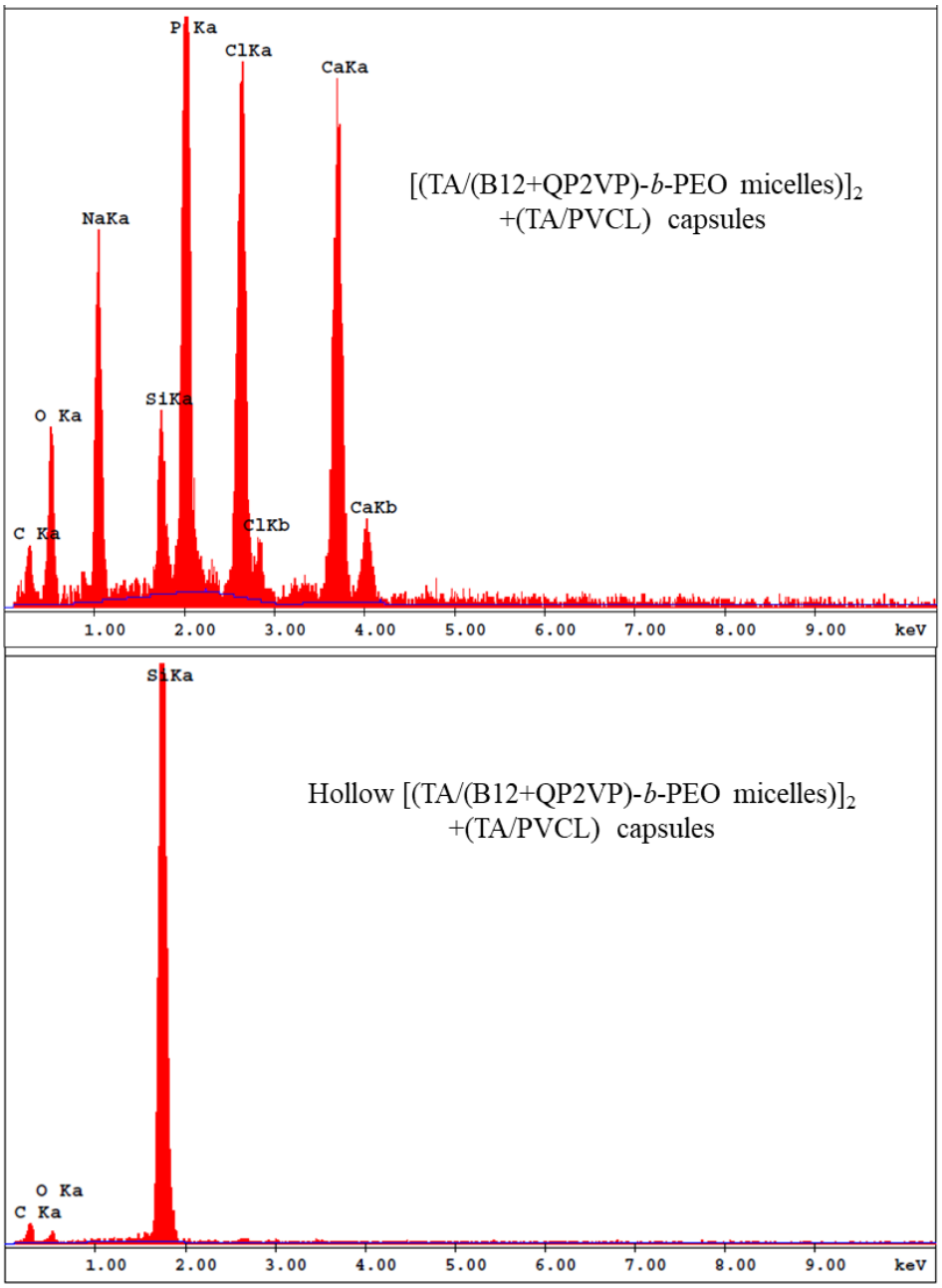

Figure 24. (A) SEM Micrograph hollow [(TA/(B12+QP2VP)-*b*-PEO)] + (TA/PVCL) and hollow [(TA/(B12+QP2VP)-*b*-PEO)] + (TA/PVCL) capsules. **(B)** EDX analysis of [(TA/(B12+QP2VP)-*b*-PEO)] +(TA/PVCL) capsules, hollow [(TA/(B12+QP2VP)-*b*-PEO)]+ (TA/PVCL) capsules, [(TA/(B12+QP2VP)-*b*-PEO)]$_2$+(TA/PVCL) capsules and hollow [(TA/(B12+QP2VP)-*b*-PEO

micelles)]$_2$+(TA/PVCL) capsules. In the EDX spectra of the hollow capsules, no trace of Ca was detected.

The stability of hollow capsules was studied by dispersing the capsules in EMEM (Figure 25) and following the zeta potential as a function of time. Zeta potential of both [(TA/(B12+QP2VP)-*b*-PEO micelles)] +(TA/PVCL) and [(TA/(B12+QP2VP)-*b*-PEO micelles)]$_2$ +(TA/PVCL) capsules remained almost constant, pointing out the stability of hollow capsules.

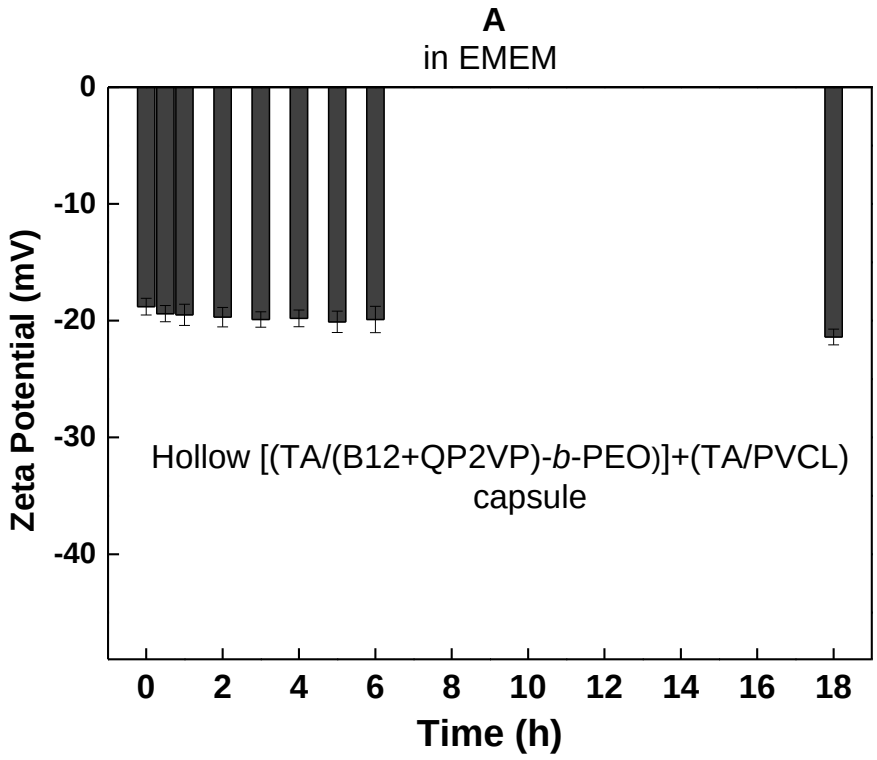

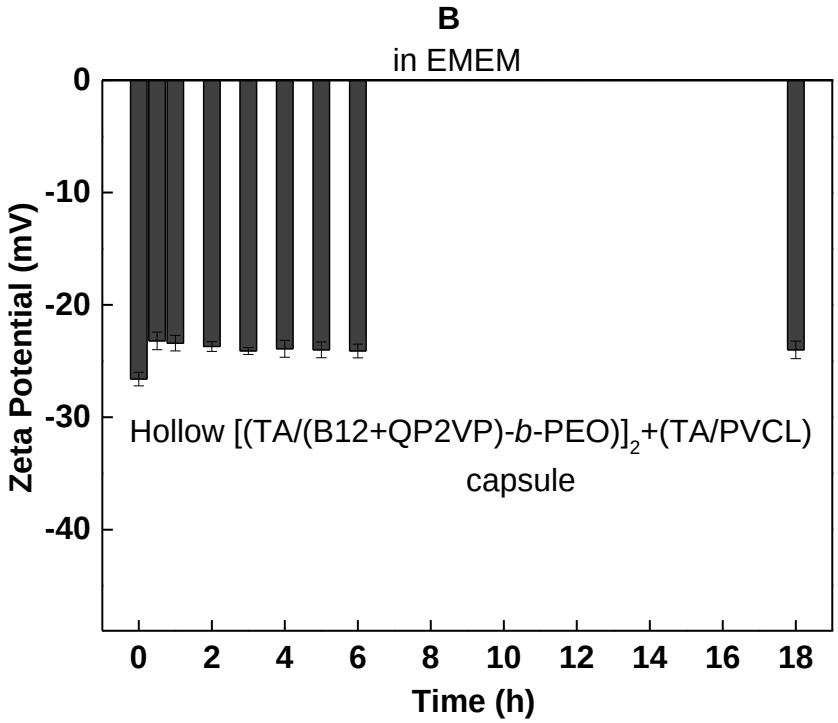

Figure 25. The EMEM stabilities of **(A)** Hollow [(TA/(B12+QP2VP)-*b*-PEO)] +(TA/PVCL) and **(B)** Hollow [(TA/(B12+QP2VP)-*b*-PEO)]$_2$+(TA/PVCL) capsules.

3.6 Determination of Boron Concentration in LbL Capsules

The boron concentration of non-hollow and hollow LbL capsules containing either one or two micellar layers were examined (Table 3). For non-hollow capsules the capsule concentration was ~ 10 mg/mL but the capsule concentrations of hollow capsules were not determined. The highest boron concentration was achieved with non-hollow capsules with 2 micellar layers - [(TA/(B12+QP2VP)-*b*-PEO)]$_2$+(TA/PVCL), indicating an increase in boron concentration with increasing number of micellar layers. Hollow [(TA/(B12+QP2VP)-*b*-PEO)]$_2$+(TA/PVCL) capsules were lower in boron concentration when compared with non-hollow [(TA/(B12+QP2VP)-*b*-PEO)]$_2$+(TA/PVCL). This may be correlated with the partial disruption of micellar layers during EDTA treatment. Similar decrease in boron

concentration upon dissolution of micellar cores was also recorded for capsules with one micellar layer, [(TA/(B12+QP2VP)-*b*-PEO)]+(TA/PVCL).

Table 3. Boron concentration of LbL capsules determided by ICP-OES.

Capsules	**Boron Concentration**
[(TA/(B12+QP2VP)-*b*-PEO)]$_2$+(TA/PVCL) capsules (10 mg/mL)	180 ±5 ppm (0.18 mg/mL)
Hollow [(TA/(B12+QP2VP)-*b*-PEO)]$_2$+(TA/PVCL) capsules	162 ±7 ppm (0.16 mg/mL)
[(TA/(B12+QP2VP)-*b*-PEO)]+(TA/PVCL) capsules (10 mg/mL)	140 ±2 ppm (0.14 mg/mL)
Hollow [(TA/(B12+QP2VP)-*b*-PEO)]+(TA/PVCL) capsules	113 ±4 (0.11 mg/mL)

3.7 Cell Viability

The survival of Hep G2 cells, a liver cancer model that is commonly employed in cytotoxicity research, was investigated in a concentration-dependent manner for cytotoxicity studies. The cytotoxicity of B12, QP2VP-*b*-PEO, [(TA/(B12+QP2VP)-*b*-PEO)]+(TA/PVCL) capsules, hollow [(TA/(B12+QP2VP)-*b*-PEO)]+(TA/PVCL) capsules, [(TA/(B12+QP2VP)-*b*-PEO)]$_2$+(TA/PVCL) capsules and hollow

[(TA/(B12+QP2VP)-*b*-PEO)]$_2$+(TA/PVCL) capsules were investigated. As seen in Figure 26, B12 showed IC_{50} which is the concentration that the proliferation of cells was reduced by 50 %. This was possibly caused from the counter cation of B12, triethylammonium.

Besides these results, QP2VP-*b*-PEO polymer reduced proliferation by ~35% regardless of its concentration. Since the (B12+QP2VP)-*b*-PEO micelles disintegrated in EMEM, the cytotoxicity data of micelles could not be determined. Promisingly, [(TA/(B12+QP2VP)-*b*-PEO)]$_2$+(TA/PVCL) capsules and hollow [(TA/(B12+QP2VP)-*b*-PEO)]$_2$+(TA/PVCL) capsules showed approximately 75% proliferation where the survival rate of [(TA/(B12+QP2VP)-*b*-PEO)]+(TA/PVCL) capsules and hollow [(TA/(B12+QP2VP)-*b*-PEO)]+(TA/PVCL) capsules were generally above 80%. These hybrid capsules may be promising for BNCT applications in the sense that capsules can reach the target site without causing any cytotoxic effect and ^{10}B isotopes found inside the structure of B12 can only be activated radio-chemically by thermal neutrons in order to show therapeutic effect. The cytotoxicity results are all tabulated on Figure 25.

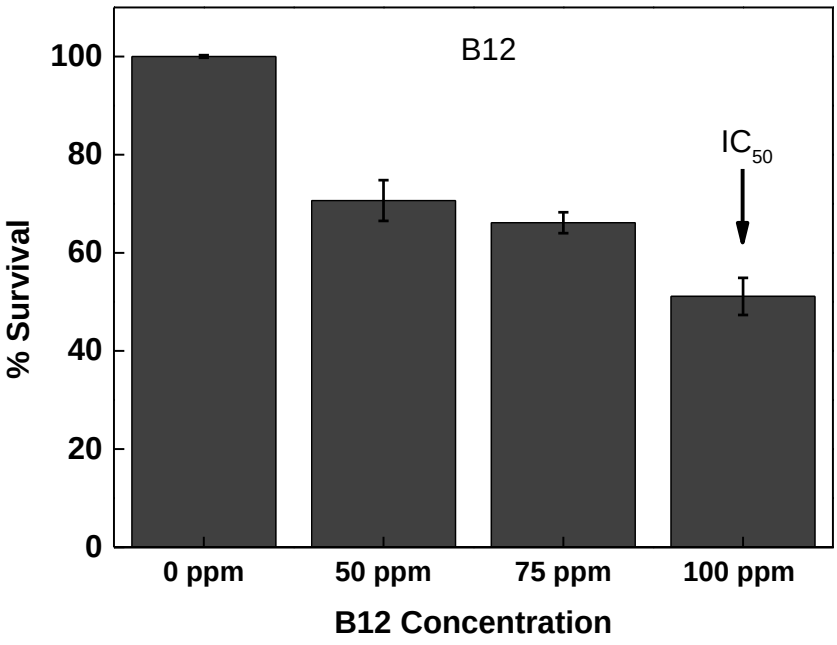
B12
IC50
% Survival
100
80
60
40
20
0
0 ppm
50 ppm
75 ppm
100 ppm
B12 Concentration

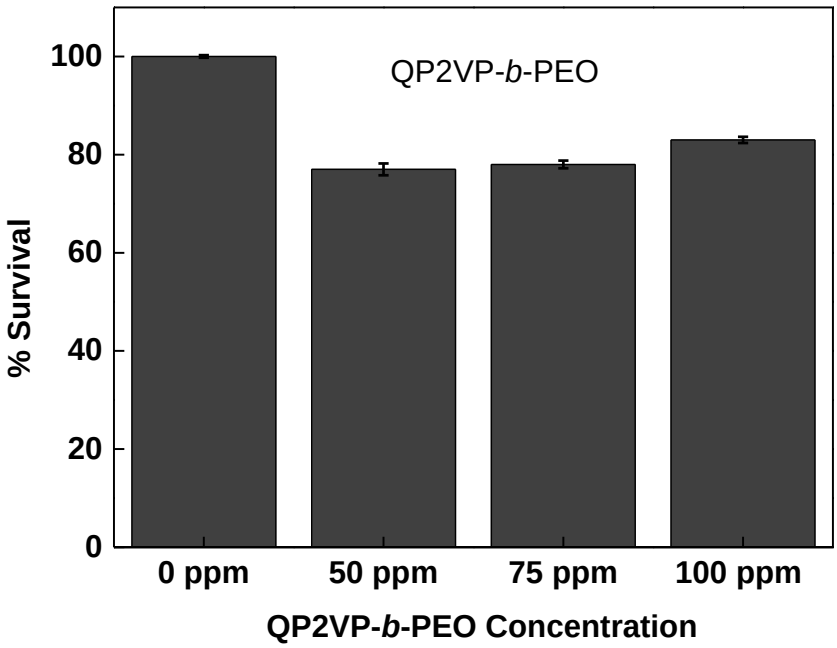
QP2VP-b-PEO
% Survival
100
80
60
40
20
0
0 ppm
50 ppm
75 ppm
100 ppm
QP2VP-b-PEO Concentration

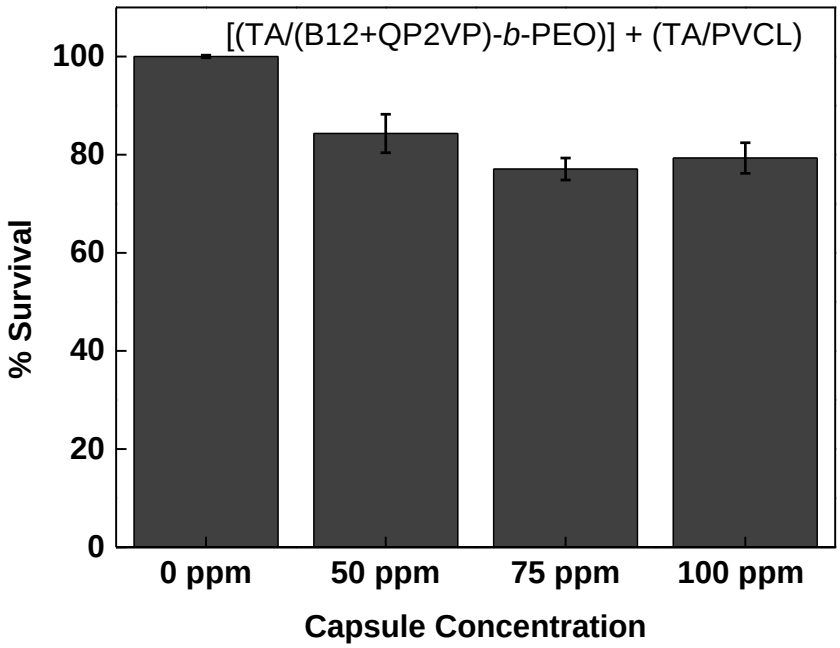
[(TA/(B12+QP2VP)-b-PEO)] + (TA/PVCL)
% Survival
100
80
60
40
20
0
0 ppm
50 ppm
75 ppm
100 ppm
Capsule Concentration

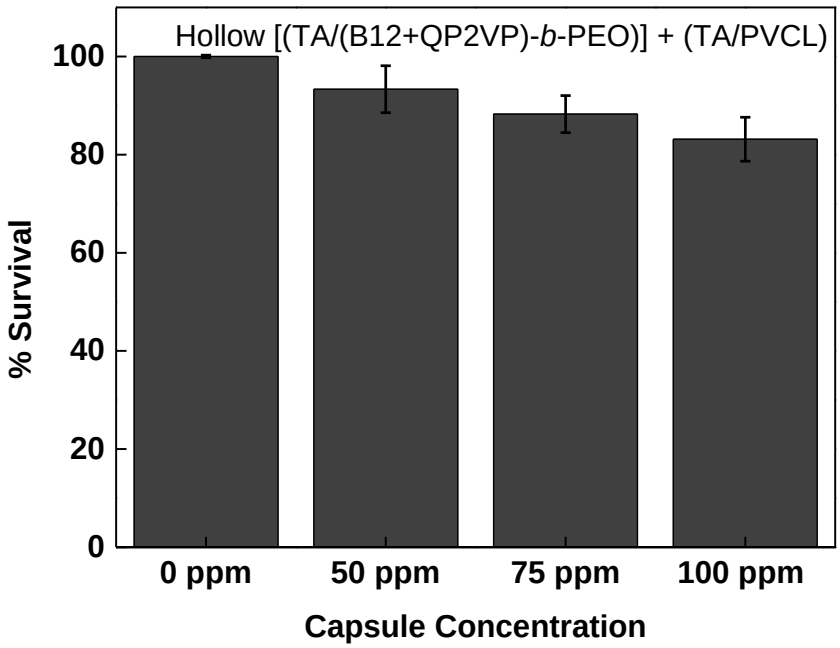
Hollow [(TA/(B12+QP2VP)-b-PEO)] + (TA/PVCL)
% Survival
100
80
60
40
20
0
0 ppm
50 ppm
75 ppm
100 ppm
Capsule Concentration

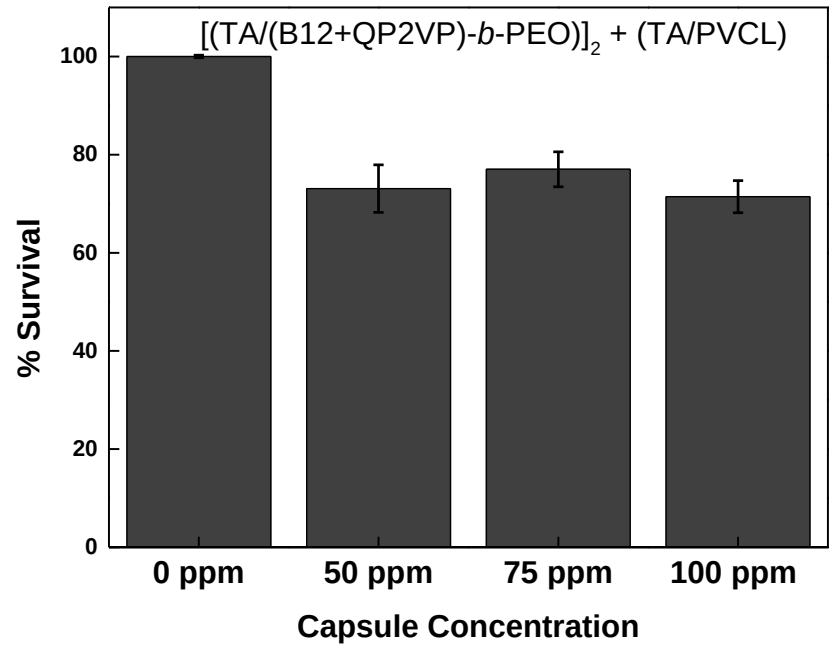

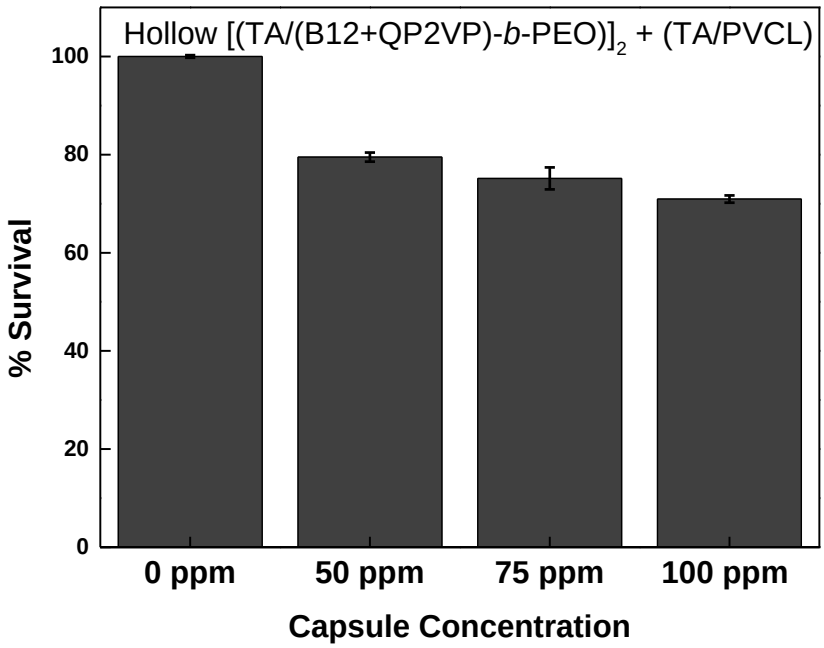

Figure 26. Proliferation of Hep G2 cells upon treatment with B12, QP2VP-*b*-PEO,

[(TA/(B12+QP2VP)-*b*-PEO)]+(TA/PVCL) capsules, hollow [(TA/(B12+QP2VP)-*b*-PEO)]+(TA/PVCL) capsules, $[(TA/(B12+QP2VP)\text{-}b\text{-}PEO)]_2$+(TA/PVCL) capsules, $[(TA/(B12+QP2VP)\text{-}b\text{-}PEO)]_2$+(TA/PVCL) capsules and hollow $[(TA/(B12+QP2VP)\text{-}b\text{-}PEO)]_2$+(TA/PVCL) capsules at 0, 50, 75 and 100 ppm concentrations after 24 hours.

3.8 Cellular Associations of LbL capsules

Cellular associations of LbL capsules were investigated by treating HepG2 cells with [(TA/(B12+QP2VP)-*b*-PEO)]+(TA/PVCL), [(TA/(B12+QP2VP)-*b*-PEO)]+(TA/PVCL), hollow $[(TA/(B12+QP2VP)\text{-}b\text{-}PEO)]_2$+(TA/PVCL) capsules and hollow $[(TA/(B12+QP2VP)\text{-}b\text{-}PEO)]_2$+(TA/PVCL) capsules at 100 ppm concentration for 24 hours. The cells were stained with phalloidin-iFluor 405 which binds strongly to the actin filaments of cytoskeleton and can be detected by an emission band and fluorescence intensity at ~400 nm. The capsules were loaded with curcumin (CUR), which has an excitation wavelength of 420 nm and emission wavelength of 470 nm [186]. Since the outermost layer of the capsule architecture is neutral PVCL, the electrostatic repulsion upon contact with the negatively charged cell membrane and polymer was eliminated. Additionally, PVCL has a LCST around 32^{o}C and hydrophobic interactions between the hydrophobic phospholipid tails and capsule shell might be enhanced at the incubation temperature of 37 ^{o}C. All capsules were seen to be associated with the cell membrane.

Figure 27 demonstrates a successful association between the cells and LbL capsules with 1 and 2 micellar layers. To confirm the loading of CUR in the capsules, a 150 μL aliquot of each capsule sample was dropped onto a glass slide and observed in the GFP channel (Figure 27A). All capsules were seen to emit florescence in the GFP channel (510 nm) suggesting that CUR could be effectively used as a reporter for these capsules.

An increment in layer number of the capsules did not result in any significant difference in the association of the capsules with HepG2 cells (Figure 27B and Figure 27D). Moreover, the hollow capsule architecture (Figure 27C and Figure 27E) did not change the association of the capsules with HepG2 cells either. Thus, all capsules were seen to be well-associated with cells and none of the capsules showed any major toxicity on HepG2 cells. However, none of the capsules were seen to be internalized by the cells. This is most likely because the capsule sizes were about 6 μm, which is too large for endocytosis; additionally, since HepG2 cells do not have any phagocytic characteristics[187], it was not possible for these cells to internalize the capsules by phagocytosis either. The size of the capsule in its current state may be too large for *in-vivo* applications that rely on internalization of the capsules. The capsule surface has been functionalized to be extremely hydrophilic and is therefore likely to attract a shell of water around it. Although this shell of water may hide the capsules from circulating immune cells, future studies are required to establish extent of activation of immune cells.

Based on the successful association of the capsules with epithelial cells, the capsules in their current form are more suited to deliver their cargo by cell association rather than internalization. The leaky nature of the blood vessels near a tumor site can ensure enrichment of the capsules in the tumor microenvironment [188]. Future studies will show whether thermal neutron flux exposure of the multilayer capsules containing B12 can kill cancer cells upon association with the cell surface.

A

100 µm
98 µm
98 µm
98 µm
[(TA/(B12+QP2VP)-b-PEO)] + (TA/PVCL) capsules
Hollow [(TA/(B12+QP2VP)-b-PEO)] + (TA/PVCL) capsules
[(TA/B12+QP2VP)-b-PEO)]2 + (TA/PVCL) capsules
Hollow [(TA/B12+QP2VP)-b-PEO)]2 + (TA/PVCL) capsules

B

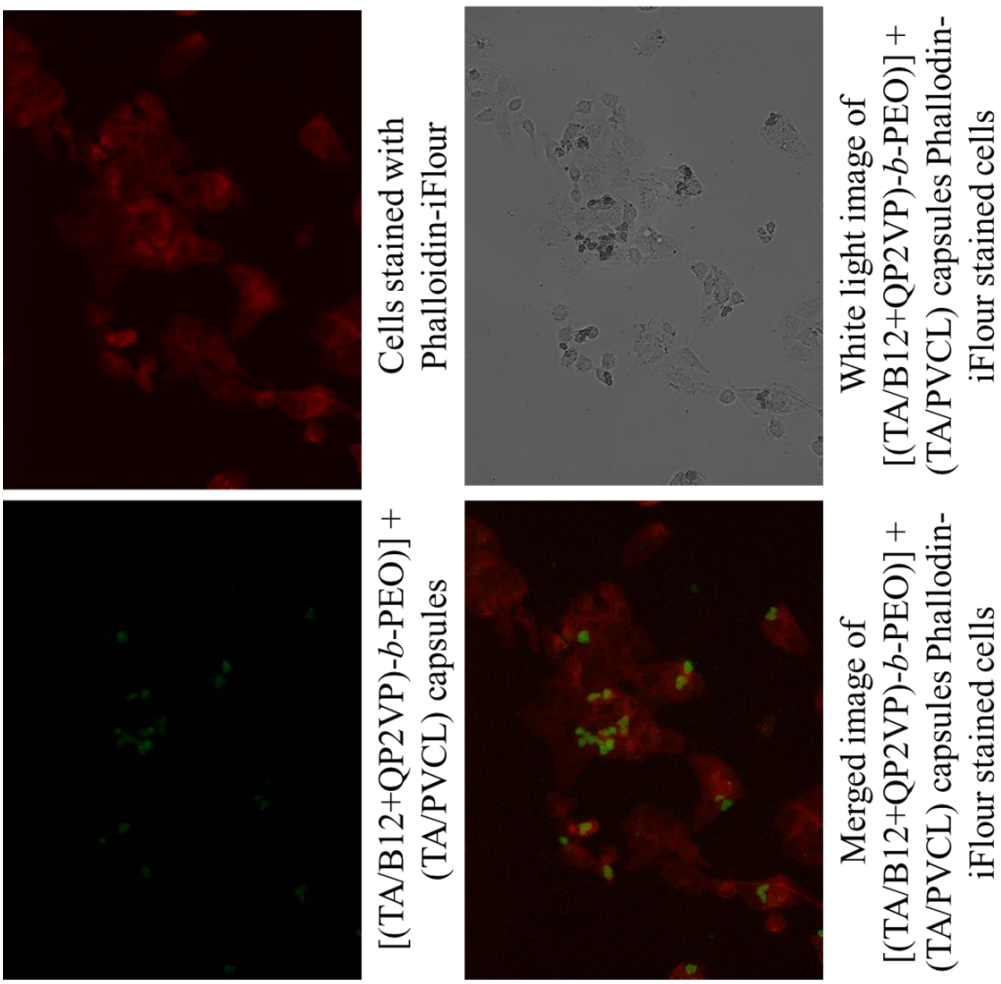
Cells stained with Phalloidin-iFlour
[(TA/B12+QP2VP)-b-PEO)] + (TA/PVCL) capsules
White light image of [(TA/B12+QP2VP)-b-PEO)] + (TA/PVCL) capsules Phallodin-iFlour stained cells
Merged image of [(TA/B12+QP2VP)-b-PEO)] + (TA/PVCL) capsules Phallodin-iFlour stained cells

C

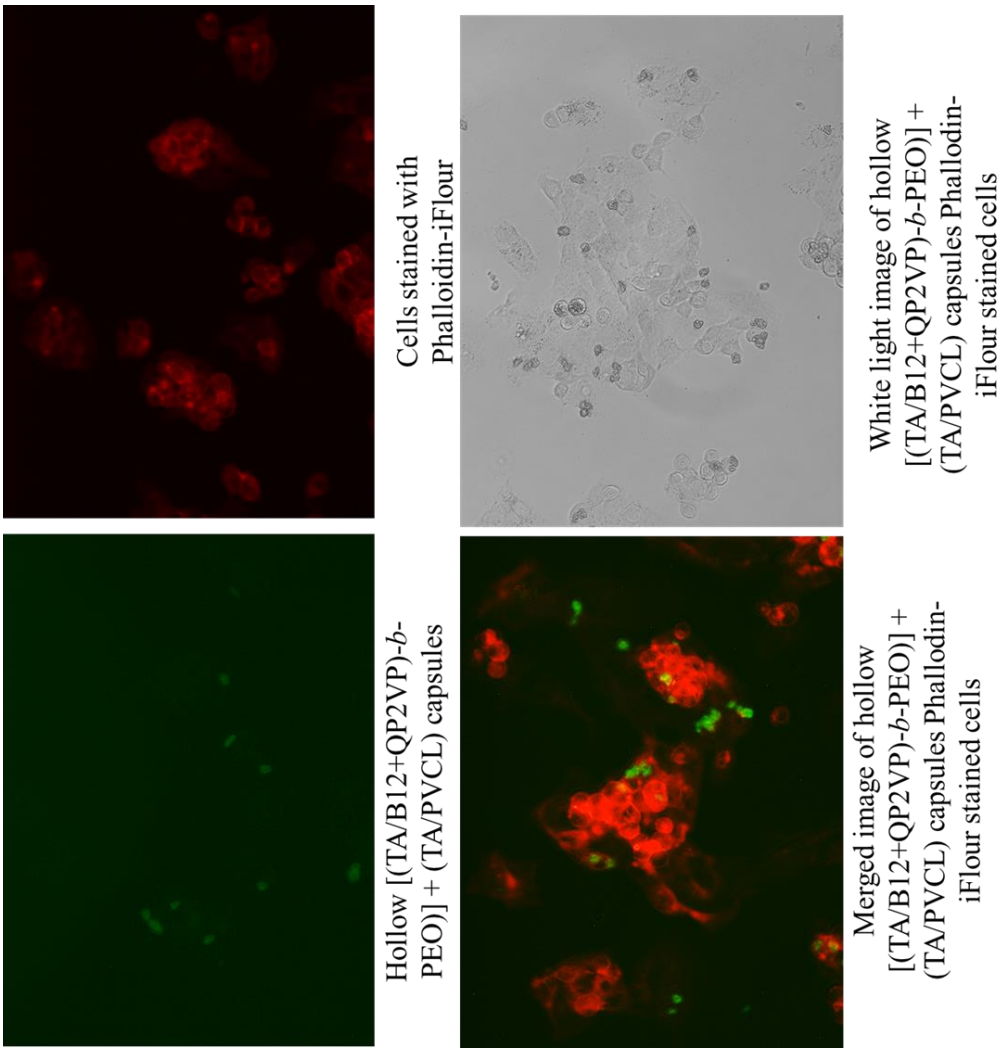
Cells stained with Phalloidin-iFlour
Hollow [(TA/B12+QP2VP)-b-PEO)] + (TA/PVCL) capsules
White light image of hollow [(TA/B12+QP2VP)-b-PEO)] + (TA/PVCL) capsules Phallodin-iFlour stained cells
Merged image of hollow [(TA/B12+QP2VP)-b-PEO)] + (TA/PVCL) capsules Phallodin-iFlour stained cells

D

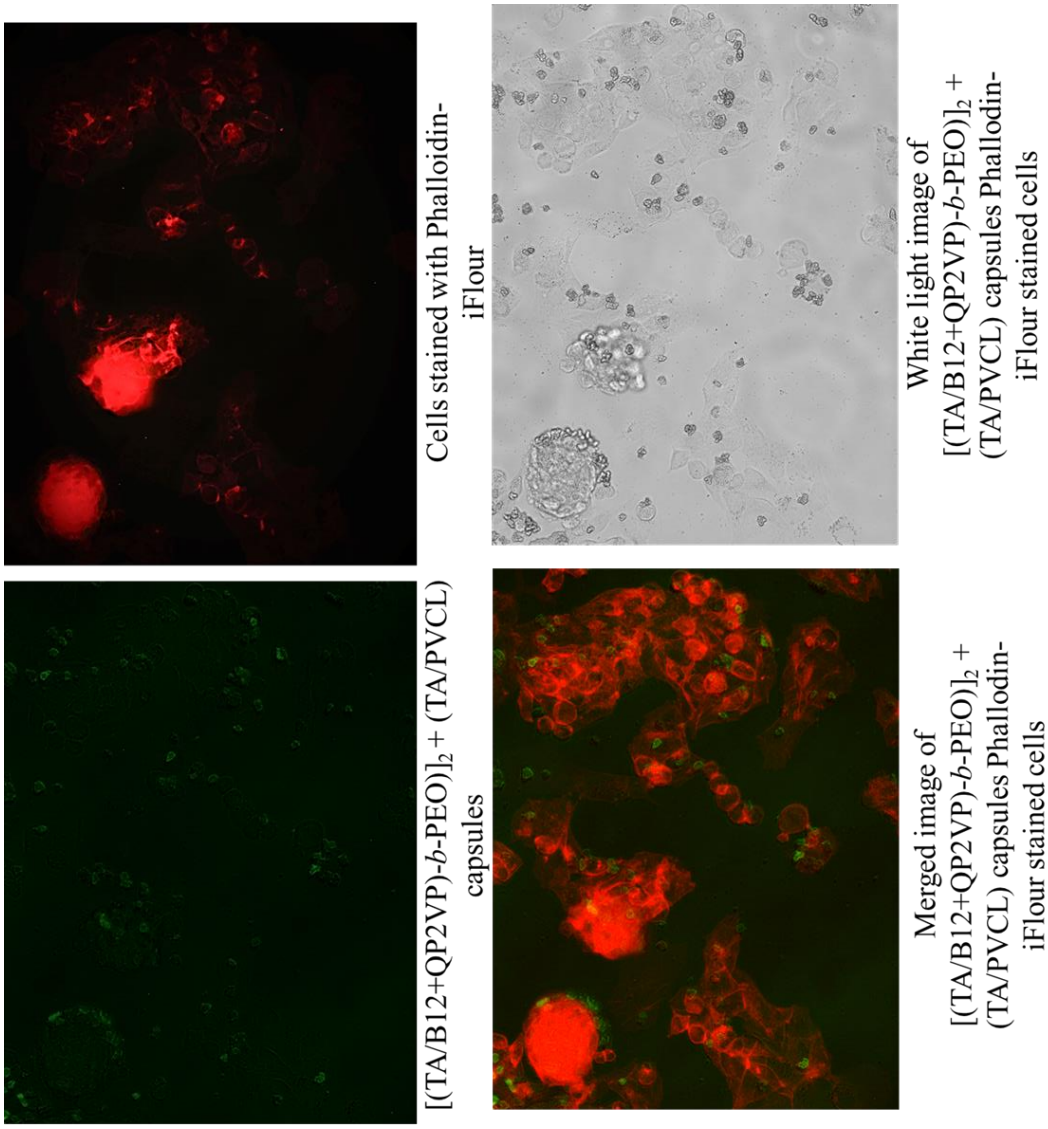
[(TA/B12+QP2VP)-b-PEO)]2 + (TA/PVCL) capsules
Cells stained with Phalloidin-iFlour
White light image of [(TA/B12+QP2VP)-b-PEO)]2 + (TA/PVCL) capsules Phallodin-iFlour stained cells
Merged image of [(TA/B12+QP2VP)-b-PEO)]2 + (TA/PVCL) capsules Phallodin-iFlour stained cells

E

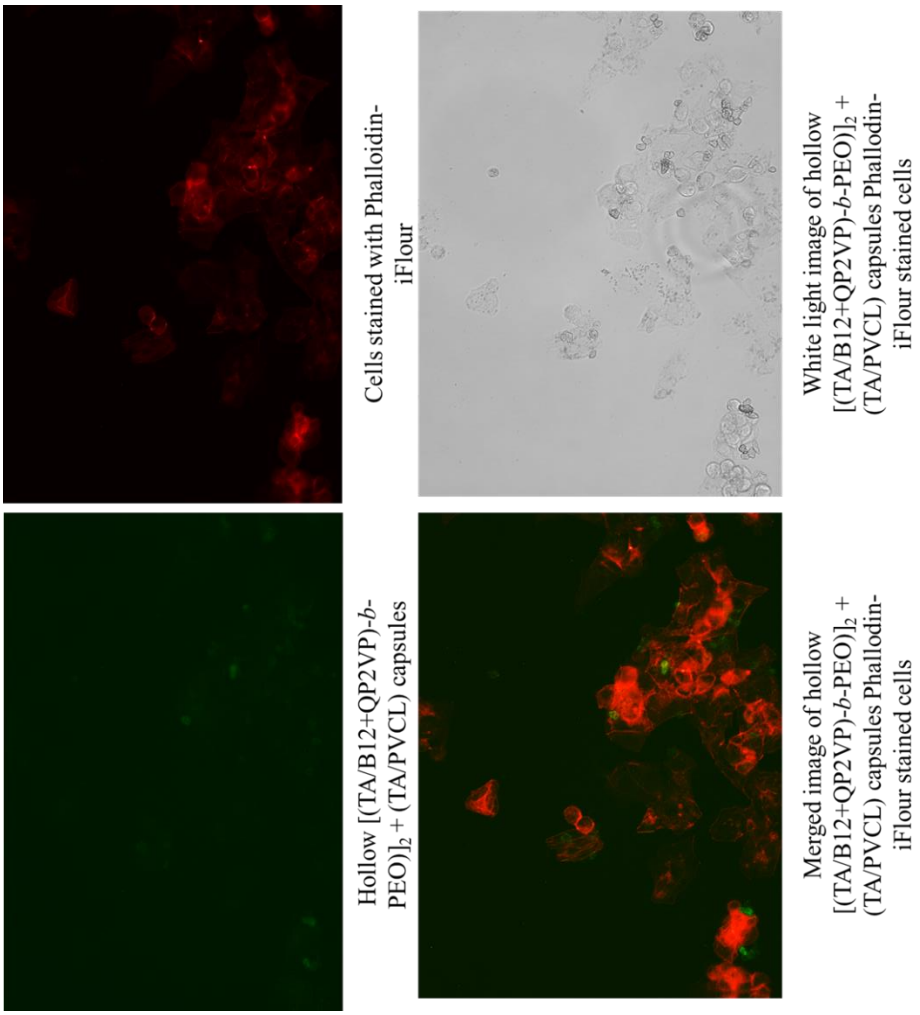

Figure 27. Cellular associations of [(TA/(B12+QP2VP)-*b*-PEO)]+(TA/PVCL) capsules, hollow [(TA/(B12+QP2VP)-*b*-PEO)]+(TA/PVCL) capsules $[(TA/(B12+QP2VP)\text{-}b\text{-}PEO)]_2$+(TA/PVCL) and hollow $[(TA/(B12+QP2VP)\text{-}b\text{-}PEO)]_2$+(TA/PVCL) capsules. The capsules were treated at 100 ppm concentration for 24 hours.

3.9 Determination of Boron Concentration of Capsule-Associated Cells with ICP-OES

The concentration of boron in non-hollow and hollow LbL capsules associated with Hep G2 cells were examined. Non-hollow capsules with either 1(labelled as A in Figure 28) or 2 micellar layers (labelled as C in Figure 28) as well as hollow capsules with 1 micellar layer (labelled as B in Figure 28) provided similar boron concentration. However, hollow capsules with 2 micellar layers (labelled as D in Figure 28) showed the lowest boron concentration. Considering the similar results obtained for the rest of the capsules, the cellular association of hollow capsules with 2 micellar layers need to be further conducted prior to suggest a clear conclusion.

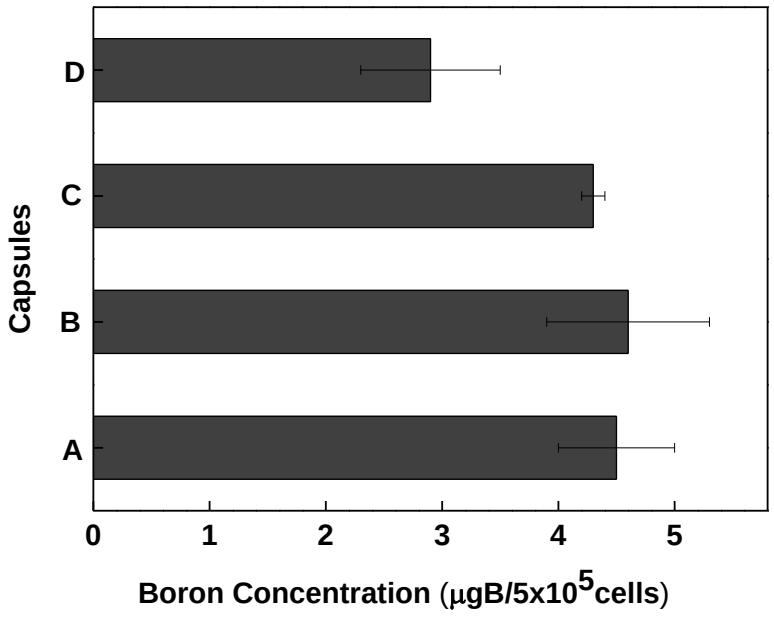

Figure 28. Boron concentration of **(A)** [(TA/(B12+QP2VP)-*b*-PEO)]+(TA/PVCL) capsules treated Hep G2 cells, **(B)** hollow [(TA/(B12+QP2VP)-*b*-PEO)]+(TA/PVCL) capsules treated Hep G2 cells, **(C)** [(TA/(B12+QP2VP)-*b*-PEO)]$_2$+(TA/PVCL) and **(D)** hollow [(TA/(B12+QP2VP)-*b*-PEO)]$_2$+(TA/PVCL) capsules treated cells.

CHAPTER 4

CONCLUSION AND OUTLOOK

This thesis study examined encapsulation of B12 by P2VP-*b*-PEO. Self-assembly of P2VP-*b*-PEO was induced through electrostatic association between protonated pyridine units of P2VP and B12 at acidic conditions. However, the resulting (B12+P2VP)-*b*-PEO micelles were found to be unstable as the pH was increased due to unprotonation of P2VP and loss of electrostatic association among P2VP and B12. To obtain stable micelles at physiological pH (pH 7.4), permanent charge was introduced to P2VP block through quaternization reaction of P2VP-*b*-PEO with CH_3I. The self-assembly of the quaternized polymer, QP2VP-*b*-PEO, in the presence of B12 molecules resulted in formation of micelles with (B12+QP2VP)-core and PEO-corona. (B12+QP2VP)-*b*-PEO micelles were stable against dilution with PBS at neutral pH. However, dilution with EMEM medium resulted in disintegration of micelles probably due to competitive interactions between B12 and EMEM ingredients, i.e. biological molecules and salt ions which resulted in loss of electrostatic association between QP2VP blocks and B12. This finding was critical when potential application of these aggregates for BNCT was considered. Because dissolution of micellar aggregates at an early stage can result in release of B12 before reaching the target site. For this reason, (B12+QP2VP)-*b*-PEO micelles were self-assembled onto CaCO3 microparticles through LbL self-assembly to enhance the stability of micelles at physiological conditions. TA was used to drive LbL assembly through hydrogen bonding interactions between ether oxygens of PEO-coronal chains and hydroxyl groups of TA. Increasing layer number induced aggregation of LbL capsules. Therefore, maximum two micellar layers could be deposited at the surface. LbL capsules were rendered stable in EMEM when a barrier stack composed of PVCL and TA was deposited onto multilayers containing (B12+QP2VP)-*b*-PEO

micelles and TA. For comparison purposes in biochemical assays, LbL capsules were also made hollow through EDTA treatment.

The capsules showed minimum cytotoxicity by screening B12's cytotoxicity at 100 ppm concentration due to the triethylammonium counter cation. All capsules promoted cell viability over 70%.

Cellular incorporation experiments showed associations with Hep G2 cells regardless of number of the layers deposited or dissolution of sacrificial $CaCO_3$ cores. The cells were not able to internalize the capsules since the capsule sizes (~6 μm) exceeds the phagocytotic ability due to the epithelial nature of Hep G2 cells. However, all capsules associated with cellular membranes which is promising to carry boron cargo to cells. According to ICP-OES experiments, all types of capsules delivered boron to the cells.

Use of the LbL capsules for BNCT applications need to be further evaluated through thermal neutron illumination.

REFERENCES

[1] D. Patel, R. Jana, M. Lin, K. Kuperkar, D. Seth, L. Chen, P. Bahadur, Revisiting the salt-triggered self-assembly in very hydrophilic triblock copolymer Pluronic ® F88 using multitechnique approach, Colloid Polym. Sci. 1 (2021) 1113-1126.

[2] A. Gandini, H. Cheradame, Advances in Polymer Science, in: V. Abetz (Ed.), Block copolymers I, Springer-Verlag Berlin 2005: pp. 5-6.

[3] C.J. Hawker, K.L. Wooley, The Convergence of Synthetic Organic and Polymer Chemistries, Science. 309 (2005) 1200.

[4] P. Alexandridis, B. Lindman, eds., Amphiphilic Block Copolymers, Elsevier, Amsterdam, The Netherlands, 2000.

[5] N. Rapoport, Physical stimuli-responsive polymeric micelles for anti-cancer drug delivery, Prog. Polym. Sci. 32 (2007) 962–990.

[6] S. Förster, M. Antonietti, Amphiphilic block copolymers in structure-controlled nanomaterial hybrids, Adv. Mater. 10 (1998) 195–217.

[7] H.K. Cho, I.W. Cheong, J.M. Lee, J.H. Kim, Polymeric nanoparticles, micelles and polymersomes from amphiphilic block copolymer, Korean J. Chem. Eng. 27 (2010) 731–740.

[8] K.J. Hanley, T.P. Lodge, Phase behavior of a block copolymer in solvents of varying selectivity, Macromolecules. 33 (2000) 5918–5931.

[9] A. Blanazs, S.P. Armes, A.J. Ryan, Self-assembled block copolymer aggregates: From micelles to vesicles and their biological applications, Macromol. Rapid Commun. 30 (2009) 267–277.

[10] S. Whitelam, R.L. Jack, The statistical mechanics of dynamic pathways to self-assembly, Annu. Rev. Phys. Chem. 66 (2015) 143–163.

[11] G.M. Whitesides, B. Grzybowski, Self-assembly at all scales, Science 295 (2002) 2418–2421.

[12] S. Bekiranov, R. Bruinsma, P. Pincus, Solution behavior of polyethylene oxide in water as a function of temperature and pressure, Phys. Rev. E. 55 (1997) 577–585.

[13] U. Tritschler, S. Pearce, J. Gwyther, G.R. Whittell, I. Manners, 50th Anniversary Perspective: Functional Nanoparticles from the Solution Self-Assembly of Block Copolymers, Macromolecules 50 (2017) 3439–3463.

[14] J.N. Israelachvili,Thermodynamic Principles of Self-Assembly, in: Intermolecular and Surface Forces, Academic Press, 2011, pp. 503-534.

[15] Y. Lu, E. Zhang, J. Yang, Z. Cao, Strategies to improve micelle stability for drug delivery, Nano Res. 11 (2018) 4985–4998.

[16] S. Kim, Y. Shi, J.Y. Kim, K. Park, J.X. Cheng, Overcoming the barriers in micellar drug delivery: Loading efficiency, in vivo stability, and micelle-cell interaction, Expert Opin. Drug Deliv. 7 (2010) 49–62.

[17] M.-C. Jones, J.-C. Leroux, Polymeric micelles – a new generation of colloidal drug carriers, Eur. J. Pharm. Biopharm. 48 (1999) 101–111.

[18] A. Vonarbourg, C. Passirani, P. Saulnier, J.-P. Benoit, Parameters influencing the stealthiness of colloidal drug delivery systems, Biomaterials. 27 (2006) 4356–4373.

[19] G. Kwon, S. Suwa, M. Yokoyama, T. Okano, Y. Sakurai, K. Kataoka, Enhanced tumor accumulation and prolonged circulation times of micelle-forming poly (ethylene oxide-aspartate) block copolymer-adriamycin conjugates, J. Control. Release. 29 (1994) 17–23.

[20] H. Cui, Z. Chen, S. Zhong, K.L. Wooley, D.J. Pochan, Block Copolymer Assembly via Kinetic Control, Science 317 (2007) 647 – 650.

[21] S. Li, C.J. Clarke, R.B. Lennox, A. Eisenberg, Two-dimensional self

assembly of polystyrene-b-poly (butyl-methacrylate) diblock copolymers, Colloids Surfaces A Physicochem. Eng. Asp. 133 (1998) 191–203.

[22] T. Nicolai, O. Colombani, C. Chassenieux, Dynamic polymeric micelles versus frozen nanoparticles formed by block copolymers, Soft Matter. 6 (2010) 3111–3118.

[23] K.S. Soppimath, T.M. Aminabhavi, A.R. Kulkarni, W.E. Rudzinski, Biodegradable polymeric nanoparticles as drug delivery devices, J. Control. Release. 70 (2001) 1–20.

[24] G.S. Kwon, T. Okano, Soluble Self-Assembled Block Copolymers for Drug Delivery, Pharm. Res. 16 (1999) 597–600.

[25] K. Khougaz, I. Astafieva, A. Eisenberg, Micellization in Block Polyelectrolyte Solutions. 3. Static Light Scattering Characterization, Macromolecules. 28 (1995) 7135–7147.

[26] L. Illum, S.S. Davis, The organ uptake of intravenously administered colloidal particles can be altered using a non-ionic surfactant (Poloxamer 338), FEBS Lett. 167 (1984) 79–82.

[27] L. Ilium, I.M. Hunneyball, S.S. Davis, The effect of hydrophilic coatings on the uptake of colloidal particles by the liver and by peritoneal macrophages, Int. J. Pharm. 29 (1986) 53–65.

[28] E. Evans, D. Needham, Physical properties of surfactant bilayer membranes: thermal transitions, elasticity, rigidity, cohesion and colloidal interactions, J. Phys. Chem. 91 (1987) 4219–4228..

[29] F. Meng, Z. Zhong, Polymersomes Spanning from Nano- to Microscales: Advanced Vehicles for Controlled Drug Delivery and Robust Vesicles for Virus and Cell Mimicking, J. Phys. Chem. Lett. 2 (2011) 1533–1539.

[30] M.E. Yildiz, R.K. Prud'homme, I. Robb, D.H. Adamson, Formation and characterization of polymersomes made by a solvent injection method, Polym.

Adv. Technol. (2008)

[31] X. Hu, Y. Zhang, Z. Xie, X. Jing, A. Bellotti, Z. Gu, Stimuli-Responsive Polymersomes for Biomedical Applications, Biomacromolecules. 18 (2017) 649–673.

[32] Y. Kotsuchibashi, M. Ebara, T. Aoyagi, R. Narain, Recent advances in dual temperature responsive block copolymers and their potential as biomedical applications, Polymers (Basel). 8 (2016).

[33] P. Ray, N. Kale, M. Quadir, New side chain design for pH-responsive block copolymers for drug delivery, Colloids Surfaces B Biointerfaces. 200 (2021) 111563.

[34] Y.C. Chung, C.H. Yang, R.H. Lee, T.L. Wang, Dual Stimuli-Responsive Block Copolymers for Controlled Release Triggered by Upconversion Luminescence or Temperature Variation, ACS Omega. 4 (2019) 3322–3328.

[35] B. Ozbas, J. Kretsinger, K. Rajagopal, J.P. Schneider, D.J. Pochan, Salt-triggered peptide folding and consequent self-assembly into hydrogels with tunable modulus, Macromolecules. 37 (2004) 7331–7337.

[36] E. Cabane, X. Zhang, K. Langowska, C.G. Palivan, W. Meier, Stimuli-responsive polymers and their applications in nanomedicine, Biointerphases. 7 (2012) 1–27.

[37] D. Schmaljohann, Thermo- and pH-responsive polymers in drug delivery, Adv. Drug Deliv. Rev. 58 (2006) 1655–1670.

[38] A.A. Moghanjoughi, D. Khoshnevis, A. Zarrabi, A concise review on smart polymers for controlled drug release, Drug Deliv. Transl. Res. (2016) 333–340.

[39] H. Mao, C. Li, Y. Zhang, D.E. Bergbreiter, P.S. Cremer, Measuring LCSTs by Novel Temperature Gradient Methods: Evidence for Intermolecular Interactions in Mixed Polymer Solutions, J. Am. Chem. Soc. 125 (2003)

2850–2851..

[40] G. Molinaro, J.-C. Leroux, J. Damas, A. Adam, Biocompatibility of thermosensitive chitosan-based hydrogels: an in vivo experimental approach to injectable biomaterials, Biomaterials. 23 (2002) 2717–2722.

[41] H. Priya James, R. John, A. Alex, K.R. Anoop, Smart polymers for the controlled delivery of drugs - a concise overview., Acta Pharm. Sin. B. 4 (2014) 120–127.

[42] M.I. Gibson, R.K. O'reilly, To aggregate, or not to aggregate? Considerations in the design and application of polymeric thermally-responsive nanoparticles, Chem. Soc. Rev. 42 (2013) 7204–7213.

[43] A. Chan, R.P. Orme, R.A. Fricker, P. Roach, Remote and local control of stimuli responsive materials for therapeutic applications, Adv. Drug Deliv. Rev. 65 (2013) 497–514.

[44] G. Kocak, C. Tuncer, V. Bütün, PH-Responsive polymers, Polym. Chem. 8 (2017) 144–176.

[45] S. Kalepu, V. Nekkanti, Insoluble drug delivery strategies: review of recent advances and business prospects, Acta Pharm. Sin. B. 5 (2015) 442–453.

[46] G. Gaucher, M.H. Dufresne, V.P. Sant, N. Kang, D. Maysinger, J.C. Leroux, Block copolymer micelles: Preparation, characterization and application in drug delivery, J. Control. Release. 109 (2005) 169–188.

[47] N.A.N. Hanafy, M. El-Kemary, S. Leporatti, Micelles Structure Development as a Strategy to Improve Smart Cancer Therapy, Cancers . 10 (2018) 238.

[48] X. Zhang, H.M. Burt, G. Mangold, D. Dexter, D. Von Hoff, L. Mayer, W.L. Hunter, Anti-tumor efficacy and biodistribution of intravenous polymeric micellar paclitaxel, Anticancer. Drugs. 8 (1997) 696–701.

[49] N.Y. Rapoport, J.N. Herron, W.G. Pitt, L. Pitina, Micellar delivery of doxorubicin and its paramagnetic analog, ruboxyl, to HL-60 cells: effect of

micelle structure and ultrasound on the intracellular drug uptake, J. Control. Release. 58 (1999) 153–162.

[50] X. Zhang, J.K. Jackson, H.M. Burt, Development of amphiphilic diblock copolymers as micellar carriers of taxol, Int. J. Pharm. 132 (1996) 195–206.

[51] T. Hamaguchi, Y. Matsumura, M. Suzuki, K. Shimizu, R. Goda, I. Nakamura, I. Nakatomi, M. Yokoyama, K. Kataoka, T. Kakizoe, NK105, a paclitaxel-incorporating micellar nanoparticle formulation, can extend in vivo antitumour activity and reduce the neurotoxicity of paclitaxel, Br. J. Cancer. 92 (2005) 1240–1246.

[52] N. Nishiyama, K. Kataoka, Current state, achievements, and future prospects of polymeric micelles as nanocarriers for drug and gene delivery, Pharmacol. Ther. 112 (2006) 630–648.

[53] A.S. Deshmukh, P.N. Chauhan, M.N. Noolvi, K. Chaturvedi, K. Ganguly, S.S. Shukla, M.N. Nadagouda, T.M. Aminabhavi, Polymeric micelles: Basic research to clinical practice, Int. J. Pharm. 532 (2017) 249–268.

[54] R.D. Issels, Hyperthermia adds to chemotherapy, Eur. J. Cancer. 44 (2008) 2546–2554.

[55] Y. Li, T. Zhao, C. Wang, Z. Lin, G. Huang, B.D. Sumer, J. Gao, Molecular basis of cooperativity in pH-triggered supramolecular self-assembly, Nat. Commun. 7 (2016) 1–9.

[56] E.S. Lee, K. Na, Y.H. Bae, Polymeric micelle for tumor pH and folate-mediated targeting, J. Control. Release. 91 (2003) 103–113.

[57] Y. Bae, N. Nishiyama, S. Fukushima, H. Koyama, M. Yasuhiro, K. Kataoka, Preparation and biological characterization of polymeric micelle drug carriers with intracellular pH-triggered drug release property: Tumor permeability, controlled subcellular drug distribution, and enhanced in vivo antitumor efficacy, Bioconjug. Chem. 16 (2005) 122–130.

[58] E.S. Lee, K. Na, Y.M. Bae, Super pH-sensitive multifunctional polymeric micelle, Nano Lett. 5 (2005) 325–329.

[59] W.C. Hess, M.X. Sullivan, pH-Dependent Micellization of Poly(2-vinylpyridine)-block-poly(ethylene oxide), J. Am. Chem. Soc. 63 (1941) 882–884.

[60] F.C. Giacomelli, P. Stepánek, C. Giacomelli, V. Schmidt, E. Jäger, A. Jäger, K. Ulbrich, PH-triggered block copolymer micelles based on a pH-responsive PDPA (poly[2-(diisopropylamino)ethyl methacrylate]) inner core and a PEO (poly(ethylene oxide)) outer shell as a potential tool for the cancer therapy, Soft Matter. 7 (2011) 9316–9325.

[61] F. Colotta, P. Allavena, A. Sica, C. Garlanda, A. Mantovani, Cancer-related inflammation, the seventh hallmark of cancer: links to genetic instability, Carcinogenesis. 30 (2009) 1073–1081.

[62] S. Purushotham, P.E.J. Chang, H. Rumpel, I.H.C. Kee, R.T.H. Ng, P.K.H. Chow, C.K. Tan, R. V. Ramanujan, Thermoresponsive core-shell magnetic nanoparticles for combined modalities of cancer therapy, Nanotechnology. 20 (2009).

[63] S. Chen, Y. Li, C. Guo, J. Wang, J. Ma, X. Liang, L.-R. Yang, H.-Z. Liu, Temperature-Responsive Magnetite/PEO−PPO−PEO Block Copolymer Nanoparticles for Controlled Drug Targeting Delivery, Langmuir. 23 (2007) 12669–12676.

[64] D. Roy, W.L.A. Brooks, B.S. Sumerlin, New directions in thermoresponsive polymers, Chem. Soc. Rev. 42 (2013) 7214–7243.

[65] D. Neradovic, O. Soga, C.F. Van Nostrum, W.E. Hennink, The effect of the processing and formulation parameters on the size of nanoparticles based on block copolymers of poly(ethylene glycol) and poly(N-isopropylacrylamide) with and without hydrolytically sensitive groups, Biomaterials. 25 (2004) 2409–2418.

[66] H. Wei, X.-Z. Zhang, Y. Zhou, S.-X. Cheng, R.-X. Zhuo, Self-assembled thermoresponsive micelles of poly(N-isopropylacrylamide-b-methyl methacrylate), Biomaterials. 27 (2006) 2028–2034.

[67] S. Glatzel, N. Badi, M. Päch, A. Laschewsky, J.F. Lutz, Well-defined synthetic polymers with a protein-like gelation behavior in water, Chem. Commun. 46 (2010) 4517–4519.

[68] J. Seuring, F.M. Bayer, K. Huber, S. Agarwal, Upper Critical Solution Temperature of Poly(N-acryloyl glycinamide) in Water: A Concealed Property, Macromolecules. 45 (2012) 374–384.

[69] M. Arotçaréna, B. Heise, S. Ishaya, A. Laschewsky, Switching the Inside and the Outside of Aggregates of Water-Soluble Block Copolymers with Double Thermoresponsivity, J. Am. Chem. Soc. 124 (2002) 3787–3793.

[70] P. Yusan, I. Tuncel, V. Bütün, A.L. Demirel, I. Erel-Goktepe, PH-responsive layer-by-layer films of zwitterionic block copolymer micelles, Polym. Chem. 5 (2014) 3777–3787.

[71] S.M.N. Simões, A.R. Figueiras, F. Veiga, A. Concheiro, C. Alvarez-Lorenzo, Polymeric micelles for oral drug administration enabling locoregional and systemic treatments, Expert Opin. Drug Deliv. 12 (2015) 297–318.

[72] P. Alexandridis, J.F. Holzwarth, Differential scanning calorimetry investigation of the effect of salts on aqueous solution properties of an amphiphilic block copolymer (poloxamer), Langmuir. 13 (1997) 6074–6081.

[73] P. Alexandridis, J.F. Holzwarth, T.A. Hatton, Micellization of Poly(ethylene oxide)-Poly(propylene oxide)-Poly(ethylene oxide) Triblock Copolymers in Aqueous Solutions: Thermodynamics of Copolymer Association, Macromolecules. 27 (1994) 2414–2425.

[74] K. Patel, P. Bahadur, C. Guo, J.H. Ma, H.Z. Liu, K. Nakashima, Salt-induced micellization of pluronic F88 in water, J. Dispers. Sci. Technol. 29 (2008)

748–755.

[75] Y.L. Su, X.F. Wei, H.Z. Liu, Effect of sodium chloride on association behavior of poly(ethylene oxide)-poly(propylene oxide)-poly(ethylene oxide) block copolymer in aqueous solutions, J. Colloid Interface Sci. 264 (2003) 526–531.

[76] A. Bahadur, S. Cabana-Montenegro, V.K. Aswal, E. V. Lage, I. Sandez-Macho, A. Concheiro, C. Alvarez-Lorenzo, P. Bahadur, NaCl-triggered self-assembly of hydrophilic poloxamine block copolymers, Int. J. Pharm. 494 (2015) 453–462.

[77] H. Hooshyar, R. Sadeghi, Influence of sodium salts on the micellization and interfacial behavior of cationic surfactant dodecyltrimethylammonium bromide in aqueous solution, J. Chem. Eng. Data. 60 (2015) 983–992.

[78] M.S. Cretan, V. Purcar, M. Popa, M. Daraba, L.I. Atanase, L. Ochiuz, Drug Delivery System Based on pH-Sensitive Biocompatible Poly (2-vinyl pyridine) -*b*- poly (ethylene oxide) Nanomicelles Loaded with Curcumin and 5-Fluorouracil, 12 (2020) 1–19.

[79] C. Ustoglu, E. Cagli, I. Erel-Goktepe, Layer-by-layer films of block copolymer micelles with cores exhibiting upper critical solution temperature behaviour, Eur. Polym. J. 96 (2017) 278–294.

[80] X. Jia, D. Chen, M. Jiang, Preparation of PEO-b-P2VPH+-S2O82- micelles in water and their reversible UCST and redox-responsive behavior, Chem. Commun. 16 (2006) 1736–1738.

[81] D.S. Linnik, Y. V. Tarakanchikova, M. V. Zyuzin, K. V. Lepik, J.L. Aerts, G. Sukhorukov, A.S. Timin, Layer-by-Layer technique as a versatile tool for gene delivery applications, Expert Opin. Drug Deliv. (2021) 1–19.

[82] K.C. Krogman, R.E. Cohen, P.T. Hammond, M.F. Rubner, B.N. Wang, Industrial-scale spray layer-by-layer assembly for production of biomimetic

photonic systems, 8 (2013) 1-11.

[83] D. Alkekhia, P.T. Hammond, A. Shukla, Layer-by-Layer Biomaterials for Drug Delivery, (2020).

[84] X. Zhang, T. Liang, Q. Ma, Layer-by-Layer assembled nano-drug delivery systems for cancer treatment, Drug Deliv. 28 (2021) 655–669.

[85] Y. Fukuda, T. Akagi, T. Asaoka, H. Eguchi, K. Sasaki, Y. Iwagami, D. Yamada, T. Noda, K. Kawamoto, K. Gotoh, S. Kobayashi, M. Mori, Y. Doki, M. Akashi, Layer-by-layer cell coating technique using extracellular matrix facilitates rapid fabrication and function of pancreatic β-cell spheroids, Biomaterials. 160 (2018) 82–91.

[86] M.M. Barsan, M. David, M. Florescu, L. Ţugulea, C.M.A. Brett, A new self-assembled layer-by-layer glucose biosensor based on chitosan biopolymer entrapped enzyme with nitrogen doped graphene, Bioelectrochemistry. 99 (2014) 46–52.

[87] X. Cai, X. Gao, L. Wang, Q. Wu, X. Lin, A layer-by-layer assembled and carbon nanotubes/gold nanoparticles-based bienzyme biosensor for cholesterol detection, Sensors Actuators B Chem. 181 (2013) 575–583.

[88] R.K. Iler, Multilayers of colloidal particles, J. Colloid Interface Sci. 21 (1966) 569–594.

[89] G. Decher, Fuzzy nanoassemblies: Toward layered polymeric multicomposites, Science. 277 (1997) 1232–1237.

[90] F. Caruso, G.K. Such, A.P.R. Johnston, F. Caruso, Chem Soc Rev Engineered hydrogen-bonded polymer multilayers : from assembly to biomedical applications, 40 (2011) 19-29.

[91] W.B. Stockton, M.F. Rubner, Molecular-level processing of conjugated polymers. 3. Layer-by-layer manipulation of polyaniline via electrostatic interactions, Macromolecules. 30 (1997) 2712–2716.

[92] D.M. Delongchamp, P.T. Hammond, Highly Ion Conductive Poly (ethylene oxide) -Based Solid Polymer Electrolytes from Hydrogen Bonding Layer-by-Layer Assembly, Langmuir, 20 (2004) 5403–5411.

[93] E. Kharlampieva, S.A. Sukhishvili, Hydrogen - Bonded Layer - by - Layer Polymer Films Hydrogen-Bonded Layer-by-Layer Polymer Films, Journal of Macromolecular Science, Part C: Polymer Reviews, 46 (2006) 377-395.

[94] O.S. Fenton, K.N. Olafson, P.S. Pillai, M.J. Mitchell, R. Langer, Advances in Biomaterials for Drug Delivery, Adv. Mater. 30 (2018) 1705328.

[95] G.B. Sukhorukov, A.L. Rogach, B. Zebli, T. Liedl, A.G. Skirtach, K. Köhler, A.A. Antipov, N. Gaponik, A.S. Susha, M. Winterhalter, W.J. Parak, Nanoengineered Polymer Capsules : Tools for Detection , Controlled Delivery , and Site-Specific Manipulation, (2005) 194–200.

[96] D.A. Links, A.G. Skirtach, A.M. Yashchenok, H. Mo, Encapsulation, release and applications of LbL polyelectrolyte multilayer capsules, Chem. Commun. 47 (2011) 12736–12746.

[97] A. Mateos-Maroto, I. Abelendan, F. Ortega, G. Rubio, E. Guzman, Polyelectrolyte Multilayers on Soft Colloidal Nanosurfaces : A New Life for the Layer-By-Layer Method, Polymers. 13 (2021) 1221.

[98] E. Donath, G.B. Sukhorukov, F. Caruso, S.A. Davis, H. Möhwald, Novel Hollow Polymer Shells by Colloid-Tem- plated Assembly of Polyelectrolytes, Angew. Chem. Int. Ed. 37 (1998) 2201–2205.

[99] Y. Yan, M. Bjo, F. Caruso, Assembly of Layer-by-Layer Particles and Their Interactions with Biological Systems, Chem. Mater. 26 (2014) 452-460.

[100] K. Ariga, Y.M. Lvov, K. Kawakami, Q. Ji, J.P. Hill, Layer-by-layer self-assembled shells for drug delivery, Adv. Drug Deliv. Rev. 63 (2011) 762–771.

[101] S.J. Son, X. Bai, S.B. Lee, Inorganic hollow nanoparticles and nanotubes in

nanomedicine: Part 1. Drug/gene delivery applications, Drug Discov. Today. 12 (2007) 650–656.

[102] Y. Zhang, S. Yang, Y. Guan, W. Cao, J. Xu, Fabrication of stable hollow capsules by covalent layer-by-layer self-assembly, Macromolecules. 36 (2003) 4238–4240.

[103] L. Dähne, S. Leporatti, E. Donath, H. Möhwald, Fabrication of Micro Reaction Cages with Tailored Properties, J. Am. Chem. Soc. 123 (2001) 5431–5436.

[104] W. Song, Q. He, H. Möhwald, Y. Yang, J. Li, Smart polyelectrolyte microcapsules as carriers for water-soluble small molecular drug, J. Control. Release. 139 (2009) 160–166.

[105] L.L. Del Mercato, P. Rivera-Gil, A.Z. Abbasi, M. Ochs, C. Ganas, I. Zins, C. Sönnichsen, W.J. Parak, LbL multilayer capsules: Recent progress and future outlook for their use in life sciences, Nanoscale. 2 (2010) 458–467.

[106] J. Campbell, J. Abnett, G. Kastania, D. Volodkin, A.S. Vikulina, Which Biopolymers Are Better for the Fabrication of Multilayer Capsules ? A Comparative Study Using Vaterite CaCO 3 as Templates, ACS Appl. Mater. Interfaces. 13 (2021) 3259-3269.

[107] A. Vikulina, D. Voronin, V. Vinokurov, Naturally derived nano- and micro-drug delivery vehicles: halloysite, vaterite and nanocellulose, New J. Chem. 44 (2020). 5638–5655.

[108] F. Liu, V. Kozlovskaya, V. Zavgorodnya, O. Martinez-Lopez, C. Catledge, E. Kharlampieva. Encapsulation of anticancer drug by hydrogen-bonded multilayers of tannic acid, Soft Matter. 10 (2014) 9237-9247.

[109] J. Xing, Y. Cai, Y. Wang, H. Zheng, Y. Liu, Synthesis of Polymer Assembled Mesoporous CaCO 3 Nanoparticles for Molecular Targeting and pH-Responsive Controlled Drug Release, 2020 (2020).

[110] N. Sudareva, O. Suvorova, N. Saprykina, H. Vlasova, Doxorubicin delivery systems based on doped CaCO 3 cores and polyanion drug conjugates, J. Microencapsul. 38 (2021) 164–176.

[111] L.J. De Cock, J. Lenoir, S. De Koker, V. Vermeersch, A.G. Skirtach, P. Dubruel, E. Adriaens, C. Vervaet, J.P. Remon, B.G. De Geest, Mucosal irritation potential of polyelectrolyte multilayer capsules, Biomaterials. 32 (2011) 1967–1977.

[112] B.G. De Geest, R.E. Vandenbroucke, A.M. Guenther, G.B. Sukhorukov, W.E. Hennink, N.N. Sanders, J. Demeester, S.C. De Smedt, Intracellularly Degradable Polyelectrolyte Microcapsules, Adv. Mater. 18 (2006) 1005–1009.

[113] V. Strehlow, J. Lessig, M. Göse, U. Reibetanz, Development of LbL biopolymer capsules as a delivery system for the multilayer-assembled anti-inflammatory substance α1-antitrypsin, J. Mater. Chem. B. 1 (2013) 3633–3643.

[114] A. Szarpak, D. Cui, F. Dubreuil, B.G. De Geest, L.J. De Cock, C. Picart, R. Auzély-Velty, Designing Hyaluronic Acid-Based Layer-by-Layer Capsules as a Carrier for Intracellular Drug Delivery, Biomacromolecules. 11 (2010) 713–720.

[115] K. Yoshida, T. Ono, Y. Kashiwagi, S. Takahashi, K. Sato, J.I. Anzai, pH-dependent release of insulin from layer-by-layer-deposited polyelectrolyte microcapsules, Polymers. 7 (2015) 1269–1278.

[116] O. Kopach, A.M. Pavlov, O.A. Sindeeva, G.B. Sukhorukov, D.A. Rusakov, Biodegradable microcapsules loaded with nerve growth factor enable neurite guidance and synapse formation, Pharmaceutics. 13 (2021) 1–15.

[117] K.C. Wood, H.F. Chuang, R.D. Batten, D.M. Lynn, P.T. Hammond, Controlling interlayer diffusion to achieve sustained, multiagent delivery from layer-by-layer thin films, Proc. Natl. Acad. Sci. 103 (2006) 10207 LP –

10212..

[118] F. Caruso, W. Yang, D. Trau, R. Renneberg, Microencapsulation of Uncharged Low Molecular Weight Organic Materials by Polyelectrolyte Multilayer Self-Assembly, Langmuir. 16 (2000) 8932–8936.

[119] B. Thierry, P. Kujawa, C. Tkaczyk, F.M. Winnik, L. Bilodeau, M. Tabrizian, Delivery Platform for Hydrophobic Drugs: Prodrug Approach Combined with Self-Assembled Multilayers, J. Am. Chem. Soc. 127 (2005) 1626–1627.

[120] B. Kim, S.W. Park, P.T. Hammond, Hydrogen-Bonding Layer-by-Layer Assembled Biodegradable Polymeric Micelles as Drug Delivery Vehicles from Surfaces, ACS Nano. 2 (2008) 386–392.

[121] A. Zhuk, L. XU, J.F. Anker, S.A. Sukhishvili, Selective water uptake within micelle-containing layer-by-layer fi lms of various architectures : a neutron reflectometry study , Soft Matter. (2013) 410–417.

[122] Z. Zhu, S.A. Sukhishvili, Temperature-Induced Swelling and Small Molecule Release with Hydrogen-Bonded Multilayers of Block Copolymer Micelles, ACS Nano. 3 (2009) 3595–3605.

[123] I. Erel, Z. Zhu, A. Zhuk, S.A. Sukhishvili, Hydrogen-bonded layer-by-layer films of block copolymer micelles with pH-responsive cores, J. Colloid Interface Sci. 355 (2011) 61–69.

[124] D. Gundogdu, V. Bütün, I. Erel-Göktepe, Preparation of Layer-by-Layer Films with Remarkably Different pH-Stability and Release Properties Using Dual Responsive Block Copolymer Micelles, Macromol. Chem. Phys. 219 (2018) 1800128.

[125] K. Yoshida, Y. Hasebe, S. Takahashi, K. Sato, J. Anzai, Layer-by-layer deposited nano- and micro-assemblies for insulin delivery: A review, Mater. Sci. Eng. C. 34 (2014) 384–392.

[126] F. Cavalieri, A. Postma, L. Lee, F. Caruso, Assembly and functionalization of

DNA-polymer microcapsules, ACS Nano. 3 (2009) 234–240.

[127] L. Xu, H. Wang, Z. Chu, L. Cai, H. Shi, C. Zhu, D. Pan, J. Pan, X. Fei, Y. Lei, Temperature-Responsive Multilayer Films of Micelle-Based Composites for Controlled Release of a Third-Generation EGFR Inhibitor, ACS Appl. Polym. Mater. 2 (2020) 741–750.

[128] A. Aliakseyeu, V. Albright, D. Yarbrough, S. Hernandez, Q. Zhou, J.F. Ankner, S.A. Sukhishvili, Selective hydrogen bonding controls temperature response of layer-by-layer upper critical solution temperature micellar assemblies, Soft Matter. 17 (2021) 2181–2190.

[129] B.S. Kim, H. Il Lee, Y. Min, Z. Poon, P.T. Hammond, Hydrogen-bonded multilayer of pH-responsive polymeric micelles with tannic acid for surface drug delivery, Chem. Commun. (2009) 4194–4196.

[130] W. Zhou, Z. Jia, P. Xiong, J. Yan, M. Li, Y. Cheng, Y. Zheng, Novel pH-responsive tobramycin-embedded micelles in nanostructured multilayer-coatings of chitosan/heparin with efficient and sustained antibacterial properties, Mater. Sci. Eng. C. 90 (2018) 693–705.

[131] Z. Zhu, S.A. Sukhishvili, Layer-by-layer films of stimuli-responsive block copolymer micelles, J. Mater. Chem. 22 (2012) 7667–7671.

[132] N. Ma, H. Zhang, B. Song, Z. Wang, X. Zhang, Polymer micelles as building blocks for layer-by-layer assembly: An approach for incorporation and controlled release of water-insoluble dyes, Chem. Mater. 17 (2005) 5065–5069.

[133] S. Biggs, K. Sakai, T. Addison, A. Schmid, S.P. Armes, M. Vamvakaki, V. Bütün, G. Webber, Layer-by-layer formation of smart particle coatings using oppositely charged block copolymer micelles, Adv. Mater. 19 (2007) 247–250.

[134] T. Addison, O.J. Cayre, S. Biggs, S.P. Armes, D. York, Polymeric

microcapsules assembled from a cationic/zwitterionic pair of responsive block copolymer micelles, Langmuir. 26 (2010) 6281–6286.

[135] R. Atun, D.A. Jaffray, M.B. Barton, F. Bray, M. Baumann, B. Vikram, T.P. Hanna, F.M. Knaul, Y. Lievens, T.Y.M. Lui, M. Milosevic, B. O'Sullivan, D.L. Rodin, E. Rosenblatt, J. Van Dyk, M.L. Yap, E. Zubizarreta, M. Gospodarowicz, Expanding global access to radiotherapy, Lancet Oncol. 16 (2015) 1153–1186.

[136] R. Baskar, K.A. Lee, R. Yeo, K.-W. Yeoh, Cancer and radiation therapy: current advances and future directions, Int. J. Med. Sci. 9 (2012) 193–199.

[137] A.W. Braithwaite, I.A. Russell, Induction of cell death by adenoviruses, Apoptosis. 6 (2001) 359–370.

[138] R.F. Barth, J.A. Coderre, M.G.H. Vicente, T.E. Blue, Boron neutron capture therapy of cancer: Current status and future prospects, Clin. Cancer Res. 11 (2005) 3987–4002.

[139] C.K. Park, S.H. Lee, J.H. Han, C.Y. Kim, D.W. Kim, S.H. Paek, D.G. Kim, D.S. Heo, I.H. Kim, H.W. Jung, Recursive partitioning analysis of prognostic factors in WHO grade III glioma patients treated with radiotherapy or radiotherapy plus chemotherapy, BMC Cancer. 9 (2009) 5–11.

[140] T. Yamamoto, K. Tsuboi, K. Nakai, H. Kumada, H. Sakurai, A. Matsumura, Boron neutron capture therapy for brain tumors, Transl. Cancer Res. 2 (2013) 80–86.

[141] R.F. Barth, J.A. Coderre, M.G.H. Vicente, T.E. Blue, Boron Neutron Capture Therapy of Cancer : Current Status and Future Prospects, 11 (2005) 3987–4003.

[142] A. Pitto-Barry, Polymers and boron neutron capture therapy (BNCT): A potent combination, Polym. Chem. 12 (2021) 2035–2044.

[143] N. Dewi, P. Mi, H. Yanagie, Y. Sakurai, Y. Morishita, M. Yanagawa, T.

Nakagawa, A. Shinohara, T. Matsukawa, K. Yokoyama, H. Cabral, M. Suzuki, Y. Sakurai, H. Tanaka, K. Ono, N. Nishiyama, K. Kataoka, H. Takahashi, In vivo evaluation of neutron capture therapy effectivity using calcium phosphate-based nanoparticles as Gd-DTPA delivery agent, J. Cancer Res. Clin. Oncol. 142 (2016) 767–775.

[144] R.F. Barth, A critical assessment of boron neutron capture therapy: an overview, J. Neurooncol. 62 (2003) 1–5.

[145] E.C.C. Pozzi, J.E. Cardoso, L.L. Colombo, S. Thorp, A.M. Hughes, A.J. Molinari, M.A. Garabalino, E.M. Heber, M. Miller, M.E. Itoiz, R.F. Aromando, D.W. Nigg, J. Quintana, V.A. Trivillin, A.E. Schwint, Boron neutron capture therapy (BNCT) for liver metastasis: Therapeutic efficacy in an experimental model, Radiat. Environ. Biophys. 51 (2012) 331–339.

[146] K. Hu, Z. Yang, L. Zhang, L. Xie, L. Wang, H. Xu, L. Josephson, S.H. Liang, M.-R. Zhang, Boron agents for neutron capture therapy, Coord. Chem. Rev. 405 (2020) 213139.

[147] T.D. Malouff, D.S. Seneviratne, D.K. Ebner, W.C. Stross, M.R. Waddle, D.M. Trifiletti, S. Krishnan, Boron Neutron Capture Therapy: A Review of Clinical Applications, Front. Oncol. 11 (2021) 1–11.

[148] H.R. Snyder, A.J. Reedy, W.J. Lennarz, Synthesis of Aromatic Boronic Acids. Aldehydo Boronic Acids and a Boronic Acid Analog of Tyrosine, J. Am. Chem. Soc. 80 (1958) 835–838.

[149] A.H. Soloway, H. Hatanaka, M.A. Davis, Penetration of Brain and Brain Tumor. V II. Tumor-Binding Sulfhydryl Boron Compounds, J. Med. Chem. 10 (1967) 714–717.

[150] J. Carlsson, E.B. Kullberg, J. Capala, S. Sjberg, K. Edwards, L. Gedda, Ligand liposomes and boron neutron capture therapy, Journal of neuro-oncology. 62 (2003) 47–59.

[151] K. Hu, Z. Yang, L. Zhang, L. Xie, L. Wang, H. Xu, L. Josephson, S.H. Liang, M.R. Zhang, Boron agents for neutron capture therapy, Coord. Chem.

[152] B.F. Spielvogel, F.U. Ahmed, G.L. Silvey, P. Wisian-neilson, A.T. Mcphail, Boron analogs of amino acids. 4. Synthesis of glycine and N-methylated glycine ester analogs, Inorg. Chem. 23 (1984) 4322–4324.

[153] H.M. Smilowitz, D.N. Slatkin, P.L. Micca, M. Miura, H.M. Smilowitz, D.N. Slatkin, P.L. Micca, M. Miura, H.M. Smilowitz, D.N. Slatkin, P.L. Micca, M. Miura, Microlocalization of lipophilic porphyrins : Non- toxic enhancers of boron neutron-capture therapy Microlocalization of lipophilic porphyrins : Non-toxic enhancers of boron neutron-capture therapy, 89 (2013) 611-617.

[154] Y. Zhu, N.S. Hosmane, Nanostructured boron compounds for cancer therapy, Pure Appl. Chem. 90 (2018) 653–663.

[155] G. Wu, R.F. Barth, W. Yang, M. Chatterjee, W. Tjarks, M.J. Ciesielski, R.A. Fenstermaker, Site-Specific Conjugation of Boron-Containing Dendrimers to Anti-EGF Receptor Monoclonal Antibody Cetuximab (IMC-C225) and Its Evaluation as a Potential Delivery Agent for Neutron Capture Therapy, Bioconjug. Chem. 15 (2004) 185–194.

[156] R.F. Barth, D.M. Adams, A.H. Soloway, F. Alam, M. V. Darby, Boronated Starburst Dendrimer-Monoclonal Antibody Immunoconjugates: Evaluation as a Potential Delivery System for Neutron Capture Therapy, Bioconjug. Chem. 5 (1994) 58–66.

[157] D.A. Feakes, K. Shelly, C.B. Knobler, M.F. Hawthorne, Na3[B20H17NH3]: Synthesis and liposomal delivery to murine tumors, Proc. Natl. Acad. Sci. U. S. A. 91 (1994) 3029–3033.

[158] T. Takahashi, Y. Fujii, G. Fujii, H. Nariuchi, Preliminary study for application of anti-alpha-fetoprotein monoclonal antibody to boron-neutron capture therapy, Jpn. J. Exp. Med. 57 (1987) 83–91.

[159] S. Martini, S. Ristori, A. Pucci, C. Bonechi, A. Becciolini, G. Martini, C. Rossi, Boronphenylalanine insertion in cationic liposomes for Boron Neutron Capture Therapy, Biophys. Chem. 111 (2004) 27–34.

[160] E.M. Heber, M.F. Hawthorne, P.J. Kueffer, M.A. Garabalino, S.I. Thorp, E.C.C. Pozzi, A.M. Hughes, C.A. Maitz, S.S. Jalisatgi, D.W. Nigg, P. Curotto, V.A. Trivillin, A.E. Schwint, Therapeutic efficacy of boron neutron capture therapy mediated by boron-rich liposomes for oral cancer in the hamster cheek pouch model, Proc. Natl. Acad. Sci. U. S. A. 111 (2014) 16077–16081.

[161] C. Lai, N. Lai, F.-I. Chou, Y. Chuang, C. Yang, C. Lin, Trivalent galactosyl-functionalized mesoporous silica nanoparticles as a target-speci fi c delivery system for boron neutron capture therapy, 1 (2013) 9412–9418.

[162] Y.C. Lee, R.T. Lee, Accounts of Chemical Research: Carbohydrate-Protein Interactions: Basis of Glycobiology, 28 (1995) 321–327.

[163] S. Feng, H. Zhang, S. Xu, C. Zhi, H. Nakanishi, X.D. Gao, Folate-conjugated, mesoporous silica functionalized boron nitride nanospheres for targeted delivery of doxorubicin, Mater. Sci. Eng. C. 96 (2019) 552–560.

[164] S. Iijima, T. Ichihashi, Single-shell carbon nanotubes of 1 nm diameter, Nature. 363 (1993) 603-605.

[165] Z. Yinghuai, A.T. Peng, K. Carpenter, J.A. Maguire, N.S. Hosmane, M. Takagaki, Substituted carborane-appended water-soluble single-wall carbon nanotubes: New approach to boron neutron capture therapy drug delivery, J. Am. Chem. Soc. 127 (2005) 9875–9880.

[166] M. Elsabahy, K. L. Wooley, Design of polymeric nanoparticles for biomedical delivery applications, Chem. Soc. Rev. 41 (2012) 2545-2561.

[167] A.K. Azab, M. Srebnik, V. Doviner, A. Rubinstein, Targeting normal and neoplastic tissues in the rat jejunum and colon with boronated, cationic acrylamide copolymers, J. Control. Release. 106 (2005) 14–25.

[168] A.H. Soloway, W. Tjarks, B.A. Barnum, F.-G. Rong, R.F. Barth, I.M. Codogni, J.G. Wilson, The Chemistry of Neutron Capture Therapy, Chem. Rev. 98 (1998) 1515–1562.

[169] H. Xiong, X. Wei, D. Zhou, Y. Qi, Z. Xie, X. Chen, X. Jing, Y. Huang, Amphiphilic Polycarbonates from Carborane-Installed Cyclic Carbonates as Potential Agents for Boron Neutron Capture Therapy, Bioconjug. Chem. 27 (2016) 2214–2223.

[170] H. Fujii, A. Matsuyama, H. Komoda, M. Sasai, M. Suzuki, T. Asano, Y. Doki, M. Kirihata, K. Ono, Y. Tabata, Y. Kaneda, Y. Sawa, C.M. Lee, Cationized gelatin-HVJ envelope with sodium borocaptate improved the BNCT efficacy for liver tumors in vivo, Radiat. Oncol. 6 (2011) 2–13.

[171] S. Yoneoka, Y. Nakagawa, K. Uto, K. Sakura, T. Tsukahara, M. Ebara, Boron-incorporating hemagglutinating virus of Japan envelope (HVJ-E) nanomaterial in boron neutron capture therapy, Sci. Technol. Adv. Mater. 20 (2019) 291–304.

[172] J. Li, O. Janouskova, R.F. Alvarez, S. Mesikova, T. Zdenek, S. Kereiche, U. Mariusz, P. Matejicek, Designed Boron - Rich Polymeric Nanoparticles Based on Nano -ion Pairing for Boron Delivery, Chemistry (Easton). (2020).

[173] V. Geis, K. Guttsche, C. Knapp, H. Scherer, R. Uzun, Synthesis and characterization of synthetically useful salts of the weakly-coordinating dianion [B12Cl12]2−, J. Chem. Soc. Dalt. Trans. (2009) 2687–2694.

[174] S. Dogan, A. Akdag, Synthesis of Carborane Derivatives For Characterization of Carbocations, Master dissertation, Middle East Technical University, 2019.

[175] D. Zhao, J. Jiang, J. Xu, L. Yang, T. Song, P. Zhang, Synthesis of template-free hollow vaterite CaCO3 microspheres in the H2O/EG system, Mater. Lett. 104 (2013) 28–30.

[176] Y. Wang, Y. Shen, Y. Zhang, B. Yue, C. Wu, pH-sensitive Polyacrylic acid

(PAA) hydrogels trapped with polysodium-p-styrenesulfonate (PSS), J. Macromol. Sci. Part B Phys. 45 B (2006) 563–571.

[177] A. Paradkar, A.A. Ambike, B.K. Jadhav, K.R. Mahadik, Characterization of curcumin–PVP solid dispersion obtained by spray drying, Int. J. Pharm. 271 (2004) 281–286.

[178] X. Wang, L. Li, W. Huo, L. Hou, Z. Zhao, W. Li, Characterization and Stability of Tanshinone IIA Solid Dispersions with Hydroxyapatite, Mater. . 6 (2013).

[179] H. Zhou, W. Wang, H. Hu, X. Ni, S. Ni, Y. Xu, L. Yang, D. Xu, Co-precipitation of calcium carbonate and curcumin in an ethanol medium as a novel approach for curcumin dissolution enhancement, J. Drug Deliv. Sci. Technol. 51 (2019) 397–402.

[180] M. El-Shahate Ismaiel Saraya, H. Hassan Abdel Latif Rokbaa, Preparation of Vaterite Calcium Carbonate in the Form of Spherical Nano-size Particles with the Aid of Polycarboxylate Superplasticizer as a Capping Agent, Am. J. Nanomater. 4 (2016) 44–51.

[181] J. Yin, J. Hu, G. Zhang, S. Liu, Schizophrenic Core–Shell Microgels: Thermoregulated Core and Shell Swelling/Collapse by Combining UCST and LCST Phase Transitions, Langmuir. 30 (2014) 2551–2558.

[182] K. Lipponen, S. Tähkä, M. Kostiainen, M.L. Riekkola, Stable neutral double hydrophilic block copolymer capillary coating for capillary electrophoretic separations, Electrophoresis. 35 (2014) 1106–1113.

[183] Z. Dong, L. Feng, W. Zhu, X. Sun, M. Gao, H. Zhao, Y. Chao, Z. Liu, CaCO3 nanoparticles as an ultra-sensitive tumor-pH-responsive nanoplatform enabling real-time drug release monitoring and cancer combination therapy, Biomaterials. 110 (2016) 60–70.

[184] S. Singh, P.J. Hsu, J.L. Kuo, G.N. Patwari, Dipole moment enhanced π-π

stacking in fluorophenylacetylenes is carried over from gas-phase dimers to crystal structures propagated through liquid like clusters, Phys. Chem. Chem. Phys. 23 (2021) 9938–9947.

[185] M. Ghasemi, R.G. Larson, Role of electrostatic interactions in charge regulation of weakly dissociating polyacids, Prog. Polym. Sci. 112 (2021) 101322.

[186] A. Singh, N.N. Myklebust, S.M.V. Furevik, R. Haugse, L. Herfindal, Immunoliposomes in Acute Myeloid Leukaemia Therapy: An Overview of Possible Targets and Obstacles, Curr. Med. Chem. 26 (2019) 5278–5292.

[187] X. Liu, N. Huang, H. Li, Q. Jin, J. Ji, Surface and Size Effects on Cell Interaction of Gold Nanoparticles with Both Phagocytic and Nonphagocytic Cells, Langmuir. (2013).

[188] S. Azzi, J.K. Hebda, J. Gavard, Vascular permeability and drug delivery in cancers, Front. Oncol. 3 (2013) 1–14.